Generation of pacemaker cardiomyocytes based on hHCN4 overexpression in hiPSCs by the *Sleeping Beauty* transposon system

Inaugural-Dissertation

to obtain the academic degree

Doctor rerum naturalium (Dr. rer. nat.)

submitted to

the Department of Biology, Chemistry and Pharmacy

of Freie Universität Berlin

by

Angélica García Pérez

from Almería, Spain

Berlin, 2018

This work was prepared from October 2012 to January 2018 under the supervision of Dr. Zsuzsanna Izsvák (Max-Delbrück Center for Molecular Medicine, Berlin, Germany) in collaboration with Prof. Martin Morad (Cardiac Signaling Center of University of South Carolina, Medical University of South Carolina & Clemson University, Charleston, SC, USA). All the experiments were conducted in the laboratories of Dr. Izsvák and Prof. Morad.

Supervisor: Dr. Zsuzsanna Izsvák
Max-Delbrück Center for Molecular Medicine
Berlin, Germany

Second examiner: Prof. Dr. med. Simone Spuler
Institute for Chemistry and Biochemistry
Department of Biology, Chemistry and Pharmacy
Freie Universität, Berlin
and
Department of Muscle Sciences and University
Outpatient Clinic for Muscle Disorders
Experimental and Clinical Research Center, Berlin

Date of Defense: 20.12.2018

Acknowledgements

Luckily, I have many people to say 'thank you' for all the support I received during many years of career in Science pursuing a PhD in one way or another. First of all, I would like to start apologizing (typical me) for those people that I would not mention by name due to space limitation or my bad head right now, after so much lack of sleep. Thank you all.

I would like to thank my supervisor Dr. Zsuzsanna Izsvák for offering me the possibility to work in this challenging project and let my carry out my PhD in her laboratory. I would like to thank my collaborators Prof. Martin Morad and Prof. Tomo Šarić for their technical and scientific support and their hospitality when I visited their laboratories. I would also like to thank Prof. Simone Spuler for her support as Academic Supervisor in Freie Univertät Berlin and for reviewing my thesis.

I would like to thank the core facilities at the MDC for their excellent technical support. I would like to thank the Advance Light Microscopy facility, the FACS facility, especially HP for the trust and the laughs during long hours of sorting, and the Stem Cell Core Facility. I would like to thank especially Dr. Sebastian Diecke for helping me with protocols, reagents, equipment, discussion, cell lines, experiments, media change… Thank you for trusting me and make me feel one more in your lab. Thank you for picking up the phone always and being constantly willing to help. I would also like to thank Dr. Mirko Moroni for the huge help he provided with electrophysiology in this project.

I would like to thank all my past and present colleagues in the lab of Zsuzsanna Izsvák for sharing so many hours with my music in cell culture, my temper and, with me. I would like to thank especially Dr. Attila Szvetnik and Dr. Enikö Eva Nagy (Ati and Eni) for very useful scientific discussions, for all those talks in the office on Friday evenings and for being a true inspiration and reference for me as scientists. I would like to thank also Dr. Sanam Bashir, Dr. Suneel Narayanavari, Ana Jiménez, Sandra Neuendorf, Beate Valeske Martina and Patrick Wasser and Ilija Bilic, for offering me their support and friendshipand helping me so much with German, bureaucracy (thank you so much Beate), lab organization… Thank you for being a great reason to go to Buch everyday.

I would like to thank my PhD colleagues, Dr. Huiqiand Cai and Dr. Vaisha Raghunathan, for the laughs and the support in this long way and the awesome trip to India. Thank you especially to Dr. Julia Zadora and Dr. Helena Escobar, for finishing my experiments when I was late, changing media, helping so much in so many aspects, caring so much about me and let me share with so many awesome moments during these years.

I would like to thank my friends in the lab of Nikolaus Rajewsky, my second lab at MDC :). Thank you Marta Rodríguez for bringing me there to meet your colleagues, especially the ones in the bioinformatics office. Thank you for your coffee, your funny games, your scientific and emotional support, and, once more, for making me feel part of your lab, your office and your

kitchen. I would like to thank specially my good friends Jordi, Mireya, Panos, Marcel, Marvin, Mackowiak, Andrei, Petar, JJ, Ivano and Cledi for making me happier to go to MDC.

I would like to thank my colleagues during my visits in the laboratories of my collaborators. I would like to thank especially (Dr.) Narasimha Telugu for letting me learn from him so many things in the lab and in life. Thank you Anfisa, for caring so much about me and feed me during exhausting working weekends. Thank you both for letting me be part of your life and family, for taking care of Juno so many times and share with me the joy of Amritha, a continuous source of happiness and love for me.

I would like to thank my former colleagues in the IPBLN and GENyO in Granada for so many hours of hard work and fun, and for keeping in contact with me after so many years. Thank you Dr. Antonio Estévez and Dr. Francisco Martín for giving me the chance to work in their laboratories when I thought everything was lost. Thank you for your trust and support. I would like to thank especially Dr. Esther Zumaquero for being so generous with me and show me and encourage me to never give up. I would like to thank Dr. Pilar Muñoz (Pili) for transferring me her huge knowledge and being my 'mum' in cell culture. I would like to thank also 'my postdocs' Dr. Sonia Morales, Dr. Teresa del Castillo, Dr. Karim Benabdellah, Dr. Miguel Toscano and Dr. Per Anderson, for teaching me so much and so well, for so many fruitful scientific discussions, for their support and, of course, for all the fun we shared working together. I would like to thank also Dr. María Morell, Dr. Marta P (;P), Dr. Santi Morell, Dr. Damiá Romero, Dr. Virginia Delgado, Dr. Sandra Fernández and many more (los Barkis, el canario, Kiko, Poto, Talia, las Veros, Rubén, Lucía, the entire Cholo's lab…), for your friendship, for all the fun we shared in Granada and for doing 2012 a memorable year.

I would like to thank my friends for many years from Granada and Almería for their support in the distance and for being always a great reason to go back to Spain. I would like to thank especially Marina and Edu for looking after me and make me feel so loved. Thank you Avi, Sol, Carmen, Brasito, Vivi, Rafón, Jesús, Txerra, Vali, Pitu, Juanma, Tamara, David, Juanmi, Alipio, Míguel, Pedro, Loli… Thank you especially to María and Mai, for all their love and for being part of my family for more than twenty years.

I would also like to thank all the wonderful people that I have met in Berlin and have make all these years worth it. Thank you Rocío, Yuting, Marta, Jingyi, Eleonora, Robin, Tristan, Philip, Christos, Trent, Toshiaki… Thank you for your friendship and for being a true family being far from home.

I would like to thank especially my 'editors team' that help me with the thesis writing, support me so much during these tough years and are the best friends anyone would imagine. Thank you Andreia for your support and for taking me out for dancing when I am almost forgetting what that is. Thank you Charlotte for so many useful comments, being always the first ;P and thank you for your constant support and all the great movies and Berlinales we have shared together. Thank you Alena for your touch in writing, the afternoon bouldering, the trips

and the positive look you always give to my work and to myself. Thank you Mireya, for so many coffees, hugs, emergency vodkas and nights out for overcoming PhD and life crisis. Thank you Jordi, for being a reference of good Science and hard work and for supporting me at so many levels. Thank you for keep coming back and remind me all the good things that Berlin has. Thank you Helenica, for your patience, your support and all the hours in the lab. Thank you for being ALWAYS there, even when I can not see it. Thank you Antonio, for so many years of free therapy, so many hours talking about life, Science and the Universe. Thank you for finding always the way to meet me when I go to Granada and for being the best possible reference as scientist and as a person. Really, really, thank you all for the support, especially during this very tough year and during the last months, when I could not even stand myself. I will never find the words or the presents to thank you enough all you have done for me. I love you all.

I would like to thank Juno (Junícola, Boliche, Gorda), for being the best dog ever. For taking me out when I can not do anything else and being a constant source of happiness and funny moments. Thank you for the patience and the adaptation to my crazy schedules.

Last, I would like to thank my family for EVERYTHING, for making me the person and scientist that I am today. For encourage me to follow my dreams and support me always, decision after decision. For letting me be the 'crazy one' of the family and love despite all. Thank you especially to my sister, the most important person in my life, and my reason to be better everyday.

Por ultimo, me gustaría agradecer a mi familia por TODO, por hacerme la persona y científica que soy hoy. Por animarme a seguir mis sueños y apoyarme siempre, decisión tras decision. Por dejarme ser 'la loca de la familia' y quererme a pesar de todo. Gracias especialmente a mi hermana, la persona más importante en mi vida y la razón que me implusa cada día a ser mejor persona.

I would like to thank you all again. Thank you very much. This work would not be possible without you and your support. I am very lucky to count on you.

Table of contents

Summary

The sinoatrial node (SAN) initiates and regulates the heartbeat in mammals. Sinoatrial (SA) nodal cells generate spontaneous action potentials by the combination of Ca^{++} oscillatory mechanisms and the activation of membrane ion channels, including the hyperpolarization-activated cyclic nucleotide-gated channels (HCN). HCN4 is the most abundant subunit in the SAN and mediates the inward depolarizing current I_f. I_f has been suggested as isolation mechanism of the SAN to resist the hyperpolarizing force of the surrounding atrium. *HCN4* relevance to pacing has been further supported by the discovery of more than twenty different mutations associated with mild or severe forms of arrhythmias. When SA nodal cells are damaged by aging or disease, the implantation of an electronic pacemaker is required. Electronic devices have been improved for decades but they still exhibit inadequate autonomic response, limited battery life, and risk of lead corrosion and infection, often causing adverse cardiac remodeling. These limitations could be addressed by the generation of biological cell-based pacemakers.

Although different strategies have been proposed to develop biological pacemakers, to date, clinically relevant studies using human cells have not been carried out yet. In this study, we propose a cell-based gene therapy approach, where the non-viral integrating transposon system *Sleeping Beauty* (SB) is used to overexpress hHCN4 in induced pluripotent stem cells (hiPSCs) as a platform for differentiation of pacemaker cardiomyocytes. I have developed a complete workflow for the generation of hHCN4-overexpressing cardiomyocytes (hHCN4-hiPSC-CM) that includes reprogramming of human fibroblasts into hiPSCs, hHCN4 overexpression in hiPSCs by SB-mediated gene delivery, and optimal cardiomyocyte differentiation into hHCN4-hiPSC-CM.

hHCN4-overexpressing hiPSCs showed stable, long-term expression of I_f while maintaining pluripotency. These cells efficiently differentiated into cardiomyocytes showing comparable yields to control hiPSCs. hHCN4-hiPSC-CM cultures displayed robust beating and contained 80% of cells expressing cardiomyocyte-specific markers from day 9 onwards through cardiomyocyte differentiation. Compared to cardiomyocytes derived from control hiPSC lines, hHCN4-hiPSC-CM showed 3-10 fold larger I_f that, just like in pacemaker cells, activated slowly at -60mV, was blocked by Cs^+ and was susceptible to ß-adrenergic regulation. Electrophysiological and transcriptional comparison of control and hHCN4-hiPSC-CM showed equivalent action potential properties and similar expression profile of ion channels, connexins and genes involved in general cardiac function or specific to SAN function and development. The number of spontaneously beating cells was similar, being this automaticity independent of the level of expression of I_f in both control and hHCN4-hiPSC-CM. However, spontaneously beating hHCN4-hiPSC-CM displayed faster beating frequency and were enriched in cells with pacemaker-like morphology.

Further *in vitro* and *in vivo* studies, including co-culture with ventricular-like cardiomyocyte monolayers and transplantation into the heart of a large animal model, are needed to determine the ability of hHCN4-hiPSC-CM to couple electrically and pace cardiac tissue and ultimately, the heart.

Zusammenfassung

Der Sinusknoten initiiert und reguliert den Herzschlag der Säugetiere. Die Zellen des Sinusknotens generieren spontane Aktionspotentiale durch das Zusammenspiel von Ca^{++} oszillatorischen Mechanismen und der Aktivierung von in der Zellmembran verankerten Ionenkanälen, wie zum Beispiel den HCN-Kanälen (aus dem Englischen: hyperpolarization-activated cyclic nucleotide-gated channels). HCN4 ist die am häufigsten im Sinusknoten vorkommende Untereinheit und exprimiert den nach innen gerichteten depolarisierenden Strom I_f. Es wird vermutet, dass I_f als Isolationsmechanismus dient, um den Sinusknoten von der hyperpolarisierenden Kraft des Atriums abzuschirmen. Die Bedeutung von HCN4 für die Schrittmacherfähigkeit des Sinusknotens wird außerdem unterstützt durch die Entdeckung von mehr als zwanzig Mutationen, welche mit leichten bis schwerwiegenden Herzrhythmusstörungen in Verbindung gebracht wurden.

Eine Schädigung der Zellen des Sinusknotens durch Alter oder Krankheit erfordert die Implantation eines elektronischen Herzschrittmachers. Diese elektronischen Apparate sind in den letzten Jahrzehnten stets weiterentwickelt worden. Allerdings ist ihr Nutzen durch eine unzureichende Autonomie, begrenzte Batterielebensdauer sowie das Risiko von Bleikorrosion und Infektion immer noch eingeschränkt. Nicht selten sind nachteilige Veränderungen des Herzmuskels die Folge (kardiales Remodeling). Diese Einschränkungen könnten durch die Generierung von zellbasierten biologischen Schrittmachern adressiert werden.

Obwohl verschiedene Strategien zur Entwicklung von biologischen Schrittmachern vorgeschlagen wurden, konnten bisher keine klinisch relevanten Studien durchgeführt werden, die auf humanen Zellen basieren. In dieser Arbeit schlagen wir eine zellbasierte kombinierte Gentherapie vor, in der das nicht-virale integrierende Transposon System *Sleeping Beauty* (SB) verwendet wird, um eine Überexpression von hHCN4 in induzierten pluripotenten Stammzellen (hiPSCs) zu erzielen. Dies soll die Basis für eine Differenzierung dieser Stammzellen in Schrittmacher-Kardiomyozyten bilden. Ich habe einen kompletten Workflow zur Generierung von hHCN4-überexprimierenden Kardiomyozyten (hHCN4-hiPSC-KM) entwickelt. Dieser beinhaltet die Umprogrammierung von humanen Fibroblasten in hiPSCs, die Überexpression von hHCN4 in hiPSCs durch SB-vermittelten Gentransfer sowie eine optimale Differenzierung von Kardiomyozyten in hHCN4-hiPSC-KM.

Unter Beibehaltung ihrer Pluripotenz, zeigten hHCN4 überexprimierenden hiPSCs eine stabile, langfristige Expression von I_f, dem für HCN4 Kanäle charakteristischen Ionenstrom. Dabei war ihre Fähigkeit sich in Kardiomyozyten zu differenzieren vergleichbar mit der von Kontroll-hiPSCs. hHCN4-hiPSC-KM-Kulturen zeigten ein robustes Schlagen. 80% der Zellen exprimierten kardiomyozyten-spezifische Marker beginnend mit Tag 9 sowie während der Differenzierungsphase in Kardiomyozyten. Im Vergleich zu Kardiomyozyten, die aus Kontroll-hiPSC-Linien stammen, wiesen hHCN4-hiPSC-KMs einen 3-10-fach größeren I_f auf. Wie in Schrittmacherzellen, zeigte I_f eine langsame Aktivierungskinetik bei -60mV, wurde durch Cs^+

blockiert und war anfällig für ß-adrenerge Regulation. Ein elektrophysiologischer und transkriptionaler Vergleich von Kontroll- und hHCN4-hiPSC-KM zeigte äquivalente Eigenschaften von Aktionspotentialen sowie ein vergleichbares Expressionsprofil von Ionenkanälen, Connexinen und Genen, welche zur allgemeinen Funktion des Herzens beitragen oder spezifisch für die Funktion und Entwicklung des Sinusknotens sind. Die Anzahl von spontan schlagenden Zellen war vergleichbar, wobei ihre Automatik unabhängig vom Expressionslevel des I_f in Kontroll- sowie hHCN4-hiPSC-KM war. Allerdings zeigten spontan schlagende hHCN4-hiPSC-KM eine schnellere Schlagfrequenz und waren in Zellen mit Schrittmacher-ähnlicher Morphologie angereichert.

Weitere In-vitro- und In-vivo-Studien mit hHCN4-hiPSC-KM, wie zum Beispiel ihre Kokultur mit ventrikulär-ähnlichen Kardiomyozyten-Monolayern oder eine Transplantation ins Herz im Großtiermodell, würden zeigen, ob sie zur elektrischen Kopplung sowie Schrittführung des Herzgewebes, und damit letztendlich des Herzens, fähig sind.

List of figures

List of tables

List of abbreviations

AAV: adeno-associated virus

AF: atrial fibrillation

AMD: Age-related Macular Degeneration

AP: action potential

APA: action potential amplitude

APD: action potential duration

APD90: action potential duration at 90% of repolarization

APD50: action potential duration at 50% of repolarization

AV: atrioventricular

AVN: atrioventricular node

ß2AR: ß2 adrenergic receptor

BAC: bacterial artificial chromosome

BMP: bone morphogenetic proteins

bpm: beats per minute

BSA: bovine serum albumin

B-TS: bradycardia-tachycardia syndrome

cAMP: cyclic adenosine monophosphate

CAR: chimeric antigen receptor

CCS: cardiac conduction system

cDNA: complementary DNA

CDS: coding sequence

CICR: calcium-induced calcium release

CM: cardiomyocyte

CNBD: cyclic nucleotide-binding domain

CPVT: catecholaminergic polymorphic ventricular tachycardia

CRT: cardiac resynchronization therapy

Cx: connexin/s

d: day (e.g. d9: day 9)

DMEM: Dulbeco's Modified Eagle's Medium

DMSO: dimethyl sulfoxide

DNA: deoxyribonucleic acid

E8 medium: Essential 8™ Medium (Gibco™, Thermo Fisher Scientific)

EB: embryoid bodies

EDTA: ethylenediaminetetraacetic acid

ESCs: embryonic stem cells

FACS: fluorescence activated cell sorting

FBS: fetal bovine serum

FGF: fibroblast growth factors

FHF: first heart field

FSC: Forward Scatter

gDNA: genomic DNA

GFP: green fluorescent protein

GFP-hiPSC-CM: cardiomyocytes derived from GFP-overexpressing hiPSCs

GFP-hiPSCs: GFP-overexpressing hiPSCs

HCN: hyperpolarization-activated cyclic nucleotide-gated potassium channel

HEK: human embryonic kidney

hESC-CMs: cardiomyocytes derived from human embryonic stem cells

hESCs: human embryonic stem cells

hHCN4: human HCN4

hHCN4-HEK293T: hHCN4-overexpressing HEK 293T cells

hHCN4-hiPSC-CM: cardiomyocytes derived from hHCN4-hiPSCs

hHCN4-hiPSCs: human HCN4-overexpressing hiPSCs

HF: heart failure

HFF: human foreskin fibroblasts

hiPSC-CMs: cardiomyocytes derived from human induced pluripotent stem cells

hiPSCs: human induced pluripotent stem cells

hPSC-CMs: cardiomyocytes derived from human pluripotent stem cells

hPSCs : human pluripotent stem cells

HRP: horseradish peroxidase

$I_{Ca,L}$: L-type Ca^{++} current

$I_{Ca,T}$: T-type Ca^{++} current

ICDs: implantable cardioverter defibrillators

I_f: Na^+/K^+ depolarizing/funny current

I_{K1}: inward rectifier K^+ current

I_{Na}: Na^+ current

I_{NCX}: inward Na^+-Ca^{++} exchange current

IR-L: Inverted Repeat Left

IR-R: Inverted Repeat Right

IRs: inverted repeats

IRES: internal ribosome entry side

IST: inappropriate sinus tachycardia

KOSR: KnockOut™ Serum Replacement

LAS: Leica Application Suite

LCR: local Ca^{++} release

LVNC: left ventricular non compaction cardiomyopathy

MDC: Max Delbrück Center for Molecular Medicine

MDP: maximum diastolic potential

MEFs: mouse embryonic fibroblasts

mESC-CMs: mouse embryonic stem cell-derived cardiomyocytes

mESCs: mouse embryonic stem cells

mRNA: messenger RNA

Myh6: myosin heavy chain 6

NA: non available

NCX: sodium-calcium exchanger

NEAA: non-essential amino acids

NRVMs: neonatal rat ventricular cardiac myocytes

NT: non-transfected

NT-hiPSC-CM: cardiomyocytes derived from non-transfected hiPSCs

NT-hiPSCs: non-transfected hiPSCs

PBMCs: peripheral blood mononuclear cells

PCR: polymerase chain reaction

PFA: paraformaldehyde

pFAR: plasmid free of antibiotic resistance markers

PSCs: pluripotent stem cells

PVDF: polyvinylidene difluoride

qPCR: quantitative PCR

RA: retinoic acid

RNA: ribonucleic acid

ROCK: Rho-associated, coiled-coil containing protein kinase

RRID: Research Resource Identifiers

RT: room temperature

RYR2: ryanodine receptor 2, cardiac ryanodine receptor

SA: sinoatrial

SAN: sinoatrial node

SB: *Sleeping Beauty*

SBr: sinus bradycardia

SCCF: Stem Cell Core Facility

SCVI: Stanford Cardiovascular Institute

SD: standard deviation

SDS: sodium dodecyl sulfate

SDS–PAGE: sodium dodecyl sulfate–polyacrylamide gel electrophoresis

SEM: standard error of the mean

SERCA: Sarco/Endoplasmic Reticulum Ca^{++} ATPase

SHF: second heart field

SKCas: Ca^{++}-activated K^{+} channels of small and intermediate conductance

SND: sinus node dysfunction or sinoatrial node disease

SNP: single-nucleotide polymorphism

SR: sarcoplasmic reticulum

SSC: Side Scatter

SSS: sick sinus syndrome

Tbx3: T-box factor 3

TNNT2: cardiac troponin, troponin 2

TGFß: transforming growth factor ß

VTN: truncated recombinant human vitronectin

WB: western blot

WNT: Wingless/INT proteins

Introduction

I. The pacing of the heart

The human cardiovascular system is composed of the heart and the circulatory system. The heart pumps blood throughout the blood vessels to the entire body. Thereby, arterial blood provides oxygen and nutrients to every cell while venous blood transports carbon dioxide and waste back to the heart. This exchange is possible thanks to the coordinated contraction of atria and ventricles during the cardiac cycle in combination with a complex vascular system. During diastole, cardiac muscle is relaxed and the heart is filled with blood. The oxygen-poor blood from the venous system is drained into the right atrium while the oxygenated blood from the lungs is delivered through the pulmonary veins into the left atrium. At the end of the diastole, the atria pump blood into the ventricles. Next, during systole, the right and left ventricles contract simultaneously and eject blood into the pulmonary artery going to the lungs and into the aorta going to the rest of the body, respectively. This sequence of events constitutes the cardiac cycle and occurs with every heartbeat (Klabunde, 2012).

The heartbeat initiates in the right atrium at the sinoatrial node (SAN) and it is propagated through the heart by a specialized muscular tissue, the cardiac conduction system (CCS). The electrical impulse begins in the SAN and spreads rapidly through both atria to the atrioventricular node (AVN) located on the endocardial surface of the right atrium. Slow conduction of AVN is responsible for the delay between atrial and ventricular systole that allows the filling of the ventricles before their contraction. After the AVN, the conduction continues via the bundle of His that then divides into the left and right bundle branches through the ventricular septum. The branches divide in fascicles extensively intercommunicated that ramify in the ventricular apex and along the ventricular walls becoming the terminal Purkinje fibers network which propagates the electrical impulse to the working muscle at multiple sites (Purkinje-muscle junctions) simultaneously (Figure 1) (Sánchez-Quintana and Yen Ho, 2003; Unudurthi et al., 2014). The action potential (AP) is transmitted through the His-Purkinje system up to ten times faster than in the ventricular muscle, allowing the synchronous contraction of the ventricles (Boyett, 2009).

The CCS consists of specialized myocytes enveloped in a connective tissue sheath that isolate them from the working myocardium. The CCS specific function relies on automaticity and source-sink balance, distinctive properties shared by all its components. Automaticity is defined as the ability to generate spontaneous APs without external stimulus and it is required for normal pacing activity. All cells from the CCS posses this capability due to their distinctive ion channel expression profile that results in a unique electrophysiological signature. Together with a complex tissue structure, the electrophysiology of the CCS is designed to manage a balance between the current generated by driving cells (source) and the current needed to excite the downstream

latent cells (sink). Source-sink equilibrium is important along the entire heart, but it acquires special importance in CCS and pacemaker tissues (Boyett, 2009; Unudurthi et al., 2014).

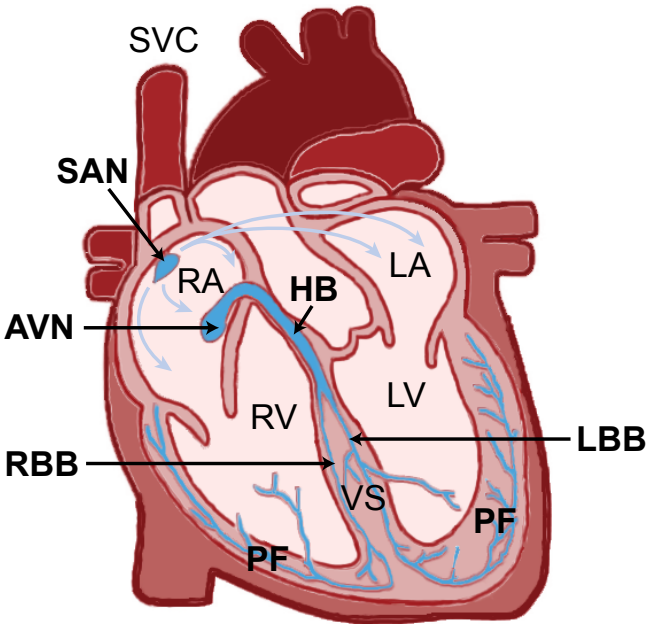

Figure 1. Schematic representation of the conduction system of the heart. Drawing of the frontal view of a longitudinal section of the heart. Anatomic regions of the heart are labeled with roman font: SVC: superior vena cava, RA: right atrium, LA: left atrium, RV: right ventricle, LV: left ventricle, VS: ventricular septum; and components of CCS are colored in blue and labeled with bold font: SAN: sinoatrial node, HB: His bundle, RBB: right bundle branch, LBB left bundle branch, PF: Purkinje fibers. Blue arrows represent the propagation of the electrical impulse through the atria (Modified from Liang *et al.*, 2015).

The SAN constitutes the primary pacemaker of the heart. Several animal models including rabbit (Brioschi et al., 2009; Brown et al., 1979; Blecker et al., 1980; Fedorov et al., 2006; Kreitner, 1981), mouse (Dobrzynski et al., 2005; Liu et al., 2007; Stieber et al., 2013; Mierop & Gessner, 1970), dog (Ambrosi et al., 2012; James et al., 1966; Lou et al., 2014; Woods et al., 1976) or guinea pig (Opthof et al., 1985; Sirenko et al., 2017) have been traditionally used to study the anatomy, morphology, electrophysiology and cell composition of the SAN. Although numerous characteristics of the SAN are common for most of mammalian hearts there are inherent differences between species. For that reason, I will be focusing on human SAN features.

I.1 The sinoatrial node: anatomy, structure and cell composition

The 'sino-auricular junction' (known nowadays as SAN) was described for the first time by Keith and Flack in 1907 as the anatomical region where the cardiac rhythm is initiated in the mammalian heart. It was primarily described as a specialized tissue structure where a central artery was surrounded by fibrous tissue, nerve fibers and 'peculiar

musculature' in very close connection with vagal and sympathetic nerves. The presence of these very well differentiated fibers in proximity to the great veins, where physiological experiments demonstrated the heart's rhythm begins, led them to propose this area as the pacemaker region of the heart (Figure 2B, C) (Keith and Flack, 1907).

The SAN is located in the subepicardial region of the right atrium at the junction of the crista terminalis and the superior vena cava (Figure 2A, B, D). It usually shows a fusiform structure that extends between the superior and the inferior vena cava except in 10% of individuals where it shows horseshoe shape around the lower part of the superior vena cava (Sánchez-Quintana and Yen Ho, 2003). Histologically, it is formed by clusters of specialized myocytes embedded in connective tissue and in close association with the autonomic nervous system. The sinus node artery typically occupies the center of the node and the rest of cells organize around it (Figure 2C, E) (Sánchez-Quintana and Yen Ho, 2003; Unudurthi et al., 2014). In the periphery of the SAN, a 'paranodal area' with nodal and atrial properties can be identified and has been proposed to have a role in pacing (Figure 2A, orange) (Chandler et al., 2009, 2011).

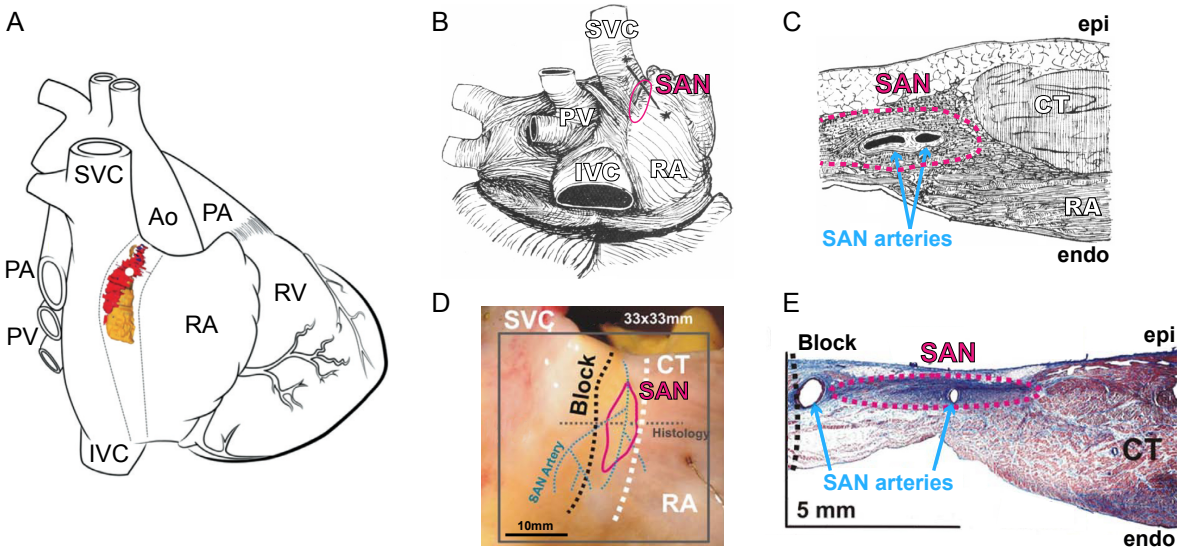

Figure 2. Anatomy and histology of the SAN. A) Schematic drawing of the human heart in dorsal view showing the computational reconstruction of the SAN (red) and the paranodal area (orange) based on imaging techniques. The leading pacemaker is labeled by a white dot (modified from Chandler et al., 2011). **B-E)** Localization of the SAN in the human heart (magenta continuous and dashed lines) and the major surrounding anatomical structures (SAN arteries: light blue; block zone intra-atrial septum: black dashed line) assessed by several procedures. **B)** Drawing of the macroscopic dorso-posterior view of the atria and **C)** the microscopic view of a histological section (*—*) of the SAN (modified from Keith and Flack, 1907). **D)** Epicardial photograph and **E)** Masson's trichrome staining of the corresponding cross-section (Histology: grey dashed line) of the SAN (modified from Fedorov et al., 2010). Ao: aorta; CT: crista terminalis; endo: endocardial; epi: epicardial; IVC: inferior vena cava; PA: pulmonary artery; PV: pulmonary veins; RA: right atrium; RV: right ventricle; SAN: sinoatrial node; SVC: superior vena cava.

It has been shown that numerous areas within the SAN are able to generate pacemaker activity (Ferrer, 1973). The 'leading pacemaker' site where the AP is originally generated (Figure 2A, white dot) is not static and can shift localization spontaneously, with vagal stimulation, during exercise or in association with heart diseases or aging (Boyett, 200). These observations suggest that heart rate changes are produced by changes in the localization of the leading pacemaker within the SAN rather than by intrinsic rhythm changes by a unique pacemaker site (Boyett et al., 2000; Choudhury et al., 2015; Ferrer, 1973).

Although the SAN functions as a single pacemaker unit, histologically it shows a marked heterogeneity between the central and peripheral areas. Original studies in rabbit, contributed with two different models to illustrate the cellular diversity of the SAN: the gradient model, which proposes a gradual transition in cell properties from the center to the periphery of the SAN; and the mosaic model that suggests a mix of pacemaker/atrial cells showing gradual decreasing ratio towards the atrium (Boyett et al., 2000; Unudurthi et al., 2014). In the human SAN, differences in the gene expression profile between the central part of the node and its interphase with the atrium have been also observed. However, the cellular distribution responsible of these differences remains unclear (Chandler et al. 2009, 2011). While it is commonly accepted that the SAN is functionally isolated from the atrium, it is still controversial how the electrical impulse is propagated to the AVN. Two main hypotheses have been proposed. Several studies suggested the existence of a structural border of fibroblasts that provides insulation and allows AP propagation only through restricted and well-defined 'SAN conduction pathways' where pacemaker cells connect with atrial cardiomyocytes (CMs) (Csepe et al., 2016; Fedorov et al., 2010). In opposition, other studies showed a lack of fibrotic insulation between the SAN and the right atrium and instead described irregular SAN borders with multiple radiations and interdigitations towards the surrounding atrium. In this case, the geometric arrangement of the atrial myocytes themselves would allow faster propagation of the AP in some areas of the atrium than others (James et al., 1966; Sánchez-Quintana et al., 2005).

At the cellular level, the SAN is formed by several thousand cells including pacemaker and atrial CMs, fibroblasts, macrophages, pericytes, adipocytes and nerve fibers, that are supported by a dense collagen matrix (Mitrofanova et al., 2018; Unudurthi et al., 2014). Only a reduced number of cells comprised in the node are putative pacemaker cells able to generate the electrical impulse. Moreover, their properties differ throughout the SAN, showing different sizes and morphology, expression of distinct gap proteins and different electrophysiological characteristics derived from variations in the density of diverse ionic currents (Baruscotti & Robinson, 2007; Boyett et al., 2000; Mitrofanova et al., 2018). Pacemaker cells are typically 5-10μm in diameter and 25-30μm long, ranging up to 125μm in length. They are mono-nucleated and display either 'spindle' morphology with increased length-to-width and surface-to-volume ratio compared with working CMs, or a 'spider' morphology with irregular and multiple prolongations

spreading from the cenll body (Satoh, 2003; Unudurthi et al., 2014). Under the electron microscope, nodal cells appear clear and with 'empty' cytoplasm due to the presence of a small number of disorganized and randomly distributed myofibrils formed by few myofilaments. SA nodal cells are weakly coupled through scattered desmosomes and are in contact with surrounding cells in all directions, in contrast with working CMs that display a polarized cell-to-cell contact by intercalated discs. In addition, nodal cells contain a low number and sparse mitochondria with few mitochondrial cristae, and a poorly developed sarcoplasmic reticulum (SR), in contrast with working CMs that contain an increased number and more complex mitochondria and SR that display an organized distribution between the myofibrils (James et al., 1966; Mitrofanova et al., 2018).

In summary, the heterogeneity of the SAN is crucial for its function for several reasons: it provides protection/isolation from the surrounding hyperpolarized atrial CMs, facilitates the generation of APs at the relative small SAN which drives the mass of atrial muscle, avoids the reentry of external APs and assures pacing function under multiple conditions by shifting the leading pacemaker site. The maintenance of these complex structural features together with other molecular mechanisms is required for the normal function of the SAN and thus the pacing of the heart.

I.2 Automaticity mechanisms and electrical coupling in the sinoatrial node

While particular architecture and heterogeneity of the SAN is crucial for robust pacing at the tissue level, automaticity is the key characteristic of nodal cells at the cellular level. Pacemaker cells are able to generate over 2.5 billion spontaneous APs without external stimuli, from the third week post-conception to the end of our life (Hornberger and Sahn, 2007).

The cardiac AP is a brief reversal of membrane potential in CMs and is produced by the orchestrated activation of ion channels. Distinct expression of these ion channels determines the shape of the AP in different types of CMs (Figure 3A). Spontaneous APs generated by SA nodal cells display different characteristics than those generated by atrial and ventricular CMs. While working CMs have a stable resting potential at ~-90mV during diastole, pacemaker CMs are characterized by a slow diastolic depolarization, the 'pacemaker potential' (Figure 3B). The cell membrane potential becomes more positive from a maximum diastolic potential of ~-60mV until it reaches the threshold potential at ~-40mV at which a new AP is triggered. In addition, the AP upstroke in pacemaker cells is slow (dV/dt_{max}~10V/s) due to low expression of voltage-gated Na^+ channels that generate a Na^+ current (I_{Na}) responsible for the fast AP upstroke in working CMs (dV/dt_{max}>100V/s) (Figure 3B). Moreover, nodal cells lack the typical 'plateau' phase present in ventricular and atrial CMs previous to the repolarization phase. Finally, repolarization of pacemaker cells to a maximum diastolic membrane potential underlies activation of several voltage-gated K^+ channels (Figure 3A, B) (Boyett, 2009; Morad & Zhang, 2017; Morris & Kalman, 2014; Satoh, 2003).

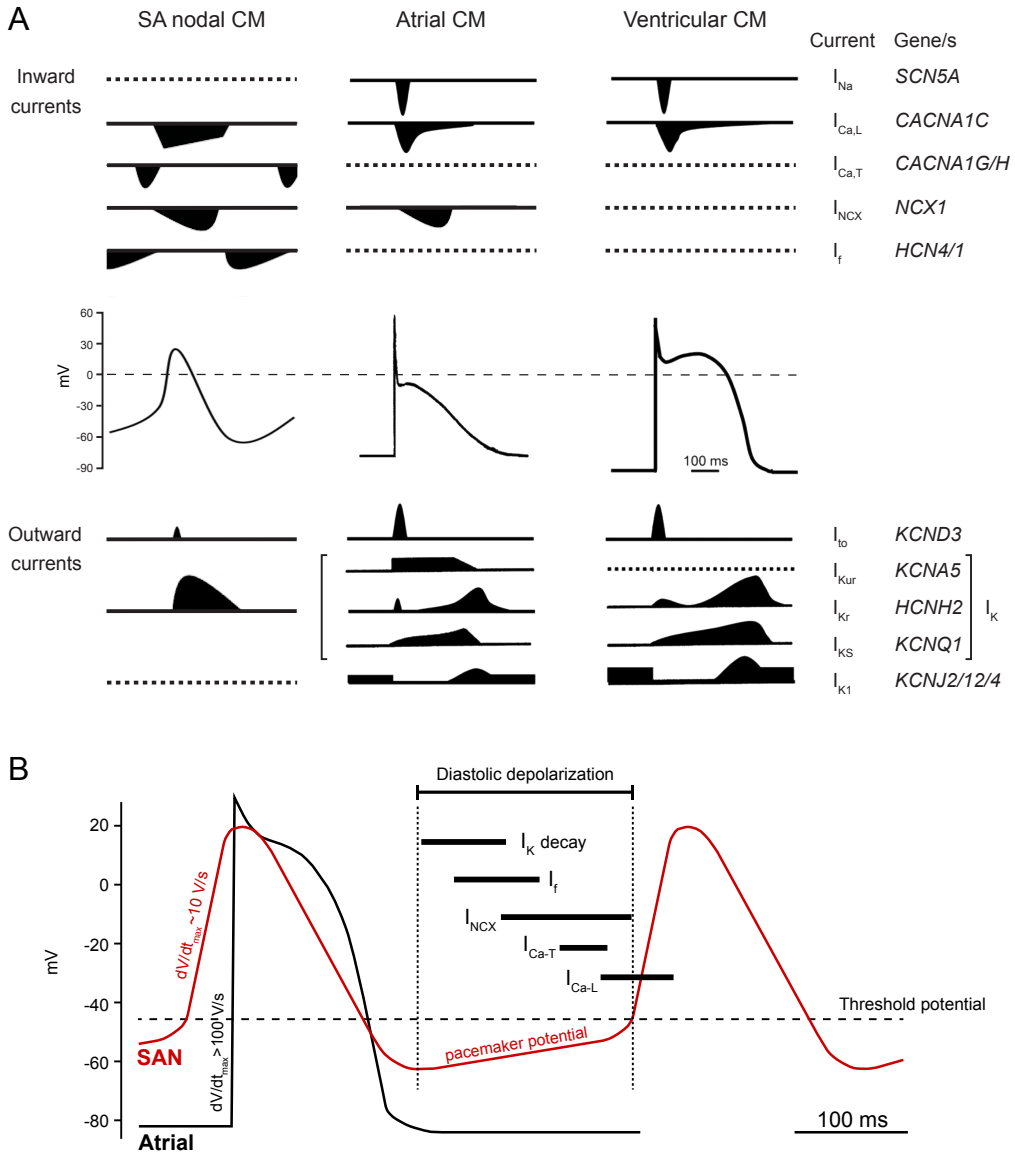

Figure 3. AP characteristics of the different CM subtypes. A) Charasteristic AP traces and contribution of the main inward (above) and outward (below) ion currents to its generation in SA nodal, atrial and ventricular CMs. Genes encoding channel subunits responsible for the ion currents are listed on the right (Modified from Park & Fishman, 2011; Ravens & Cerbai, 2008; Rezazadeh & Duff, 2017). **B)** Overlay of representative AP of working CM (atrial, black) and SA nodal cells (red). Temporal contribution of the main currents responsible for the pacemaker potential is represented in black bars (Modified from Morris & Kalman, 2014). See the main text for currents symbol description.

The diastolic depolarization is considered the electrophysiological signature of the specialized pacing tissue of the heart and occurs by the coordinated activity of a unique combination of ion channels/transporters/exchangers responsible for the pacemaker mechanisms (Morad & Zhang, 2017; Morris & Kalman, 2014). Precise interactions between membrane voltage-gated proteins (Membrane clock) and intracellular calcium dynamics (Calcium clock) are responsible for automaticity in pacemaker cells. Traditionally, five ionic currents are considered the key players in SAN pacing (Figure 3A). SAN cells lack the

inward rectifier K^+ current (I_{K1}) carried by KCNJ2, which is responsible for the maintenance of the hyperpolarized membrane potential in working CMs. Its absence in SA nodal cells contributes to the earliest phase of diastolic depolarization. The membrane clock is created by the resulting decay of outward I_{K1} and the presence of at least three voltage-activated inward currents: the Na^+/K^+ depolarizing current or funny current (I_f), L-type Ca^{++} current ($I_{Ca,L}$) and T-type Ca^{++} current ($I_{Ca,T}$). The Ca^{++} currents, also part of the calcium clock, contribute to the late phase of diastolic depolarization together with the activation of the inward Na^+-Ca^{++} exchange current (I_{NCX}) (Figure 3A, B) (Morris & Kalman, 2014).

The role of different ion channels required for the generation of the pacemaker potential has been studied using the voltage-clamp technique in combination with ion channels inhibitors. Moreover, the generation of knockout and transgenic animals has revealed the contribution of different ion channels to the global pacemaker function of the SAN in mammals. Although many studies have tried to identify the genuine spontaneous event responsible for the pacemaker potential that generates and regulates automaticity in SA nodal cells (Bogdanov et al., 2001; Brown et al., 1979; Tsutsui et al., 2018), it is currently accepted that pacemaker function can be only understood as the result of a functionally coupled-clock system where several voltage-, time- and calcium-dependent oscillatory mechanisms are responsible for the AP firing and rhythm (Maltsev & Lakatta, 2009; Tsutsui et al., 2018; Yaniv et al., 2015).

I.2.1 Calcium clock

The calcium clock mechanisms are dependent on membrane channels and intracellular calcium handling proteins. The key players of this system are the cardiac type 2 ryanodine receptors (RYR2) expressed in the membrane of the SR and the sodium-calcium exchanger (NCX), L-type calcium channels and T-type calcium channels expressed in the sarcolemma (Lyashkov et al., 2018; Tsutsui et al., 2018).

The main function of the SR is to store of Ca^{++} ions and therefore it plays a central role in AP generation. In opposition to the global Ca^{++} release from RYR2 that contributes to the AP in atrial and ventricular CMs, spontaneous and local Ca^{++} release (LCR) propagates through the subsarcolemmal space in SAN cells (Bogdanov et al., 2001; Tsutsui et al., 2018). These LCRs activate the NCX that exchanges one intracellular Ca^{++} for three extracellular Na^+ generating an inward current (I_{NCX}) by Ca^{++} removal from the cell. As the membrane potential reaches -50mV, T-type calcium channels activate, inducing further depolarization. When the membrane potential reaches -40mV, L-type calcium channels open. These Ca^{++} inward currents are amplified by calcium-induced calcium release (CICR) from the SR by RYR2 and thus increase I_{NCX} amplitude and create a positive feedback resulting in further acceleration of diastolic depolarization. The Sarco/Endoplasmic Reticulum Ca^{++} ATPase (SERCA) expressed at the membrane of the SR reuptakes

cytoplasmic Ca^{++} refilling the SR store (Lyashkov et al., 2018; Maltsev & Lakatta, 2013; Monfredi et al., 2010; Morris & Kalman, 2014).

SA nodal cells display a specific spatial distribution of LCRs during spontaneous AP generation. Before the AP upstroke, LCR arises near the edge of the cell and propagates in waves through the subsarcolemmal space towards the center of the cell (Bogdanov et al., 2001; Tsutsui et al., 2018). This wavelike propagation and amplification is similar in working CMs and is attributed to CICR mechanisms. Recent studies have described cyclic Ca^{++} release and upstroke of different mitochondrial populations during pacing, suggesting that mitochondrial Ca^{++} oscillations also participate in the calcium-clock mechanism underlying automaticity (Yaniv et al., 2012; X. Zhang et al., 2015).

Several studies have shown that spontaneous beating and generation of LCRs occurs under voltage clamp, i.e. independently of the membrane-clock (Bogdanov et al., 2001; Y. Wu et al., 2009; X. Zhang et al., 2015). Moreover, the pharmacological blockage of I_f and I_{Ca} does not suppress automaticity of pacemaker cells (Kreitner, 1981; Noma et al., 1983; Vinogradova et al., 2010). In contrast, blockage of I_{NCX} by Ni^{++} or Cd^{++}, inhibition of RYR2 by ryanodine or tetracaine, inhibition of SERCA by thapsigargin or cyclopiazonic acid, or mitochondrial uncoupling mediated by FCCP, have shown a concentration-dependent effect and ultimate suppression of spontaneous AP generation, indicating the crucial role of SR and mitochondrial Ca^{++} handling as pacing mechanisms (Vinogradova et al., 2010; X. Zhang et al., 2015).

I.2.2 Membrane clock

Classical theories proposed that the combined activity of membrane voltage-gated ion channels, the membrane clock, would be sufficient to provide automaticity to pacemaker cells (Noble, 1962). Early studies investigating the ionic mechanisms responsible for the generation of diastolic depolarization in SA nodal cells, identified the decay of outward I_{K1} and particularly the Na^+/K^+ driven hyperpolarization-activated 'funny' inward current, I_f, as main contributors to the pacemaker potential (Brown et al., 1979; Brown & DiFrancesco, 1980; Maylie et al., 1981) (Described in detail in Introduction, section II.2: page 15). Although the first numerical models of the membrane clock included only few voltage-gated channels, they predicted quite accurately the distinctive AP shape of pacemaker cells (Noble, 1960). Later, during decades of voltage clamp studies, more than twelve ion currents have been identified that play a role in the membrane clock (Maltsev & Lakatta, 2013). The sarcolemmal T-type and L-type calcium channels and NCX are part of both Ca^{++} and membrane clock and therefore play a key role in clock coupling (Tsutsui et al., 2018). Additionally, although conventionally the inward current I_{Na} was considered absent in nodal cells, its expression was further confirmed in the periphery of the SAN where it was proposed to play a role in AP entrainment and propagation to the neighboring atrium (Chandler et al., 2009).

A numerical study developed to elucidate the minimal set of sarcolemmal and intracellular currents that would model automaticity of a single pacemaker cell, concluded that a coupled clock between $I_{Ca,L}$, I_K decay, I_{NCX} and intracellular calcium-clock would be sufficient to generate spontaneous APs. Nevertheless, when I_f was included in the simulations, the pacing model decreased in flexibility but increased in robustness, stabilizing pacing rate and showing an important role as anti-bradycardic mechanism (Maltsev & Lakatta, 2013). A recent study in human SA nodal cells has shown that spontaneous LCRs coupled to the membrane clock drive the automaticity in these cells. Several parameters: voltage, time, intrinsic cAMP signaling, PKA- and CaMKII-dependent protein phosphorylation have been shown to regulate both clocks. While intracellular Ca^{++} concentration represents the clock oscillatory substrate, I_{NCX}, I_f, I_K and I_{Ca} have been suggested to play a major role in clock coupling (Tsutsui et al., 2018).

I.2.3 Propagation of the electrical impulse

From the SAN where the AP is generated to the ventricular myocytes that contract at the end of the cardiac cycle, the propagation of the electrical impulse through the CCS and the heart tissue depends on the ability of neighboring CMs to receive and transmit electrical current. This cell-to-cell electrical communication occurs through gap junctions, nonspecific ion channels comprised of connexins (Cx) that allow intercellular cytoplasmic continuity. Different regions of the heart contain gap junctions constituted by different composition of Cx and therefore displaying different conductance properties (Davis et al., 1995; Boyett et al., 2000; Monfredi et al., 2010).

There is some level of electrical uncoupling within the SAN. This allows its conduction velocity to be slower compared to the surrounding atrium. Sparse and small gap junctions with preferential expression of low-conductance Cx have been described in the SAN (Boyett et al., 2000). Cx43 is ubiquitously and abundantly expressed in working CMs, it is responsible for the high conduction velocity of the AP through the contractile myocardium, and it is completely absent in the SAN. Instead, slowly conducting Cx, predominantly Cx45 and to less extent Cx40, are expressed in the SAN and the AVN; the latter also shows low levels of Cx43 expression. At the ventricles, Purkinje fibers display abundant and polarized expression of these three Cx, that are mostly present in the longitudinal cellular ends but almost absent in the transversal cell-to-cell contact regions (Davis et al., 1995; Kreuzberg et al., 2009).

Experimental and numerical studies have shown that synchronized activation of the atrial tissue by the SAN requires the expression of low-resistance intracellular channels. This poor electrical coupling of the SA nodal cells with the adjacent atrial CM contributes to the pacemaker activity of the SAN by two main mechanisms: i) it allows the coordinated propagation of the AP from the center to the periphery of the node and ii) it provides certain

level of isolation from the hyperpolarized myocardium (Anumonwo et al., 1992; D. Cai et al., 1994).

I.3 Aging and disease of the sinoatrial node

The SAN is a specialized plastic tissue that undergoes remodeling at different levels during human lifespan. The heart rate slows down from ~140 beats per minute in a newborn to ~70 beats per minute in an adult human. During senescence, the heart rate under autonomous control does not show significant changes, in contrast with the 'intrinsic heart rate' (the heart rate in the absence of sympathetic and parasympathetic activity), that shows an age-related decrease. Similarly, after autonomic ablation, SAN conduction tends to decrease in association with age while this correlation is absent with intact innervation. These data indicate that there are intrinsic variations in the SAN architecture and function associated with age (Kuga et al., 1988, 1993; Boyett et al., 2009).

An evident limitation when studying the consequence of aging in the SAN is to separate the real effect of aging from those changes derived from associated heart diseases. Moreover, it is difficult to differentiate compensatory mechanisms of the autonomic nervous system due to intrinsic deterioration of the SAN from primary age-related changes in this autonomic regulation. Nevertheless, common structural changes of the aging SAN have been described in humans as well as in several animal models. It is well established that the SAN undergoes a clear and significant loss of pacemaker CMs upon senescence. The muscle loss is accompanied by an increase in fibrosis (without changes in adipose tissue) and extends to the atrium, in a gradual process that starts around 60 years of age (Davies & Pomerance, 1972; Csepe et al., 2015). The remodeling of the heart by increased fibrosis relates to the mentioned reduced conductivity of the SAN by two mechanisms: i) abnormal cell-to-cell connections lead fibroblasts to depolarize adjacent CMs and ii) physical isolation of pacemaker cells by enhanced fibrosis reduces the pacing by limiting their coupling (Csepe et al., 2015). These macroscopic alterations are expected to result in changes in SAN activation and quite often an inferior shift of the leading pacemaker. Electrical remodeling of the SAN has been also proposed as a possible mechanism underlying the observed physiological changes during senescence. Altered expression of Ca^{++} handling proteins, reduction in I_f current density and peripheral loss of I_{Na} and Cx43 expression have been described in pacemaker cells subjected to aging. However, these observations have been made only in animal models, and further confirmation of these electrophysiological changes in human SA nodal cells is required (Morris & Kalman, 2014; Choudhury et al., 2015).

Whether SAN dysfunction is due to aging, genetic mutations, associated diseases, heart failure or athletic training, it results in a variety of physiological manifestations or symptoms that have been traditionally grouped under the name of sick sinus syndrome (SSS) and more recently referred as sinus node dysfunction or sinoatrial node disease (SND). Independently of

the etiology, the clinical expressions of SND are the consequence of diverse pathological mechanisms, and comprise both structural rearrangements and molecular remodeling in SA nodal and atrial cells, involving changes in ion channels and their regulatory elements (Morris & Kalman, 2014). SND affects equally men and women and can appear at any age. However, the incidence of the disease increases exponentially with age and the mean age of patients with SND is around 68 years old (Dakkak & Doukky, 2017).

The most common clinical manifestation of SND is a persistent or periodic sinus bradycardia (slow heart rate). Other symptoms associated with SAN failure are sinus arrest, that occurs when sinus rhythm stops for short times without any other compensatory rhythm, or sinus escape, that involves longer periods of sinus rhythm interruption replaced by atrial or junctional rhythm (beating initiated by the AVN). Under both conditions, long periods of SAN inactivity could result in total cardiac arrest followed by ventricular arrhythmias. Additional SND manifestations combine post-tachycardia events after decreased sinus rhythm, and are referred as bradycardia-tachycardia syndrome (Ferrer, 1973). Overall, the decreased cardiac output resulting from these alterations in the SAN activity can lead to hypoperfusion of vital organs with high demand of oxygen, especially the brain, the heart and the kidneys, causing fatal consequences.

The relation between SND and other cardiac diseases, especially atrial tachycardia and heart failure is also well studied. Frequently, SAN malfunction is associated with remodeling of right atrium that leads to atrial flutter and atrial fibrillation (AF). In turn, initial atrial arrhythmia induces as well electrical rearrangements in the SAN and causes SND (Dobrzynski et al., 2007; Morris & Kalman, 2014). In binodal disease, the transitory or persistent AF induces atrioventricular (AV) block that derives in bradycardia as result of both SAN and AVN dysfunction (Ferrer, 1973). At the beginning of the disease, atrial arrhythmogenic foci can be eliminated by catheter ablation with variable success rate. Although SAN function can be recovered to normal levels, tachycardia periods often reappear or sinus bradycardia arise as result of irreversible SND, depending on the degree of atrial and SAN tissue remodeling (Dobrzynski et al., 2007).

Lethal bradyarrhythmias account for almost half of the cases of sudden death associated to heart failure. Conversely, it has been shown that heart failure induces important SAN rearrangements leading to SND even without its clinical manifestations (Monfredi et al., 2010; Morris & Kalman, 2014). Electroanatomic mapping of patients with symptomatic heart failure revealed caudal shift of the leading pacemaker, increased intrinsic sinus cycle length and sinus recovery time, reduced SAN conduction and anomalous propagation of the AP from the SAN around the crista terminalis. In addition, this affection might be worsen by the cocktail of negatively chronotropic and antiarrhythmic drugs often used for treatment of heart failure that could lead to or aggravate an existing SAN pathology (Sanders, 2004).

There is an increased incidence of SND in endurance athletes. They show higher prevalence of sinus bradycardia and SAN and AVN conduction abnormalities resulting from intrinsic changes of the heart (Stein et al., 2002). Initially, it was proposed that this pathology was the result of alterations in the regulation by the autonomic nervous system, but reduction in the intrinsic heart rate has been demonstrated in the SAN of these athletes (Boyett, 2009). It has been suggested that the response to training is originally mediated by the autonomic nervous system, and over time the atrial and ventricular dilatation induce 'mechanoelectric feedback' that leads to irreversible structural and electrophysiological remodeling of the SAN and other components of the CCS, resulting in chronic SND (Stein et al., 2002; Monfredi et al., 2015).

Importantly, several mutations in genes encoding for proteins involved in the AP generation and propagation have been involved in familial SND. Most of mutations affect the expression of ion channels, but mutations in genes encoding structural and regulatory proteins have also been linked to congenital bradyarrhythmias. The discovery of these mutations associated with SAN pathologies has helped to understand the important role that these particular genes have in pacing mechanism in humans (Rezazadeh & Duff, 2017).

More than 200 mutations in *SCN5A*, the gene encoding the Nav1.5 channel, have been associated with cardiac disorders due to the main role of I_{Na} in the fast upstroke of the cardiac AP in working CMs. Interestingly, up to 14 mutations in *SCN5A* have been associated with SND, revealing the importance of I_{Na} for the maintenance of an appropriate SAN function (Park & Fishman, 2011). In contrast, only one mutation in *CACNA1D* has been described in association with a cardiac phenotype, and the loss of function of the Cav1.3 L-type Ca^{++} channel has been linked with congenital bradycardia and deafness (Baig et al., 2011). Similarly, point mutations and deletions in *HCN4* (Described in detail in Introduction: section II.3, page 17) have been associated with several cases of congenital bradycardia and AF (Verkerk & Wilders, 2015). A specific kind of congenital arrhythmia associated with SND, catecholaminergic polymorphic ventricular tachycardia (CPVT), has been linked with mutations in SR proteins involved in the maintenance of the calcium clock, RYR2 and cardiac calsequestrin (*CASQ2*). CPVT patients show resting sinus bradycardia and are susceptible to sudden death as the result of stress-induced ventricular tachycardia that is independent of heart structural diseases (Park & Fishman, 2011).

Not only mutations in genes coding for ion channels have been associated with hereditary SND. Mutations in scaffold proteins essential for the maintenance of the structure and function of the sarcolemma have been also identified as the underlying cause of congenital SND. Loss of function mutations in the *ANK2* gene encoding the structural protein Ankyrin-B result in defective translocation and anchoring of ion channels involved in both membrane and calcium clock to the sarcolemma, leading mainly to reduced density of $I_{Ca,L}$ and I_{NCX} (Refaey & Mohler, 2017). Similarly, malformations in the

caveolae, specialized sarcolemmal invaginations, due to mutations in *CAV3* have been identified in patients with severe bradycardia. Several channels and transporters including HCN4, Nav1.5 and NCX have been found in caveolae as part of cell-signaling transduction microdomains. Abnormal localization of these channels in the sarcolemma of the SA nodal cells interferes with Ca^{++} and Na^{++} homeostasis and lead to heart rate alterations. These mutations have been linked to CPVT, long QT-syndromes, sudden infant death syndrome and SND (Rezazadeh 6 Duff, 2017).

Although I focused in the description of SAN pathologies, dysfunction of other components of the CCS, such AVN or His-Purkinje system, can also lead to cardiac arrhythmias and sudden cardiac death. Failure of any of the components of the CCS is potentially fatal, and requires the use of cardiac implantable electrical devices such as artificial pacemakers, implantable cardioverter defibrillators (ICDs) and cardiac resynchronization therapy (CRT), the only available treatment to date.

II. HCN4

II.1 HCN family and isoforms

The hyperpolarization-activated cyclic nucleotide-gated potassium channels (HCN) are members of the voltage-gated ion channel superfamily (Yu, 2005). HCN are nonselective cation channels, conducting both Na^+ and K^+, activated by hyperpolarization and modulated by cyclic nucleotides (mostly by cAMP) (DiFrancesco & Tortora, 1991; Hayoz et al., 2017). HCN-current was first described in cardiac nodal cells and named 'funny current' (I_f) due to its peculiar characteristics, especially the fact that it is activated by hyperpolarization at membrane potentials negative to -50mV (Brown et al., 1979; Maylie et al., 1981). HCN proteins are highly conserved in mammals (>90% sequence identity). They are encoded by four genes (*HCN1-4*) and their expression depends on the tissue, cell type, developmental stage or age. They are widely expressed in brain and heart, where they contribute to the rhythmic firing of APs in neurons and CMs (Robinson & Siegelbaum, 2003). HCN3 is specifically expressed in neurons, while the other three members are expressed in both neural and cardiac tissue (Biel et al., 2002).

HCN subunits are expressed at the plasma membrane where they work as functional channels assembled as homo or heterotetramers (except for HCN2-HCN3 heterotetramers) (Baruscotti et al., 2011). Individual HCN subunits are formed by three main macrodomains: the transmembrane core and the cytoplasmic N- and C-termini. The N-terminus is involved in membrane localization (Tran et al., 2002) and, together with the most distal portion of the C-terminus, represents the most variable region between the different HCN proteins (Biel, 2009). The transmembrane core has 80-90% sequence similarity between the different members of the HCN family. It is formed by six α-helix segments (S1-6, Figure 4) and a loop between S5 and S6 that contributes to the pore of

the channel. All subunits show the GYG motif in the pore loop, which represents the selectivity filter in K^+ channels for this cation. Moreover, a highly conserved asparagine (N380) in the extracellular portion of this loop is glycosylated (white N, Figure 4) and has been shown to be crucial for membrane localization and tetramerization of the HCN subunits (Much et al., 2003). The positively charged S4 α-helix constitutes the voltage sensor while the S4-S5-linker is responsible for the differential response to voltage (Figure 4). The proximal region of the C-terminus is formed by the cyclic nucleotide-binding domain (CNBD) and the C-linker region that connects it to the S6. This region interacts with the transmembrane core during channel gating and it is responsible for the cyclic nucleotide-mediated regulation of these channels. The CNBD is formed by four α-helices and a ß-roll between A- and B-helices that consists in eight ß-strands and forms the cAMP-binding pocket together with several residues of the C-helix (Figure 4). The C-linker is formed by six α-helices (A'-F', Figure 4) and mediates most of the subunit-subunit interactions within the tetramer (Biel, 2009). Although HCN opening is mainly controlled by voltage, cAMP and cGMP are considered stimulatory modulators and their binding induce a positive shift in the channels voltage dependence, facilitating their activation. Moreover, this modulation is mediated by direct binding to the CNBD domain rather than by protein phosphorylation, which induces conformational changes that increase channels activity (DiFrancesco & Tortora, 1991; Hayoz et al., 2017).

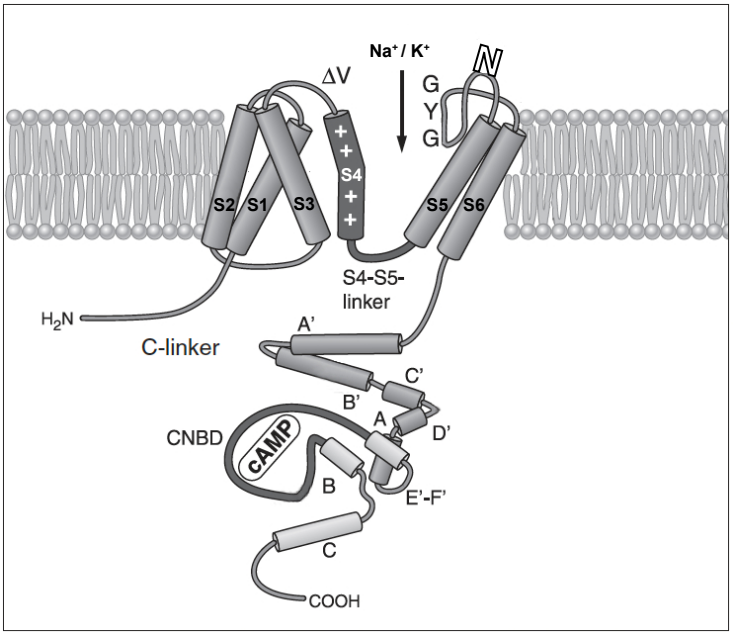

Figure 4. Schematic representation of the structure of an HCN subunit. HCN subunits are composed of six transmembrane segments (S1-S6) including the voltage sensor (S4). The permeation pathway (black arrow) contains the GYG triplet constituting the selectivity filter for K^+. The C-terminus is composed of the C-linker, consisting in six α-helices (A'-F'), and the cyclic nucleotide-binding domain (CNBD), consisting in α-helices (A-C) with a ß-roll between the A- and B-helices (thick gray line). The asparagine residue susceptible to glycosylation in the loop between S5 and S6 is indicated as a white N (Modified from Biel, 2009).

All subunits of the HCN family show currents with biophysical properties of native I_f. However, different subunits present differences in their activation kinetics, their steady-state voltage dependence and their sensitivity to cAMP modulation. HCN1 subunit presents the fastest kinetics with strong voltage-dependent activation (30-300ms at -140 to -95mV); saturating concentrations of cAMP induce only a weak shift in its activation curve. HCN4 is the subunit with the slowest activation kinetics, up to 1-2 seconds at -70mV, while HCN2 and HCN3 display intermediate opening kinetics, 200-500ms. Interetingly, human HCN3 have been shown to be insensitive to cAMP or cGMP. In contrast, HCN2, and especially HCN4 are strongly sensitive to cAMP-mediated voltage-activation shift (up to 25mV) (Biel, 2009).

I_f contributes to several processes in neurons, including determination of the resting membrane potential, dendritic integration or synaptic transmission; and plays a critical role in heart beat generation and regulation. I_f is present in all cardiac tissues, although its functional contribution under physiological conditions is restricted to the CCS (Baruscotti et al., 2010; Biel et al., 2002). While HCN2 is the most abundant subunit in atrial and ventricular CMs, HCN1 and HCN4 expression is restricted to the CCS and they are highly expressed in the SAN (Chandler et al., 2009).

II.2 HCN4 (I_f) role in pacing

For decades, many investigators concluded that the depolarizing I_f current was responsible for the diastolic depolarization observed in pacemaker cells APs, and it was recognized as the 'pacemaker current' (Brown et al., 1979; Brown and DiFrancesco, 1980; DiFrancesco and Ojeda, 1981). Later during the 1990s, HCN proteins were identified and characterized as molecular correlate of I_f. Among the four HCN subunits, HCN4 expression was shown to be restricted to the SAN within the rabbit heart and started to be referred as the pacemaker channel (Ishii et al., 1999; Vaccari et al., 1999). Later studies confirmed that HCN4 is also the most expressed subunit in the human SAN (Chandler et al., 2009). Originally, I_f activation range was proposed to overlap with membrane potential ranges (-40 to -65mV) exhibited by SA nodal cells during diastolic depolarization (Brown and DiFrancesco, 1980; Verkerk et al., 2007). The activation of an inward current leading to depolarization at maximum diastolic membrane potential could represent the molecular mechanism by which the threshold membrane potential is reached and spontaneous APs are triggered (DiFrancesco, 2007). Moreover, I_f was shown to increase upon adrenaline perfusion and to be modulated by intracellular cAMP, providing the link between HCN regulation and autonomic control of the heart rate by sympathetic ß-adrenergic and parasympathetic muscarinic stimulation (Brown et al., 1979). Taking all these evidences together, I_f current was considered for decades the main depolarizing current during diastolic depolarization and an essential mechanism for spontaneous APs generation in pacemaker cells.

Although the importance of I_f in pacing is widely accepted, its role as main contributor of the pacemaker potential is controversial. Many studies have shown discrepancies of HCN activation kinetics with diastolic depolarization duration and membrane potential ranges. While membrane potential oscillates from -60mV to -40mV during diastolic depolarization, activation of I_f current occurs from -70mV to more negative potentials and becomes stronger at higher levels of hyperpolarization ranging up to -160mV (Maylie et al., 1981; Noma et al., 1983; Verkerk et al., 2007). I_f displays a slow activation time constant of several seconds, while the AP frequency in humans ranges from 1 to 2 per second. Moreover, spontaneous APs can still be recorded upon complete blockage of I_f by Cs^{++}, zatebradine and other inhibitors, although the diastolic depolarization phase is significantly slower, and the interval between APs is prolonged (Kreitner et al., 1981; Noma et al., 1983; Boyett et al., 2000). For all these reasons, I_f in pacing has been reviewed and a modulatory function of this current has been proposed in opposition to the traditional belief that it directly contributes to the diastolic depolarization phase of pacemaker cells AP (Boyett et al., 2000; Satoh, 2003; Morad & Zhang, 2017).

When considered in the multicellular context of the SAN and its interface with the atrium, I_f expressed by pacemaker cells has been proposed to be a protective mechanism. The large mass of hyperpolarized atrium (-90mV) electrically coupled to the relative small SAN should drag pacemaker cells membrane potential to more negative voltages. The expression of I_f would oppose this effect and act as functional insulator in SA nodal cells. Consistent with the mentioned gradient model proposed for SAN structure, higher density of I_f and HCN4 expression have been described in the periphery of the rabbit SAN compared with the central region. This observation concurs with the suggested role of I_f as inward depolarizing current to overcome the hyperpolarizing influence of the surrounding atrium (Boyett et al., 2000; Morad & Zhang, 2017). However, there seem to be some discrepancies regarding human SAN, where HCN4 has been shown to be highly expressed in the central node compared to the paranodal area (Chandler et al., 2009).

The physiological role of HCN4 has been extensively studied in animal models. Mice deficient in *Hcn4* global or cardiac-specific expression died between embryonic day 9.5 and 11.5 (first heart beats in mice are observed during development at day 8.5). At this stage of embryonic development, these mice did not show structural abnormalities and heart contracted rhythmically, although at a slower rate. Moreover, electrophysiological studies in single CMs showed a 75-90% decrease of the I_f density in *Hcn4*$^{-/-}$ mice, and the current was insensitive to cAMP stimulation. The subsidiary I_f expression was proposed to be carried by Hcn1 and Hcn3. Interestingly, APs typical of mature pacemaker cells could not be recorded from *Hcn4* deficient CMs (Stieber et al., 2003). In transgenic mice where a single point mutation (R669Q) was introduced within the CNBD of *Hcn4*, resulting in cAMP insensitivity of the channel, homozygous mice died during embryonic development between day 11 and 12. Similarly to *Hcn4*$^{-/-}$ mice, they displayed a slower heart rate

although I_f densities values were comparable to those of wild type animals (Harzheim et al., 2008). Several studies investigated the effect of *Hcn4* cardiac deletion in adult animals. They developed bradycardia ranging from intermittent sinus pauses (Herrmann et al., 2007) to deep bradycardia with AV block eventually leading to complete heart block and death (Baruscotti et al., 2011). These observations confirmed that, while Hcn4 expression is not required for proper cardiac structural organization or automaticity, it plays a key role in heartbeat regulation and cardiac function during embryonic development and adulthood.

II.3 *HCN4* mutations and arrhythmia

The relevance in pacing of HCN4 has been further supported by the discovery of several mutations, most of them inducing loss-of-function, in patients with mild or severe forms of arrhythmia. The first *HCN4* mutation was identified by a gene candidate approach in a single patient with idiopathic SND. In that patient, a heterozygous 1bp deletion introduced an early stop codon in the *HCN4* sequence and resulted in a truncated HCN4 protein (537X) lacking the CNBD and the distal C-terminus residues. I_f carried by this channel was comparable to that carried by the wild type channel, but was unresponsive to cAMP modulation. Coexpression of both channels resulted in currents displaying properties similar to those of the truncated HCN4 (Schulze-Bahr et al., 2003). Since this first report, twenty-two additional mutations or variants of the *HCN4* gene have been described in association with SND or AF (summarized in Table 1).

As mentioned before, most of the identified mutations in *HCN4* cause loss-of-function of this channel and bradycardia as main clinical manifestation. Additional heart rhythm disturbances such as AV block, AF, deficient chronotopic heart rate modulation, bradycardia-tachycardia syndrome or sinus arrest have been described as well. In agreement with these observations, in vitro studies have shown decreased current intensity of I_f carried by these mutant channels, shift to more negative voltage-activation ranges, slower activation kinetics or altered response to cAMP-mediated activation. Moreover, some mutations interfere with HCN4 trafficking resulting in reduced or no expression of the channel at the cell membrane. Overall, these alterations lead to a reduced contribution of I_f during diastolic depolarization and prolongation of this AP phase resulting in slower heart rate (Baruscotti et al., 2016; Verkerk & Wilders, 2015).

In addition to bradycardia, patients carrying specific *HCN4* mutations also develop ventricular non-compaction cardiomyopathy (Table 1, LVNC). Because mice deficient in cardiac Hcn4 expression did not show structural heart defects, the mechanisms underlying this pathology in human are truly puzzling. Their clarification could be crucial for understanding the role of *HCN4* during heart development (Rezadadeh et al., 2017). Interestingly, only one gain-of-function *HCN4* mutation has been described to date. An arginine-to-glutamine mutation (R524Q) has been identified in a case of familial inappropriate sinus tachycardia (IST). The mutant channel presents higher cAMP affinity

that mimic the effect of ß-adrenergic stimulation and leads to faster basal heart rate (Baruscotti *et al.*, 2017). This finding brings insight to the molecular mechanisms underlying HCN4-linked tachyarrhythmias, and support the important role of this channel in heart beat regulation.

Mutation	Clinical manifestations	Effect on HCN4/I_f	Reference
K189R	AF	None	Macri *et al.*, 2014
P257S	AF	Deficient membrane expression	Macri *et al.*, 2014
A414G	SBr, AF, LVNC	Hyperpolarizing shift in voltage-activation	Milano *et al*, 2014
G480R	Asymptomatic SBr	Reduced membrane expression. Hyperpolarizing shift in voltage-activation, slower activation kinetics	Nof, *et al.* 2007
Y481H	SBr and LVNC	Hyperpolarizing shift in voltage-activation	Milano *et al*, 2014
G482R	SBr and LVNC	No I_f. Dominant negative effect.	Milano *et al*, 2014 Schweizer *et al.*, 2010
A485V	SBr	Reduced membrane expression. Hyperpolarizing shift in voltage-activation, slower activation kinetics	Laish-Farkash et al., 2010
R524Q	IST	Increased cAMP affinity	Baruscotti et al., 2017
K530N	AF	Hyperpolarizing shift in voltage-activation, slower activation kinetics, increased cAMP sensitivity	Duhme et al, 2013
D553N	Severe bradycardia, long QT	Reduced membrane expression. Reduced current amplitude.	Ueda et al., 2004 Duhme et al, 2013
573X	SBr, AF	cAMP insensitivity	Schulze-Bahr et al., 2003
S672R	Asymptomatic SBr	Hyperpolarizing shift in voltage-activation, faster deactivation	Milanesi et al., 2006
N688S	Asymptomatic	None	Macri *et al.*, 2014
695X	SBr, LVNC	cAMP insensitivity	Schweizer *et al.*, 2010
T822M	Early-onset AF	None	Macri *et al.*, 2014
P883R	SBr, B-TS, LVNC	NA	Schweizer *et al.*, 2010
G885R	Early-onset AF	None	Macri *et al.*, 2014
P945S	Early-onset AF	None	Macri *et al.*, 2014
A1045V	Asymptomatic	None	Macri *et al.*, 2014
R1068H	Asymptomatic	None	Macri *et al.*, 2014
G1077S	Early-onset AF	None	Macri *et al.*, 2014
G1097W	AV block	Decreased density, hyperpolarizing shift in voltage-activation, faster deactivation	Zhou et al., 2014
E1193Q	Early-onset AF	None	Macri *et al.*, 2014

Table 1. *HCN4* mutations and variants in association with SND and AF. AF: atrial fibrillation; AV: atrioventricular; B-TS: bradycardia-tachycardia syndrome; IST: inappropriate sinus tachycardia; LVNC: left ventricular non-compaction cardiomyopathy; NA: non available; SBr: sinus bradycardia.

Although it has been proven that the expression of HCN4 is not essential for spontaneous APs generation (Noma et al., 1983) and several mechanisms and currents have been shown to contribute to diastolic depolarization in addition to the 'funny current' (Tsutsui et al., 2018), there is a plethora of evidences that support the key role of this channel and thus I_f in basal heart rate maintenance and its proper modulation by the autonomic nervous system.

III. The *Sleeping Beauty* transposon system

Transposable elements or transposons are repetitive sequences with the ability to relocate themselves ('jump') within the host genome by a process called transposition.

They are present in the genome of virtually all organisms and contribute to a large fraction of the genomic DNA in numerous species. While 45% of the human genome derives from transposon sequences, this percentage can range up to 80% in the case of the maize genome (Lander et al., 2001; Muñoz-López & García-Pérez, 2010). However, only a small fraction of the transposable elements are actively 'jumping' in the genome, while the rest have been inactivated by mutations accumulation. Although these repetitive sequences were initially called 'junk DNA', the completion of the sequence of the human genome suggested that this portion of the genome has been and is still subjected to a gain of function process (Lander et al., 2001). Nowadays, it is well known that transposable elements have played an important role in shaping the genome of multiple organisms during evolution, including humans. Transposon-derived sequences are incorporated in gene coding sequences and a wide variety of regulatory elements through domestication by the host genome and have been reported to be essential for many cellular processes such as embryonic development, cell differentiation and neurogenesis (Bodega & Orlando, 2014).

Regarding their transposition mechanism, transposable elements can be categorized in two classes: retrotransposons (Class I) and DNA transposons (Class II). Retrotransposons are mobilized by a 'copy and paste' mechanism that involves two stages. First, the transcribed RNA transposon is reverse transcribed to DNA by a reverse transcriptase and then, the new DNA copy of the transposon is inserted in a new position into the genome by a transposase. This transposition mechanism results in the amplification of the transposon copy number per genome. In opposition, DNA transposons are mobilized by a 'cut and paste' mechanism in which the transposase directly excise the transposon and integrate it in a different position of the genome. Normally, this transposition mechanism does not involve copy number amplification (Muñoz-López & García-Pérez, 2010).

Sleeping Beauty (SB) is a DNA transposon belonging to the Tc1/*mariner* superfamily. These elements have been identified in several vertebrate genomes where they underwent 'vertical inactivation', a process by which the accumulation of mutations ultimately led to the loss of active transposase copies. Originally, DNA transposons consist in a single open reading frame encoding the transposase flanked by terminal inverted repeats (IRs) that constitute the recognition sequence and binding site of the transposase (Figure 6A). SB transposase was 'resurrected' by molecular reconstruction based on the consensus genomic sequence of 8 fish species of the salmonid subfamily. The synthetic transposase gene in combination with the IRs sequence previously identified from a non-autonomous Tc1 element (Ivics et al., 1996), comprised the original SB transposon system and was the first DNA transposon confirmed to be transpositionally active in vertebrate cells (Ivics et al., 1997).

As a DNA transposon, SB operates by a 'cut and paste' transposition mechanism. First, two molecules of SB transposase recognize and binds to each of the IRs. During excision, the two transposon ends are brought together and the transposase catalyze

transposon excision acting as a tetramer. The excised DNA is then integrated into the genome after a TA dinucleotide that is duplicated upon transposition (Figure 6B) (Izvák et al., 2002; Ivics et al., 1997). The two components of the SB transposon system, transposase and transposon, can work in trans. This feature allows the integration of any DNA sequence of interest flanked by the IRs into the genome by coexpression with the transposase (Izvák et al., 2002).

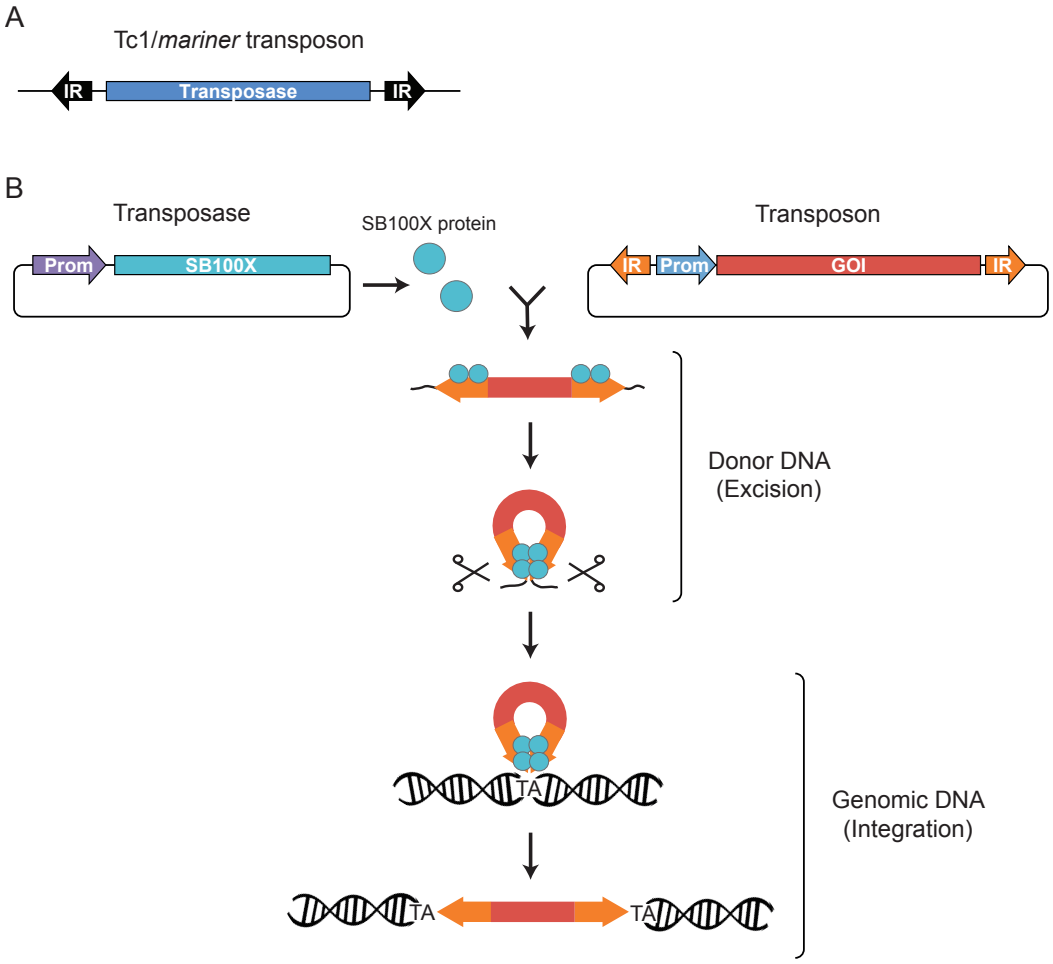

Figure 5. ***Sleeping Beauty*** **structure and transposition mechanism. A)** SB original structure. Schematic map of transposase gene and flanking IRs sequences common for the DNA transposons belonging to the Tc1/*mariner* superfamily. **B)** Schematic representation of the SB100X transposition mechanism. See the main text for detailed description. GOI: gene of interest; IR: inverted repeat; Prom: promoter.

Since the establishment of the SB transposon system, multiple groups modified the transposase sequence and the transposon vector in an attempt to enhance its transpositional activity (Baus et al., 2005; Geurts et al., 2003; Zayed et al., 2004). Using a high-throughput genetic screening, Mátés and colleagues obtained a hyperactive version named SB100X that, by substitution of only 9 amino acids, resulted in ~100-fold enhance transposition activity compared to the original SB transposase. Despite the hyperactivity of SB100X, it maintained the main characteristics of the original SB such as integration

profile, protein stability, affinity to the IRs, and transposition mechanism (Figure 5B). Moreover, SB100X transposon system was used to mediate stable transgene integration in somatic, germ line and stem cells, showing efficiency levels comparable to integrating viral systems (Mátés et al., 2009). Thanks to this feature, the SB100X system has been used as non-viral plasmid-based gene transfer tool for a wide range of applications including transgenesis, insertional mutagenesis and gene therapy (Narayanavari et al., 2016).

III.1 *Sleeping Beauty* in gene therapy

The integrating SB transposon system has been widely applied as a non-viral gene delivery vehicle to stably incorporate genes of interest into the genome of variety of cell and tissue types, particularly in therapeutically relevant primary cells such as stem or progenitor cells (Mátés et al., 2009; Katter et al., 2013). In comparison with viral integrating systems and transient DNA expression vectors, the development of the hyperactive SB100X transposase allowed the use of simple DNA-based transgenesis to provide long-term expression of any gene of interest by SB-mediated transgene integration (Ivics et al., 2009; Mátés et al., 2009).

The SB two-component system represents a flexible genetic tool susceptible to optimization at many levels. The SB transposase is available at different transpositional activities and it can be delivered to the target cell or tissue as DNA expression vector, mRNA or recombinant protein (Geurts et al., 2003; Ivics et al., 1997; Mátés et al., 2009). Additionally, the SB transposon vector has been engineered using different strategies, including minicircle technology (Holstein et al., 2018; Monjezi et al., 2017), free of antibiotic resistance marker donor molecules (pFAR) (Marie et al., 2010; Pastor et al., 2018) or a 'sandwich conformation' where duplicated IRs in an inverted orientation are flanking the cargo DNA (Zayed et al., 2004). These strategies have been mainly designed to increase the transposition efficiency for large cargo sequences. Although it is known that transposition efficiency decreases with increasing transposon size, SB does not have an upper limit of cargo sequence in contrary to viral systems. Indeed, SB has been shown to integrate large DNA fragments such as bacterial artificial chromosomes (BACs) in different mammalian systems (Rostovskaya et al., 2012, 2013).

The SB100X transposon system has comparable transgenesis efficiency to viral integration systems while overcoming many of their limitations for clinical applications. SB vectors are based on plasmid DNA, allowing easy and low cost manufacture and manipulation (Hodge et al., 2016). Therefore, this technology relies on efficient transfection or delivery methods to the target cells. Although initially this could represent an important drawback, the SB system has been successfully combined with a wide range of delivery methods both *in vitro* and *in vivo*, including hybrid approaches transposon-virus in which the stable gene integration by SB is combined with the infective capacity of integration defective lentivirus (Benati et al., 2018), adeno-associated virus (AAV) (Boehme et al., 2016; Hausl et al., 2010), herpes simplex virus (Silva et al., 2009) or baculovirus (Luo

et al., 2011). Another considerable advantage for gene therapy approaches is the close-to-random integration profile, which makes SB the safest integration genetic tool when compared to viral vectors or other transposon systems that show biased integration towards transcription start sites or transcriptionally active loci (Narayanavari et al., 2016). Moreover, the activity of the transposase is not constrained to dividing cells and no immunogenicity upon SB transgenesis has been described in preclinical studies involving several animal models (Hausl et al., 2010).

The SB system has been efficiently used for gene transfer in therapeutically relevant human cell types including hematopoietic stem cells, mesenchymal stem cells (MSCs), muscle cells, induced pluripotent stem cells and T cells (Hodge et al., 2016). Similarly, therapeutic long-term transgene expression has been achieved in animal models for a broad range of diseases such as hemophilia, muscular dystrophies or metabolic disorders among others (Escobar et al., 2016; Hausl et al., 2010; Narayanavari et al., 2016). After a decade of basic research and preclinical studies, the SB system was used for the first time in a clinical trial for cancer immunotherapy (Williams, 2008). Allogeneic or autologous T cells were expanded *ex vivo* and engineered with the SB transposon system to express a chimeric antigen receptor (CAR) recognizing tumor-associated antigens, for further transplantion into patients with B-lymphoid malignancies. Once treatment feasibility and safety was tested and sustained detection of genetically modified T cells was achieved, clinical trials moved rapidly forward to test the efficacy of this transposon-based combined gene-cell therapy. Currently, there are eleven ongoing Phase I/II clinical trials for CAR T-cell therapy development involving SB-mediated transgenesis (Kebriaei et al., 2013, 2016).

Based on a similar approach involving *ex vivo* SB-mediated gene integration, the project 'TargetAMD' funded by the European Commission aims to develop a transposon-based therapy for Age-related Macular Degeneration (AMD) and carry out the first Phase I/II clinical trial in Europe using the SB technology (http://www.targetamd.eu).

IV. Human pluripotent stem cells and cardiomyocyte differentiation

IV.1 Human pluripotent stem cells

Human pluripotent stem cells (hPSCs), that include human embryonic stem cells (hESCs) and human induced pluripotent stem cells (hiPSCs), can proliferate indefinitely and have the potential to differentiate into all cell types of the human body. The derivation of hESCs from the human blastocyst and its establishment for *in vitro* culture represented a breakthrough in the field of regenerative medicine and developmental biology. Established hESC lines remain undifferentiated for long periods of culture being passaged continuously, demonstrating self-renewal capacity. Another essential characteristic of hESCs is the conservation of their developmental capacity to generate different tissues

from all three germ layers (i.e. pluripotency) even after prolonged culture times (Thomson et al., 1998). Despite the enormous potential of this technology, hESCs derivation implies the manipulation of human embryos, which causes ethical controversy about their use. Moreover, in the frame of clinical applications, the transplantation of hESC-derived cells or tissues would require immunosuppression treatment, as allotransplants are susceptible to immune rejection by the host (Ratcliffe et al., 2011; Yoshida & Yamanka, 2011).

These drawbacks were overcome almost a decade later by the discovery of four transcription factors (i.e. POU5F1 (OCT3/4), SOX2, KLF4 and MYC) that, upon overexpression, 'reprogrammed' adult human dermal fibroblasts into the so-called 'hiPSCs'. hiPSCs retain the same core properties as hESCs such as self-renewal and pluripotency, and are similar in their morphology, gene expression and epigenetic status of pluripotent cell-specific genes. hiPSCs can be generated from autologous adult somatic cells, thereby avoiding ethical issues concerning derivation of these cells from human embryos and avoiding immunosuppressive therapy in the context of cell transplantation (Takahashi et al., 2007). After the initial approach was reported, many improvements in the reprogramming method have been made, including the substitution (MYCL instead of MYC) or addition (LIN28) of reprogramming factors, the use of non-integrating episomal vectors (Okita et al., 2011), synthetic RNA (Warren et al., 2010), recombinant proteins (D. Kim et al., 2009; H. Zhou et al., 2009), the addition of small molecules to enhance reprogramming efficiency (Yu et al., 2011), or the use of an exclusively chemical method (Hou et al., 2013). Together with the large spectrum of technology platforms successfully applied for reprogramming, hiPSCs have been generated from a broad variety of sources proving highly reproducible results. For all these reasons, the reprogramming method is used worldwide in research and pharmacological laboratories and nowadays constitutes a routine procedure in cell and tissue culture technologies.

hPSCs have become a unique tool to study developmental processes in human and to identify the differences with animal models originally used to investigate lineage commitment and early embryogenesis in mammals. Initial works in this matter have aimed to elucidate the signaling pathways involved in the generation of different human tissues in order to develop efficient differentiation protocols of hPSCs into specific cell types (Keller, 2005). Given the limited source of certain human cell types such as neurons or CMs, hPSCs have been used as unlimited source of non-proliferative cell types for basic or applied studies. The ability of this cells to proliferate indefinitely and grow clonally, have provided the opportunity to use them for genetic engineering and, upon differentiation, create transgenic effector cells otherwise difficult to obtain and manipulate. This feature has been widely used to introduce or correct disease-causing mutations to later generate the adequate cell platform for disease modeling or development of new therapy approaches (Avior et al., 2016; Sterneckert et al., 2014). Another common application has been the generation of reporter hPSC lines to track or select specific cell populations based on the

expression of marker genes. These reporter cell lines have been used to identify progenitor populations, study lineage commitment or enrich particular somatic cell types upon differentiation (Den Hartogh & Passier, 2016; Giudice & Trounson et al., 2008; Sharma et al., 2018). In addition, transgenic hPSC lines overexpressing particular genes in a constitutive or inducible manner have been generated to study the contribution of these genes in self-renewal and pluripotency maintenance, during differentiation processes or in relevant somatic cell types (Darr et al., 2006; Lavon et al., 2006; Li et al., 2017; Takayama et al., 2012).

The first decade of research with hiPSCs has given great results and insights on their potential for developmental studies, drug testing, disease modeling and regenerative therapies development. Differentiation protocols to derive specific cell types are being developed and improved constantly, increasing our understanding of human early embryogenesis and cell fate commitment (Ayabe et al., 2018; Lee et al., 2017; Protze et al., 2017; Trillhaase et al., 2018). A large number of patient-derived hiPSC lines have been established (Dimos et al., 2008; Park et al., 2008; Robbins & Price, 2017) and keep being generated (Lee et al., 2018; Sommer et al., 2018), representing an exceptional tool to understand underlying pathological mechanisms of complex diseases and a valuable cell source to develop new therapies (Giadone et al., 2018; Sharma et al., 2014). In a similar way, hiPSCs derivation into cell types especially susceptible to pharmacological toxicity, such as CMs, neurons or hepatocytes, has provided robust cell and tissue-based platforms for drug toxicity testing, providing relevant data in the human context and reducing the use of experimental animals for this purpose (Deshmukh et al., 2012; J. H. Kim et al., 2017; Magdy et al., 2018; Sharma et al., 2017). Regarding clinical applications, the world's first trial involving these cells was performed in 2014 in a patient with AMD that received an autologous transplantation of hiPSC-derived RPE cells. Although there were no changes in disease symptoms one year after cell transplantation, the graft was retained, as shown by the presence of functional RPE-like cells. Moreover, the patient did not show tumor development or immune rejection in the absence of immunosuppressive therapy. This study confirmed for the first time the safe and feasible application of hiPSC-derived cells for human transplantation (Mandai et al., 2017).

IV.2 Cardiomyocyte differentiation

Since hESCs were established they have been used to understand and control their differentiation towards different tissues and cell types of the organism. In analogy to mouse ESCs (mESCs) differentiation experiments, hESCs were cultured in low-attachment surfaces, allowing them to spontaneously differentiate forming 3D structures called 'embryoid bodies' (EB). Mesoderm-derived lineages seemed easier to differentiate and the presence of CMs within these structures was easily detected by the appearance of spontaneously beating areas (Kehat et al., 2001). Later studies confirmed the same

differentiation outcome using hiPSCs (J. Zhang et al., 2009). Since these initial approaches, many improvements in CM differentiation protocols have been made.

IV.2.1 Developmentally staged cardiomyocyte differentiation

CM differentiation protocols *in vitro* can be established by recapitulating the different phases of embryonic development towards cardiac tissue. The cardiac tissue is derived from the mesoderm and, during early stages of development, its commitment to cardiac mesoderm is regulated by sequential activation or inhibition of three main signaling pathways: bone morphogenetic proteins (BMP) as members of the transforming growth factor ß (TGFß) pathway, Wingless/INT proteins (WNT) and fibroblast growth factors (FGF). Once the cardiac mesoderm is induced, MESP1, which has been described as master regulator of cardiac progenitor specification, is expressed and activates through inhibition of WNT/ß-catenin signaling a set of highly conserved transcription factors, including NKX2-5, TBX5, MEF2C, GATA4 and ISL1 that regulates the heart-specific transcriptional program (Burridge et al., 2012).

In agreement with this data in heart morphogenesis, several protocols based in EB formation have been designed following three sequential stages: i) induction of mesoderm by BMP4 and activin A treatment, ii) induction of cardiac mesoderm by WNT signaling inhibition combined with the expansion of the cardiovascular progenitors by VEGF and iii) expansion of cardiovascular lineages by addition of FGF2. Although initial 'developmentally staged' protocols showed higher CM differentiation efficiency, they required cardiac progenitors selection by fluorescence activated cell sorting (FACS) based on the expression of surface markers, limiting their scalability (Kattman et al., 2011; L. Yang et al., 2008). Continuation of this work in the Keller lab has recently led to the development of protocols to enrich or specifically differentiate the different subtypes of CM. First, they identified NKX2-5^{-} population as SAN-like pacemaker cells and based the protocol optimization on its enrichment. Among multiple conditions, the addition of retinoic acid (RA) together with the inhibition of the TGFß and FGF pathways after mesodermal induction resulted in the enrichment of NKX2-5^{-} population and the generation of up to 30% of SAN-like pacemaker cells (Protze *et al.*, 2017. See also Introduction: section V.2, page 32). In a parallel publication, they identified the different mesodermal precursors for atrial and ventricular CMs, characterized by RALDH2 and CD235a expression respectively, and identified the modulatory role of the RA signaling pathway for the commitment into one or another lineage (Lee et al., 2017).

While these protocols have shown efficient differentiation of hPSCs into different subtypes of CM, they rely on EB formation that is intrinsically variable, involve the monitoring or cell selection by specific gene markers expression and require individual optimization for different hPSC lines. Nevertheless, they have proven their efficiency to analyze accurately both the timing and growth factor concentrations to induce each phase

of cardiac development. These data reveal that the differentiation into CM subtypes rely on the specification of the appropriate mesoderm progenitor at early stages, which is crucial for the development of highly efficient and reproducible directed protocols into atrial, ventricular and nodal CMs.

IV.2.2 Directed cardiomyocyte differentiation

Given the intrinsic variability of differentiation protocols based in EB formation and thanks to the development of new feeder-free culture techniques, hPSC monolayers began to be used to optimize CM differentiation. Early studies already reported the importance of hPSCs culture conditions prior or at the start of the differentiation process for final CM yield (Mohr et al., 2010). Thus, monolayer homogeneity facilitated the optimization of initial culture conditions and the controlled application of small molecules and growth factors. In analogy to initial EB differentiation protocols, the addition of BMP4 and activin A during early differentiation induced mesodermal lineage and ultimately up to 30% of CMs was obtained after differentiation (Lafflame et al., 2007). In parallel, controversial results were reported about the contribution of WNT/ß-catenin activation or inhibition in CM differentiation, until several studies discovered the biphasic role of WNT canonical pathway in cardiac differentiation. They concluded that this effect was stage specific and, while WNT signaling activation was required at early stages of mesodermal induction, it reduced cardiogenesis at later time points. Although addition of WNT3A to BMP4 treatment increased differentiation efficiency, the final CM yield was highly variable among different hPSC lines (Paige et al., 2012; Ueno et al., 2007).

Finally, Lian and collaborators showed that the modulation of the canonical WNT signaling pathway alone was enough to obtain >80% of CMs upon differentiation. They showed that sequential activation of WNT/ß-catenin pathway by using a GSK3 inhibitor followed by WNT inhibition, either by ß-catenin knockdown or the addition of small molecules, produced high CM yield from different hPSC lines without any purification step (Lian et al., 2012, 2013). Soon after that, another study described a similarly efficient, fully chemically defined and free of animal-derived products protocol for CM differentiation also based in WNT signaling modulation and producing up to 95% $TNNT2^{+}$ CMs (Burridge et al., 2014). These protocols produced high efficient, reproducible and easily scalable CM populations that, just like in human heart, were mostly composed by ventricular-like CMs, followed by atrial-like and with a very low yield of nodal-like CMs (0-10%) (Burridge et al., 2014; Karakikes et al., 2014; Lian et al., 2012, 2013).

IV.3 hPSC-derived cardiomyocytes in cardiovascular research

Cardiovascular diseases have been the leading cause of mortality in the world for the last fifteen years. Due to the non-proliferative nature of CMs and the limited regeneration capacity of the heart, there is a need for new sources of CMs to understand disease

progression and develop regenerative therapies in order to replace the damaged cardiac tissue. As in many other fields, animal models have covered for decades the lack of human relevant tissue and cell samples for studying cardiovascular diseases and perform drug testing. However, there are many interspecies differences regarding heart development, structure and physiology (e.g. the basal heart rate in mice is ~600bpm vs. ~70bpm in humans). The discovery and establishment of hPSCs and the development of efficient CM differentiation protocols represent an unlimited source of human CMs and they have become an extraordinary tool to understand early heart development and cardiac diseases in the human context (Oikonomopoulos et al., 2018; Sayed et al., 2016).

Many hiPSC lines have been generated from patients suffering from different cardiac diseases. Surprisingly, most of the patient-specific hiPSC-derived CM (hiPSC-CMs) resemble structural, molecular and electrophysiological features of the studied diseases, and have been extremely useful to understand pathology mechanisms. Recapitulation of disease events by hiPSC-CMs have been possible not only in the case of monogenic diseases, but also in the context of complex syndromes, viral infections and disease-associated cardiomyopathies (Fonoudi & Bosman, 2017; Sayed et al., 2016). In addition, many groups have been working in the generation of hPSC-CMs and engineered human cardiac tissue for transplantation purposes. Most of these strategies have been focused in the replacement of damaged areas of the ventricles or atria, which requires a large number of CMs (10^7-10^9) with robust contractile capacity. Early studies with hESCS-derived CMs (hESC-CMs) (Kehat et al., 2004; Lafflame et al., 2007; Shiba et al., 2012) and hiPSC-CMs (Chauveau et al., 2017; Chong et al., 2014; Ye et al., 2014) already demonstrated their ability to engraft and couple electrically when transplanted into healthy and injured hearts. However, albeit an efficient remuscularization, the heart function was poorly or not improved at all, and transplanted animals developed ventricular arrhythmias. These conflicting results highlight the two major limitations of hPSC-derived CMs (hPSC-CMs) generated by any of the existing protocols: lack of maturation and heterogeneity of the resulting CM population (Oikonomopoulos et al., 2018).

As previously mentioned, hPSC-CMs resemble most metabolic, molecular, electrophysiological and functional features of native CMs. However, these characteristics are closer to those displayed by fetal rather than adult CMs (Keung et al., 2014; Sayed et al., 2016). In general, hPSC-CMs show smaller size and rounder morphology compared with the brick-like shape of working CMs and they have short and disorganized sarcomeres that lead to a reduced contractile force. hPSC-CMs are usually mononucleated and display an even distribution of gap junctions compared with multinucleated mature CMs that show the typical polarized pattern of Cx in intercalated disks. Mitochondria are less abundant and irregularly distributed, in agreement with a predominant glycolytic metabolism in hPSC-CMs vs. abundant and highly developed mitochondria aligned between the sarcomeres linked to the oxidative metabolism typical of adult CMs (Kehat et al., 2001; Keung et al., 2014; Snir et

al., 2003). In addition, they display electrophysiological features analogous to fetal CMs (e.g. presence of I_f and decreased I_{Na} and I_{K1}) that lead them to beat spontaneously (Ma et al., 2011; Sayed et al., 2016). Although many groups have tried to mature hPSC-CMs by prolonged culture, mechanical or electrical stimuli, soluble compounds addition or stiffness variation of the culture substrate, the higher degree of maturation achieved is still insufficient and resembles neonatal CMs properties (Denning et al., 2016).

Regardless of the approach used to differentiate hPSCs into CMs, a heterogeneous population of CMs is generated, comprising CMs with ventricular, atrial and nodal features (Kehat et al., 2001; J. Zhang et al., 2009). The CM subtypes have been traditionally divided by their anatomical localization. However, during in vitro differentiation from hPSCs the developing CMs lack anatomical and spatial information and therefore the generation and identification of specific subtypes is challenging. In addition, this classification also reflects differences in the main physiological role of CMs. Working CMs, composed of atrial and ventricular, are responsible for the contraction of the cardiac muscle; whereas CMs of the CCS are specialized in AP generation and propagation. Thus, specific applications of hPSC-CMs, e.g. myocardial repair after infarction or generation of a biological pacemaker, require the generation of particular CM subtypes (Kane & Terracciano, 2017).

The cardioprotective and cardiac regeneration capacity of multiple cell substrates, including bone marrow derived cells and progenitors, MSCS, skeletal myoblasts and autologous or allogeneic cardiac progenitor cells, have been tested in different clinical trials. Although all the approaches proved to be safe, these treatments achieve only marginal efficacy or show inconsistent outcomes (Fernández-Avilés et al., 2017; Hastings et al., 2015). Despite all the advances achieved during the last years in CM generation from hPSCs, its use in clinical procedures is still limited, and requires further optimization. The maintenance of hPSCs genomic stability after prolonged culture and differentiation, the risk of tumor formation by transplantation of not fully differentiated cells and the immune rejection associated with allotransplants, are still main concerns for the clinical use of hPSC-CMs (Oikonomopoulos et al., 2018; Sayed et al., 2016). Moreover, the appearance of arrhythmia after transplantation due to the electrophysiological heterogeneity of hPSC-CMs represents another major limitation. Thus, an important challenge for cardiac regenerative medicine falls in the development of particular cell substrates or specific protocols for the differentiation of the different subtypes of CMs. In addition, elucidating the signaling pathways underlying atrial, ventricular and nodal CMs specification would contribute to a better understanding of the human cardiac development and, ultimately, to control commitment, proliferation and differentiation of hPSC-CMs (Kane & Terracciano, 2017; Karakikes et al., 2014; Lee et al., 2017; Protze et al., 2017).

V. Biological pacemaker strategies

As mentioned before, pacemaker cells are susceptible to damage as the result of normal aging, associated heart diseases or hereditary conditions. SND can be initially treated with chronotropic drugs, but in most of the cases the implantation of an electronic pacemaker is ultimately required. Although electronic devices have been used for more than five decades and have been continuously improved, up to 6% of patients undergoing pacemaker implantation develops complications that may require removal or replacement of the device. Most complications are caused by the lead that is intrinsically thrombogenic, it is susceptible to corrosion and fracture, promotes fibrosis at the lead-tissue interface and provides surface for bacterial growth leading to infections. During pacemaker implantation, pneumothorax, hemothorax and cardiac perforation can occur and after surgery the most common complication is pocket hematoma with risk of systemic infection (Madhavan et al., 2017; Mulpuru et al., 2017). Further limitations of artificial pacemakers are their limited battery life, sensitivity to electromagnetic fields, the inadequate autonomic response and the adverse cardiac remodeling due to the lead positioning, especially in pediatric patients. These obstacles could be addressed by the development of biological pacemakers that, ideally, would fire APs throughout the entire life of the patient without replacements, adapting the heart rate to physiologic requirements and without immunogenic, tumor formation or arrhythmogenic risks (Rosen et al., 2004).

Among the diverse approaches that have been undertaken to develop a biological pacemaker, three different cell substrates have been mainly used: MSCs, working CMs and PSCs. MSCs can be efficiently differentiated in different mesodermal cell types including chondrocytes, adipocytes and osteoblasts. Although their ability to differentiate into CMs remains controversial (Choi et al., 2010; Takahashi et al., 2015), several studies showed Cx-mediated cell-to-cell functional coupling (Valiunas et al., 2004) or cardiac properties acquisition via cell fusion between MSCs and CMs (Freeman et al., 2015). For these reasons, they have been used as a platform to deliver in situ overexpression of different ion channels to induce biological pacemaker function. In a similar way, some approaches involved direct delivery in the myocardium of overexpression viral vectors with the aim of conferring automaticity and pacing ability to atrial or ventricular CMs. Finally, genetically modified or non-modified PSCs have been subjected to diverse differentiation protocols in order to obtain CMs with SA nodal cells characteristics and the capacity to pace the heart.

V.1 Gene-transfer mediated

The first attempt to achieve cardiac pacing by gene therapy was published by Edelberg and collaborators in 1998. They tested the effect of human ß2 adrenergic receptor (ß2AR) overexpression in heart rate regulation, both *in vitro*, in mouse embryonic CMs, and *in vivo*, by injection of naked DNA in the right atrium of murine hearts (Edelberg

et al., 1998). They demonstrated increased beating rates and chronotropic modulation in modified CMs and further validated this result in a large animal model (Edelberg et al., 2001). Although the effect was short (24h) and the pacing ability upon heart block was not proven, they established the initial proof-of-principle for heart rate regulation by gene therapy. Later studies investigated *in vivo* adenoviral gene transfer of adenylate cyclase 6, a downstream target of ß2AR, in a large animal model. After AVN ablation, ventricular CMs localized at the site of injection were able to generate pacemaker rhythm (Ruhparwar et al., 2010). The main limitation of these approaches was that pacemaker activity was induced only upon catecholamine stimulation and not in basal conditions.

V.1.1 Ion channels

Following studies exploring the generation of biological pacemakers focused on mirroring the ion channel profile of SA nodal cells. Initially, a study investigated the inhibition of I_{K1} that is absent in SA nodal cells but highly expressed in atrial and ventricular CMs. Suppression of Kir2.1 channel by adenoviral gene transfer of a dominant-negative construct induced automaticity in ventricular CMs in guinea pigs (Miake et al., 2002). To date, no further studies have explored this strategy.

The HCN family, long known as pacemaker channels, became an obvious candidate for pacemaker function induction by overexpression. These channels are responsible of I_f, traditionally considered the only current activated at the membrane potential ranges during diastolic depolarization, and are susceptible of autonomic regulation by cAMP. Several *in vitro* studies showed that genetically modified MSCs, neonatal rat ventricular cardiac myocytes (NRVMs) or mESC-CMs carrying *HCN1* (Y. Zhou et al., 2013), *HCN2* (Bruzauskaite et al., 2016; Jin et al., 2010; Qu et al., 2001) or *HCN4* gene overexpression cassettes (Boink et al., 2008; Feng et al., 2016; Saito et al., 2015; X. Yang et al., 2008), expressed functional I_f showing chronotropic response and induced an increase in the rate of spontaneously beating myocytes. These results were then confirmed *in vivo*. HCN-overexpressing MSCs were able to engraft, coupling through gap junctions formation with host CMs, and deliver functional I_f when transplanted into the heart. Pacemaker rhythm generation at the site of injection was confirmed both in intact hearts (Jun et al., 2012; Nong et al., 2013; Plotnikov et al. 2007; Potapova et al., 2004) and upon AV block (Lu et al., 2013). Similarly, mESC-CMs overexpressing HCN4 were able to integrate in the host myocardium and generate sustained ectopic rhythm when transplanted into the heart of rats subjected to AV block (Saito et al., 2018). Although these cell-based strategies achieved partial biological pacemaker function, cell engraftment consisted in disperse heterogeneous clusters of cells, not all the animals generated pacemaker rhythm, pacing was irregular and required the use of backup electronic devices in large animal models and the duration of the studies was restricted to just several weeks.

In parallel, strategies using *in situ* adenoviral vectors delivery demonstrated that overexpression of HCN proteins in the myocardium was enough to induce regular spontaneous activity at the site of injection in animals with induced heart block. However, HCN2-based strategies showed low basal heart rates and limited autonomic responsiveness (Plotnikov et al., 2004; Qu et al., 2003). On the contrary, when researchers used a mutant HCN2, with faster and more positive current activation (Bucchi et al., 2006), a chimeric HCN212, with HCN1 transmembrane region and HCN2 N- and C-termini (Plotnikov et al., 2008), or HCN4 (Cai et al., 2007), tachycardia and unstable pacing rhythm were induced, being necessary the backup use of electronic pacemakers. To overcome these disadvantages, other studies tested the expression in tandem of HCN2 with modulatory proteins (Boink et al., 2012, 2013) that led to physiological heart rates recovery and showed more robust pacemaker activity.

V.1.2 Transcription factors

While ion channels overexpression strategies reported encouraging results, there are many differences between working and pacemaker CMs that might not be achieved by manipulation of a single ion channel. In order to confer complete pacemaker gene expression profile to CMs, several studies investigated the effect of overexpressing transcription factors involved in SAN development in mature CMs or during cardiac differentiation. However, all these approaches have been established in animal models and further relevance and applicability in human pacemaker cells should be addressed.

In mouse models, T-box factor 3 (Tbx3) expression is restricted to the CCS in developing and adult heart (Hoogaars et al., 2004). Moreover, ectopic expression of Tbx3 in atrial CMs resulted in the downregulation of working CM genes (i.e. *Cx40*, *Kir2.1*, *Nav1.5*) and upregulation of pacemaker genes, (i.e. *Hcn4*, *Hcn1*, *Cx30.2*) (Hoogars et al., 2007). To explore the applicability of Tbx3 overexpression for the generation of a biological pacemaker, Bakker and collaborators tested the effect of *Tbx3* gene transfer in NRVMs *in vitro*. These cells displayed reduced intercellular coupling and I_{K1} but did not express I_f (Bakker et al., 2012). A later study investigated the generation of pacemaker cells by differentiation of Tbx3-overexpressing mESCs in combination with myosin heavy chain 6 (Myh6)-promoter-selection. Resulting CMs showed pacemaker-like morphology and expressed Hcn4, Cx45 and Cx30.2 (Rimmbach et al., 2015) but did not show enhanced automaticity. Thus, Tbx3 expression alone conferred certain pacemaker features but was not sufficient to transform working CMs into functional SA nodal cells.

Shox2 expression is restricted to the SAN during early development. It has been shown to repress the expression of Nkx2.5, resulting in the expression of Tbx3, which downstream activates the already mentioned set of pacemaker genes (Espinoza-Lewis et al., 2009). Additionally, the *SHOX2* promoter was used in *in vitro* studies to identify SA nodal-like cells within beating aggregates derived from mESCs (Hashem et al., 2013;

Hashem & Claycomb, 2013). When overexpressed transiently at early stages of EB differentiation using mESCs, it increased automaticity (i.e. number of spontaneously beating EB) and induced upregulation of pacemaker genes (i.e. *Hcn4*, *Cx45*, *Ncx1*). SHOX2-overexpressing EB were then transplanted into rat hearts with induced heart block and, although injected hearts showed higher ectopic rates, the basal beating rate was not restored (Ionta et al., 2015).

In an adenoviral-mediated overexpression screening of embryonic SAN transcription factors in NRVMs, Tbx18 induced increased automaticity, pacemaker cells-like morphology and SAN-specific epigenetic changes. These cells were able to generate ectopic rhythm under SAN arrest after transplantation into guinea pig hearts (Kapoor et al., 2013). The follow-up *in vivo* study tested the effect of *TBX18* adenoviral-transfer by intramyocardial injection in pigs with complete heart block. *TBX18*-transduced animals displayed higher heart rate and required less use of the backup electronic pacemaker. Moreover, the induced pacemaker activity was susceptible to autonomic regulation and chronotropic response to exercise. Since these effects decreased 2 weeks after injection and transduced cells are known to be rapidly eliminated by the immune system, this strategy was proposed as a 'bridge-to-device' biological pacemaker for pacemaker-dependent patients requiring temporal device removal (Hu et al., 2014).

Regardless of the nature of the overexpressed gene, none of these strategies have been further tested in human CMs. Ion channels responsible for the automaticity in SA nodal cells show high degree of homology throughout mammals and the strategies involving their expression could be easier to extrapolate to human context (Biel, 2009; Saito et al., 2018). However, the signaling pathways involved in SAN development, and thus the required transcription factors, have been elucidated mainly in mouse models. Since differentiation and transdifferentiation protocols based in the manipulation of cardiac transcription factors expression have given discrepant outcomes in mouse and hPSCs (Ieda et al., 2010; Kattman et al., 2011; Nam et al., 2013; Takeuchi & Bruneau, 2009), these strategies might be more difficult to apply in human cells.

V.2 Gene-transfer independent

At early stages of differentiation and embryonic development, all CMs display pacemaker activity (i.e. spontaneous beating), a property that disappears upon maturation to working CMs (Christoffels & Moorman, 2009). Since early differentiation protocols were tested *in vitro*, beating cells could be identified within EB undergoing spontaneous differentiation. Based on this observation, early studies used spontaneously contracting areas or complete beating EB to investigate their ability to integrate structurally and functionally with the cardiac tissue. *In vitro*, these cells coupled by gap junctions and were able to electrically drive NRVM monolayers. Further *in vivo* experiments demonstrated the potential of these cells to generate pacemaker activity and to respond to chronotropic

modulation when transplanted into hearts with induced AV block in pigs (Kehat et al., 2004) or guinea pigs (Xue et al., 2005). With the constant improvement of directed differentiation protocols, these strategies were further tested using pure populations of beating CMs derived from hESCs (Shiba et al., 2012) or hiPSCs (Chauveau et al., 2017) with similar results. In general, the response of the different experimental animals was heterogeneous, the basal heart rate, although responsive to autonomic modulation, did not reach physiological values and reproducible robust pacing could not be achieved in any of the studies. These inconsistent results could be partially due to the cell heterogeneity present in hPSC-CMs and motivated other investigators to find specific differentiation protocols to enrich or directly derive SA nodal cells from PSCs.

Using mESCs, the addition of an activator of Ca^{++}-activated K^{+} channels of small and intermediate conductance (SKCas) induced cardiac differentiation during EB formation. Moreover, resulting CMs showed low expression of *Cx43* and *Myl2v* ventricular markers and upregulation of pacemaker marker genes (i.e. *Shox2*, *Tbx3*, *Hcn4*, *Cx30.2* and *Cx45*) compared to CMs derived from untreated EB. These differences were functionally validated by electrophysiology studies that confirmed the enrichment in CMs displaying pacemaker-like APs upon SKCas activation. However, the pacing ability of these cells was not further tested (Kleger et al., 2010).

Two recent studies have developed different protocols to differentiate hPSCs into pacemaker CMs. Protze and collaborators used a reporter hESC line expressing GFP under *NKX2-5* promoter to select NKX2-5^{-} CMs after differentiation by a developmentally staged protocol. These CMs expressed low levels of ventricular markers, high levels of SAN-associated genes and represented 4-10% of the final CM population. Upon modification of the differentiation conditions, the authors were able to obtain up to a 55% of NKX2-5^{-} CM population. Additionally, they validated the generation of SA nodal-like cells from transgene-free hPSCs using this optimized protocol. The pacing ability of these cells was validated both *in vitro*, using ventricular CM monolayers, and *ex vivo*, in rat hearts upon induced AV block. Transplanted cells showed low survival, coupling with the host myocardium through Cx and functional pacing which efficiency ranged from isolated ectopic beats to sustained pacemaker activity (Protze et al., 2017).

Another study developed an empirical protocol where hPSCs were differentiated into beating aggregates by co-culture with the visceral endoderm-like cell line END-2 and subsequent cultured in Fetal Bovine Serum (FBS)-enriched medium. They observed an enrichment of pacemaker genes expression at day 10 of differentiation that increased after 8 weeks. At this time point, cells showed increased expression of transcription factors, ion channels and ß-adrenergic receptors associated with pacemaker cell function. However, levels of cardiac troponin were low at every differentiation stage tested, and comparison to working CMs under parallel differentiation conditions was missing. Nevertheless,

generated cells showed pacemaker-like APs and morphology and were able to initiate and synchronize the beating of NRVM monolayers (Schweizer et al., 2017).

The generation of pacemaker-like cells from non-genetically modified PSCs represents an important step forward for therapeutic applications. However, reproducibility of these protocols, production of a homogeneous pacemaker-CM population and confirmation of their ability to generate robust pacing activity in large animals models are still required. Nonetheless, these differentiation protocols are helping to understand and study the development and function of human SA nodal cells and create a cell platform suitable for disease modeling and gene and cell-therapies improvement.

Aim of the study

The sinoatrial node is the primary pacemaker of the human heart. Sinoatrial nodal cells generate spontaneous action potentials by the combination of a Ca^{++} oscillatory mechanism and voltage- and time-dependent currents, including I_f and I_{NCX}, generated by sarcolemmal ion channels. When sinoatrial nodal cells are damaged due to aging or disease, the only therapy available to date is the implantation of an electronic pacemaker. Electronic devices have been improved for decades but they still exhibit important limitations that could be addressed by the generation of alternative biological cell-based pacemakers. Although different strategies have been used to develop biological pacemakers, most of them have been established using animal models and, to date, only few approaches have been tested in a human context.

Several studies have suggested that cardiomyocytes derived from human pluripotent stem cells possess the subcellular oscillatory Ca^{++} mechanism that provides the basis for automaticity independently of the sarcolemma, leading them to spontaneously beat. Therefore, we hypothesize that the expression of HCN4, and thus I_f current, in these cells would be enough to provide the functional insulation required for pacemaker cells to efficiently generate and propagate action potentials to the surrounding cardiac tissue. The automaticity properties of hiPSC-derived cardiomyocytes coupled with strong I_f expression could be enough to provide robust pacemaker activity to these cells, allowing them to pace the heart when transplanted into the myocardium.

Our ultimate goal is the generation of patient-specific pacemaker-like cells for autologous transplantation. For that purpose, I designed and tested and experimental strategy taking into account possible future clinical applications. I established the working pipeline as follows:

1. Generation of hiPSC by reprogramming of human fibroblasts using non-viral non-integrating episomal vectors.
2. Generation of hiPSC overexpressing human HCN4 (hHCN4-hiPSCs) using non-viral gene delivery by the *Sleeping Beauty* transposon system.
3. Differentiation of hHCN4-hiPSCs into cardiomyocytes.
4. Characterization of the resulting hHCN4-overexpressing cardiomyocytes by monitoring pacemaker cells specific features:
    a. hHCN4 gene transfer validation.
    b. Functional characterization of I_f current.
    c. Beating rate and action potential characterization.
    d. Cell morphology evaluation.
    e. Gene expression profile analysis.

Material and methods

I. Plasmid vectors and cloning

The plasmids pCAGGS-SB100X (map in page 126) and pT2-GFP (map in page 127) were already available in the laboratory. The control plasmid pT2-IRES-GFP (also known as pLICU1, map in page 128) was generated as follows: Internal Ribosome Entry Site (IRES) sequence was amplified by PCR using pT2CVIneo3 plasmid as template (map in page 126) (kindly provided by Dr. Ivana Grabundzija, laboratory of Dr. Zsuzsanna Izsvák) and the forward 5'-ATCTATGCTAGCCAATTCCGCCCCTCTCC-3' (AGP9) and reverse 5´-CGACC GGTGGCAAGCTTATCATCGTGTT-3' (AGP10) primers, adding NheI and AgeI target sequences (underlined) upstream and downstream of the IRES sequence respectively. The PCR product was cloned using CloneJET PCR Cloning Kit (Thermo Scientific™, Thermo Fisher Scientific) generating the plasmid pJET1.2-IRESreverse (map in page 127). IRES sequence was extracted from pJET1.2-IRES by digestion with NheI and AgeI and cloned into pT2-GFP previously digested with NheI and AgeI.

The coding sequence (CDS) of the human gene HCN4 was amplified by PCR from the plasmid pcDNA3.1B-hHCN4-myc-His (kindly provided by Dr. Naohiro Yamaguchi, laboratory of Prof. Martin Morad) using the forward 5'-ATGGACAAGCTGCCGCCGTCC AT-3' (AGP6) and reverse 5'-GGCTCGAGCTAGC**TCA**TAGATTGGATGGCAGTTTGGAGC GCA-3' (AGP7) primers. After amplification, the stop codon (bold) was restored and NheI and XhoI target sequences (underlined) were added downstream the hHCN4 CDS. The PCR product was digested with NheI and cloned into pT2-IRES-GFP previously digested with MluI, treated with Klenow fragment of DNA Polymerase I and later digested with *Nhe* I, generating the final overexpression vector pT2-hHCN4-GFP (also known as pLICU2, map in page 128). After cloning, pT2-hHCN4-GFP plasmid was sequenced and validated the presence of Kozak sequence followed by the complete hHCN4 CDS on frame and with stop codon using the following primers: 5'-CGAACAGGAGAGGGTCAAGTC-3' (AGP1), 5'-TCAGCATGATCGTGGGTGC-3' (AGP2), 5'-GAGATCATCCAGCAGATTGTGC-3' (AGP3), 5'-CAATCCAGGGTGTGGTGTTC-3' (AGP4), 5'-TCCTCCTCGGCGTCCTCTTC-3' (AGP5) and 5'-TTTACTCCCCGAGGAGGTC-3' (AGP11).

II. Cell culture

All the cell cultures were kept and handled in sterile conditions. *Mycoplasma* contamination was regularly checked by PCR analysis of culture supernatants from at least 48h or >80% confluency cell cultures (Young et al., 2010). Only *Mycoplasma*-free cultures were used to perform experiments.

II.1 Coatings

II.1.1 0.1% gelatin

Stock solution of 2% gelatin from porcine skin (Sigma-Aldrich) was prepared in purified water and autoclaved. Working solution of 0.1% gelatin was prepared by dissolving the corresponding amount of 2% gelatin stock solution (previously melted at 37°C) in PBS (PAA). Enough volume of gelatin 0.1% solution to cover the bottom of cell culture-treated plates (e.g. 3ml for a 10cm plate) was poured in the dish, evenly distributed and incubated for at least 20min at 37°C. After incubation, the remaining gelatin solution was aspirated and the corresponding culture media was added avoiding well desiccation.

II.1.2 Matrigel

hESC-qualified Matrigel® (Corning®) was aliquoted, diluted in KnockOut™ DMEM (Dulbecco's Modified Eagle's Medium) (Gibco™, Thermo Fisher Scientific) and stored according to manufacturer's instructions considering lot-specific dilution factor. ~50µl per cm^2 of Matrigel® working solution was poured in the corresponding tissue culture-treated plate format (e.g. 0.5ml per well of a 6-well plate), evenly distributed and incubated at least 1h at room temperature (RT) in a flat surface. When plates were not used immediately, they were kept at 4°C wrapped in Parafilm® M (Bemis Company, Inc) for no longer than a week and pre-warmed at RT for 30min before use. Before plating the cells, the remaining Matrigel® solution was aspirated and the corresponding culture media was added avoiding well desiccation.

II.1.3 Vitronectin

Truncated recombinant human vitronectin (VTN) (Gibco™, Thermo Fisher Scientific) at stock concentration (0.5mg/ml) was aliquoted and stored according to manufacturer's instructions. Aliquots were thawed at RT shortly before use and working solution was always prepared fresh in PBS. For hiPSCs culture, working solution was prepared at a final concentration of 5µg/ml and 100µl per cm^2 were used, resulting in a final coating concentration of 0.5µg/cm^2. For CM differentiation and culture, working solution was prepared at a final concentration of 7.5µg/ml and 100µl per cm^2 were used, resulting in a final coating concentration of 0.75µg/cm^2. Plates were incubated for at least 1h30min and no longer than 3h at RT. When plates were not used immediately, they were kept at 4°C wrapped in Parafilm® M (Bemis Company, Inc) for no longer than a week and pre-warmed at RT for 30min before use. Before plating the cells, the remaining VTN solution was aspirated and the corresponding culture media was added avoiding well desiccation.

II.2 HEK293T culture and transfection

HEK293T were maintained in a humidified incubator at 37°C and 5%CO_2 in DMEM with 4.5g/l glucose and GlutaMAX™ (Gibco™, Thermo Fisher Scientific) supplemented with 10% FBS, (PAA), 1xAA (Gibco™, Thermo Fisher Scientific) and 100µg/ml G418 (Gibco™, Thermo Fisher Scientific). Medium change was performed every 2-3 days and cells were split with 0.05% trypsin-EDTA (Gibco™, Thermo Fisher Scientific) 2-3 times per week before reaching 90% confluency at 1:5-1:10 ratio.

The day before transfection, HEK293T cells were detached with 0.05% trypsin-EDTA (Gibco™, Thermo Fisher Scientific), plated at density of 100,000 cells per cm^2 in 12-well plates (~350,000 per well) and placed in the incubator for 24h. The day of transfection cells were typically at 80-90% of confluency and media change was performed at least 30min prior transfection. Cells were transfected with different transposons in equimolar amounts using the transfection reagent jetPRIME® (Polyplus-transfection®) according to manufacturer's instructions. In the final experiment, one well of a 12-well plate of HEK293T cells was transfected with 150ng of pT2-GFP (5.6kb), 166ng of pT2-IRES-GFP (6.2kb) or 262ng of pT2-hHCN4-GFP (9.8kb) with or without transposase expression plasmid. For *Sleeping Beauty* mediated transgenesis, cells were also cotransfected with 15ng of pCAGGS-SB100X (ratio 1:10 transposase:transposon). Gene expression was monitored by GFP expression 24h after transfection under the fluorescence microscope and 48h after transfection by FACS, calculating transfection efficiency.

For cryopreservation, subconfluent cultures were detached with 0.05% trypsin-EDTA (Gibco™, Thermo Fisher Scientific), washed with PBS (PAA) and prepare as cell suspension at 0.5-1·10^6 cells/ml in freezing medium consisting of 90% culture medium and 10% DMSO (Sigma-Aldrich). 1ml aliquots were prepared in cryogenic tubes, placed at -80°C for 24h and later transferred to a liquid nitrogen tank for long-term storage.

II.3 Mouse embryonic fibroblasts culture

Mouse embryonic fibroblasts (MEFs) isolated from CF-1 mouse strain were kindly provided by Dr. Alessandro Prigione. CF-1 MEFs were maintained in a humidified incubator at 37°C and 5% CO_2 in MEFs medium, consisting of DMEM with 4.5g/l glucose and GlutaMAX™ (Gibco™, Thermo Fisher Scientific) supplemented with 15% Fetal Bovine Serum (FBS, PAA), 1xAA (Gibco™, Thermo Fisher Scientific) and 0.75g of $NaHCO_3$ (Sigma-Aldrich). Passage 1 MEFs were expanded for 3 passages splitting them at 1:3 ratio with 0.05% trypsin-EDTA (Gibco™, Thermo Fisher Scientific) until the day of inactivation.

Inactivated MEFs were plated 24h before using them as feeder cells in 0.1% gelatin-coated dishes with MEFs medium at seeding densities of ~20,000/cm^2 for reprogramming and ~25,000/cm^2 for hiPSC maintenance, and kept in a humidified incubator at 37°C and 5% CO_2.

II.4 MEFs inactivation

Mycoplasma-free passage 4 highly proliferative cultures of MEFs were inactivated for using them as feeder cells for hiPSC maintenance and reprogramming experiments. Before being used as feeder cells, inactivated MEFs were cultured for a week in standard conditions and monitored daily to confirm that they do not proliferate.

II.4.1 Inactivation by irradiation

The day of inactivation, cells were prepared in cell suspension using 0.05% trypsin-EDTA (Gibco™, Thermo Fisher Scientific), washed, placed in a 10cm dish and exposed to 40Gy of gamma irradiation using a Cs-137 irradiator model OB 29 (STS). After irradiation, cells were washed, counted and resuspended in 90% FBS (PAA) and 10% DMSO (Sigma-Aldrich) at concentration of $1 \cdot 10^6$cells/ml. 1ml aliquots were prepared in cryogenic tubes, placed in a Mr. Frosty™ (Thermo Scientific™, Thermo Fisher Scientific) freezing container for 24h at -80°C and transferred to liquid nitrogen for long-term storage.

II.4.2 Inactivation by mitomycin C

The day of inactivation, cells were cultured with MEFs medium supplemented with 10µg/ml mitomycin C (Sigma-Aldrich) for 2-3h in a humidified incubator at 37°C and 5% CO_2. After incubation with mitomycin C, cells were washed three times with PBS (PAA), prepared in cell suspension using 0.05% trypsin-EDTA (Gibco™, Thermo Fisher Scientific). MEFs were counted, washed and resuspended in 90% FBS (PAA) and 10% DMSO (Sigma-Aldrich) at concentration of $1 \cdot 10^6$cells/ml. 1ml aliquots were prepared in cryogenic tubes, placed in a Mr. Frosty™ (Thermo Scientific™, Thermo Fisher Scientific) freezing container for 24h at -80°C and later transfer to liquid nitrogen for long-term storage.

II.5 Human foreskin fibroblasts culture

The human foreskin fibroblast cell line HFF-1 (ATCC® SCRC-1041™) was maintained in a humidified incubator at 37°C and 5% CO_2 in HFF medium, consisting of DMEM with 4.5g/l glucose and GlutaMAX™ (Gibco™, Thermo Fisher Scientific) supplemented with 15% Fetal Bovine Serum (FBS, PAA) and 1xNEAA (non-essential aminoacids, Gibco™, Thermo Fisher Scientific). Cells were split with 0.05% trypsin-EDTA (Gibco™, Thermo Fisher Scientific) every 3-4 days at confluency <90% in order to maintain them actively proliferating, in exponential phase of growing. Typically, 1:4-1:5 splitting ration and seeding density ~10,000 cells/cm^2 were used.

II.6 Reprogramming of HFF into hiPSCs

Low passage and actively proliferating HFF-1 (ATCC® SCRC-1041™) cultures were used for reprogramming experiments. HFF were detached using 0.05% trypsin-EDTA

(Gibco™, Thermo Fisher Scientific), prepared in single cell suspension and transfected with Neon™ Transfection System (Invitrogen™, Thermo Fisher Scientific) in sterility, using a 100µl tip and 1700V 10ms 3pulses as electroporation conditions. $1 \cdot 10^6$ cells were transfected with 2.5µg of each plasmid for the reprogramming factors expression: pCXLE-hOCT3/4-shp53-F (Addgene plasmid # 27077), pCXLE-hSK (Addgene plasmid # 27078), pCXLE-hUL (Addgene plasmid # 27080) gift from Prof. Shinya Yamanaka (Okita *et al.*, 2011). After transfection, cells were plated on a 10cm plate previously coated with 0.1% gelatin and containing pre-warmed HFF medium supplemented with 10µM ROCK inhibitor (Y-27632) (Calbiochem). Cells were cultured for a week in HFF medium performing medium change every second day and kept in a humidified incubator at 37°C, 5% CO_2 and 5% O_2 until the end of the reprogramming experiment.

Seven days after transfection, $1.2 \cdot 10^6$ of inactivated MEFs were plated in a 10cm plate previously coated with 0.1% gelatin (~20,000/cm^2 seeding density) and kept in a humidified incubator at 37°C, 5% CO_2 for 24h. Next day (i.e. eight days after transfection), transfected fibroblasts were split with 0.05% trypsin-EDTA (Gibco™, Thermo Fisher Scientific) and $0.1 \cdot 10^6$ cells were transferred onto previously prepared feeder cells with HFF medium supplemented with 10µM ROCK inhibitor (Y-27632) (Calbiochem). From next day on, culture medium was changed daily and cells were maintained until the end of the reprogramming experiment in embryonic stem cells (ESCs) medium consisting of DMEM/F12 (1:1) with GlutaMAX™ (Gibco™, Thermo Fisher Scientific) supplemented with 20% KnockOut™ Serum Replacement (KOSR) (Gibco™, Thermo Fisher Scientific), 1xNEAA (Gibco™, Thermo Fisher Scientific), 100µM ß-mercaptoethanol (Gibco™, Thermo Fisher Scientific), 10ng/ml bFGF (Preprotech), 50µg/ml Vitamin C (Sigma-Aldrich) and 500µM sodium butyrate (Sigma-Aldrich). During the first week after reseeding the transfected cells, ESCs medium was additionally supplemented with four small molecules to enhance reprogramming efficiency: 1µM CHIR99021 (Axon MedChem), 5µM PD0325901 (Sigma-Aldrich), 2µM SB431542 (Calbiochem) and 0.5µM Thiazovivin (Calbiochem).

21 to 30 days after transfection, fully reprogrammed colonies displaying ES-like morphology could be easily identified. Colonies were manually picked under a scope cut from the surrounding tissue with a Sterican® needle (27Gx3/4) (B. Braun) and transferred with a 200µl tip to a well of a 24-well plate previously coated with Matrigel® (Corning®) containing 1ml of mTeSR™-1 medium (STEMCELL™ Technologies) supplemented with 10µM ROCK inhibitor (Y-27632) (Calbiochem). mTeSR™-1 medium (STEMCELL™ Technologies) was changed daily. After 5-7 days, established colonies were expanded splitting them with EDTA 0.5mM (1:1000 dilution in PBS of EDTA 0.5M, pH8.0, Invitrogen™, Thermo Fisher Scientific) or Versene solution (Gibco™, Thermo Fisher Scientific) at 1:2-1:4 ratio depending on the size of the colony. Once cell number was enough to be cultured in wells of a 6-well plate (typically at passage 2 or 3), hiPSCs were

maintained in this plate format and subsequently adapted to VTN-coated plates and Essential 8™ Medium (Gibco™, Thermo Fisher Scientific) culture (See following section).

II.7 hiPSCs culture and transfection

hiPSCs were kept routinely in a humidified incubator at 37°C, 5%CO_2 and 5%O_2. hiPSCs cultures for maintenance and cryopreservation were split exclusively using EDTA (section II.7.4) and kept in uninterrupted culture for no longer than 2 months. hiPSCs splitting ratio was adjusted every time depending on proliferation rate, colony number and size, varying from 1:3 to 1:12. Typical splitting ratios for hiPSCs maintenance in each culture condition are mentioned below and are approximately equivalent to seeding 20,000-30,000 cells per cm^2. All material, reagents, media and solutions used for hiPSCs culture were always equilibrated at RT prior its use when no other working temperature is specified. Typical volumes used for hiPSCs culture are summarized in Table 2 at the end of this section, page 45.

For cryopreservation, subconfluent cultures (less than 85% confluency) in exponential phase of growth were split with EDTA (section II.7.4) and colonies were disrupted mechanically (by gentle pipetting with a 5ml pipette) to obtain the optimal clump size for freezing (~50µm). Clumps were washed and resuspended in cold (4°C) 0.8ml Bambamker™ freezing medium (Lymphotec, Inc) per cryogenic tube. Typically, 3 wells of a 6-well plate of hiPSCs cultures 3-4 days after splitting were frozen in 5 cryogenic tubes. Cryogenic tubes were immediately placed in a precooled (4°C) Mr. Frosty™ (Thermo Scientific™, Thermo Fisher Scientific) freezing container, kept for 24h at -80°C and later transfer to liquid nitrogen for long-term storage. Frozen hiPSCs were thawed in the same culture conditions they were cultured before freezing, with the medium supplemented with ROCK inhibitor: 10µM Y-27632 (Calbiochem) or 2µM Thiazovivin (Calbiochem). Typically, thawed hiPSCs were changed to normal culture medium without ROCK inhibitor immediately after cell attachment and first passage after thawing was always performed with EDTA (section II.7.4).

II.7.1 hiPSCs culture on feeder cells with ESCs medium

hiPSCs cultured on feeder cells (section II.3) were kept in ESCs medium changed daily. When colonies size was higher than 700µm (before differentiation starts to appear in the center of the colony) or maximum one week after the last passage, hiPSCs were split with collagenase IV (section II.7.3). Typically, hiPSCs cultured on feeder cells were split at 1:4-1:6 splitting ratio every 4-5 days. When hiPSCs cultured on feeder cells were changed to feeder-free culturing conditions (always during splitting), hiPSCs were split with EDTA and cultured on matrigel or VTN-coated plates directly with mTeSR™-1 medium, without any intermediate adaptation step.

II.7.2 Feeder-free hiPSCs culture

Under feeder-free conditions, hiPSCs were cultured directly on matrigel or VTN-coated plates (section II.1) and medium change was performed daily.

Routine culture of hiPSCs was carried on VTN-coated plates with E8 medium (Essential 8™ Medium (Gibco™, Thermo Fisher Scientific)) and cell passage was performed with EDTA (section II.7.4) at 1:6-1:12 splitting ratio twice a week (every 3-4 days), when confluency was ~85% or colony size exceeded 700μm. When mentioned, mTeSR™-1 medium (STEMCELL™ Technologies) was also used in a similar manner. When changing from one medium to another, hiPSCs cultures were always kept for 24h in 1:1 mTeSR™-1:E8 medium for adaptation to the new medium, never concurring with cell passage.

II.7.3 hiPSCs passage with collagenase IV

Collagenase IV working solution was prepared by reconstituting the necessary amount of lyophilized Collagenase Type IV (Gibco™, Thermo Fisher Scientific) in KnockOut™ DMEM (Gibco™, Thermo Fisher Scientific) to obtain a final 200U/ml working concentration. Working solution was sterilized by filtration and stored according to manufacturer's instructions. For splitting, ESCs spent medium was aspirated from hiPSCs cultured on feeder cells and cells were washed with PBS (PAA). Corresponding volume of collagenase IV working solution (Table 2) was poured in the culture dish and cells were incubated for 5-10min at 37°C until the edges of the hiPSC colonies started to detach from the feeder cells monolayer. Collagenase IV solution was then aspirated, new ESCs medium was added and hiPSC colonies were detached by gentle pipetting with a 5ml pipette and washed by centrifuging at 200*g* for 3min. Supernatant was discarded, was hiPSC colonies were resuspended in new ESCs medium by gentle pipetting with a 5ml pipette until an optimal average clump size ~50μm was obtained. hiPSC clumps solution was distributed evenly in plates previously prepared with feeder cells or appropriate coating and placed in the incubator undisturbed until colony clumps were attached.

II.7.4 hiPSCs passage with EDTA

For hiPSCs passage, a working solution of 0.5mM EDTA was prepared by diluting 1:1000 EDTA 0.5M pH8 solution suitable for cell culture (Ambion™, Invitrogen™, Thermo Fisher Scientific) in PBS (PAA) and kept at 4°C for no longer than one month. For splitting, spent medium was aspirated from hiPSCs cultures and cells were washed with DMEM/F12 (1:1) with GlutaMAX™ (Gibco™, Thermo Fisher Scientific). An equivalent volume of EDTA (Table 2) was added to the culture dish and cells were incubated 4-8min at 37°C until the edges of hiPSC colonies started to detach. EDTA solution was aspirated and an equivalent volume of DMEM/F12 was added. The plate was gently rocked on the sides for 30-60 seconds until colonies detached from the coating, colonies were collected in a tube and washed by centrifugation at 200*g* for 5min. After centrifugation, supernatant was aspirated

and colonies were resuspended in culture medium and mechanically disrupted by gentle pipetting with a 5ml pipette until obtaining the optimal clump size of ~50µm. hiPSCs clumps solution was distributed evenly in coated plates previously prepared and placed in the incubator undisturbed until colony clumps were attached.

II.7.5 hiPSCs passage with Accutase

For single-cell hiPSCs preparation and passage, StemPro™ Accutase™ Cell Dissociation Reagent (Accutase) (Gibco™, Thermo Fisher Scientific) was used. Spent medium was aspirated from hiPSCs cultures and cells were washed with DMEM/F12 (1:1) with GlutaMAX™ (Gibco™, Thermo Fisher Scientific). Corresponding volume of Accutase (Table 2) was added to the culture dish and cells were incubated 4-8min at 37°C until colonies were completely detached in small clumps. Directly after incubation, DMEM/F12 medium volume equivalent to culture volume was added to dilute Accutase and clumps were mechanically disrupted by pipetting gently with a micropipette with a 1ml tip 5-10 times until single cell suspension was obtained. Cells were then collected in a tube and washed by centrifugation at 300*g* for 5min. After centrifugation, supernatant was aspirated and cells were resuspended in culture medium supplemented with ROCK inhibitor: 10µM Y-27632 (Calbiochem) or 2µM Thiazovivin (Calbiochem). hiPSCs single-cell solution was distributed in coated plates previously prepared, distributed evenly and placed in the incubator undisturbed until cells were attached. Typically, hiPSCs split with Accutase were changed to normal culture medium without ROCK inhibitor immediately after cell attachment.

II.7.6 hiPSCs transfection

hiPSCs were transfected with Neon™ Transfection System (Invitrogen™, Thermo Fisher Scientific) in sterile conditions. Subconfluent hiPSCs cultures at ~80% confluency in exponential phase of growth were used for transfection. hiPSCs cultures were prepared in single-cell suspension with Accutase as described before (section II.7.5) and washed by centrifugation in DMEM/F12 (1:1) with GlutaMAX™ (Gibco™, Thermo Fisher Scientific). To minimize single-cell hiPSCs manipulation time, no cell counting was performed. Instead, one well of a 6-well plate (~1.2-1.5·10^6 cells) was used for each transfection condition and seeded after transfection in a well of a 6-well plate. After centrifugation, cells were resuspended in 120µl of R buffer containing the corresponding plasmid DNA mixed for each transfection condition. hiPSCs were then transfected using the 100µl tip and 1050V 30ms 2pulses as electroporation protocol. After transfection, hiPSCs were immediately seeded in VTN-coated plates with E8 medium supplemented with ROCK inhibitor: 10µM Y-27632 (Calbiochem) or 2µM Thiazovivin (Calbiochem) previously prepared and kept at 37°C. Transfected hiPSCs were evenly distributed and placed in the incubator undisturbed until cells were attached. Typically, E8 medium without ROCK inhibitor was changed immediately after cell attachment.

For SB-mediated transgenesis, 5-7µg of pT2-hHCN4-GFP (section I) overexpressing plasmid were transfected. The control plasmids were transfected at equimolar amount depending on their size. SB100X expression plasmid was transfected at 1:10 transposase:transposon mass ratio. 5-7 µg of the plasmid pcDNA3.1B were used as control for viability during the transfection procedure and GFP expression negative control for FACS experiments and gating.

Plate format	Surface area (cm2)	Volume of culture medium		Volume of EDTA 0.5mM	Volume of DMEM/F12 or PBS (washing)	Volume of Accutase or Collagenase IV
		Regular	Confluent			
1xw6wp	9.6	2ml	4ml	1ml	1-2ml	0.5ml
1xw12wp	3.5	1ml	2ml	0.5ml	0.5-1ml	0.3ml
1xw24wp	1.9	0.5ml	1ml	0.25ml	0.5ml	0.2
60mm	20	3ml	5ml	2ml	1.5-3ml	1ml
100mm	60	10ml	15ml	6ml	5-10ml	2ml

Table 2. Volumes used for hiPSCs culture adjusted by culture dish area. w: well, wp: well plate.

II.8 Cardiomyocytes culture

II.8.1 CM differentiation and maintenance

Highly proliferative and synchronized hiPSCs cultures growing on VTN-coated plates and E8 medium in a humidified incubator at 37°C, 5%CO_2 and 5%O_2 were used for CM differentiation. For that purpose, hiPSCs cultures showing 80% confluency were split with Accutase (section II.7.5) every 4 days and plated at 25,000 cells per cm^2 seeding density 3-5 times before starting the differentiation protocol.

At day -3 of differentiation, hiPSCs were prepared in single-cell suspension with Accutase, washed by centrifugation with DMEM/F12 (1:1) with GlutaMAX™ (Gibco™, Thermo Fisher Scientific) and resuspended in E8 supplemented with 2µM Thiazovivin (Calbiochem) for counting. Typically, 250,000 cells per well of a 6-well plate were seeded in VTN-coated plates at 0.75µg/cm^2 (section II.1). hiPSCs were evenly distributed and placed in the incubator undisturbed until cells were attached. E8 medium without Thiazovivin was changed immediately after cell attachment and daily until day 0 of differentiation.

At day 0 of differentiation, spent medium was aspirated and replaced by CM differentiation medium consisting of RPMI Medium 1640 supplemented with GlutaMAX™ (Gibco™, Thermo Fisher Scientific) and 1xB-27™ Supplement minus insulin (Gibco™, Thermo Fisher Scientific) supplemented with 6µM CHIR99021 (Axon MedChem. Cells were transferred to a humidified incubator at 37°C, 5%CO_2 and maintained in normoxia conditions during and after the differentiation protocol. 24h later, medium was changed to

CM differentiation medium and kept for 48h. At day 3 of differentiation, spent medium was aspirated and CM differentiation medium supplemented with 5μM IWR-1-endo (Cayman Chemical) was added and kept for 48h. From day 5 of differentiation, cells were kept in CM differentiation medium and medium change was performed every second day. Media change during the first days of differentiation was performed always at the same time of the day for better differentiation efficiency. When robust beating appeared in the culture, usually around day 9 of differentiation, medium was changed to CM medium consisting of RPMI Medium 1640 supplemented with GlutaMAX™ (Gibco™, Thermo Fisher Scientific) and 1xB-27™ Supplement (Gibco™, Thermo Fisher Scientific). Differentiated CMs were maintained up to 2 months in CM medium and medium change was performed every 2-3 days. Normally, CMs cultures showing ~75-80% TNNT2-expressing cells were obtained upon CM differentiation. CMs at day 9 and 20 of differentiation were typically used for characterization experiments.

II.8.2 CMs dissociation and single-cell suspension preparation

CMs cultures were dissociated and prepared in cell suspension for subsequent characterization analysis (e.g. FACS analysis, electrophysiology…). Spent CM medium was aspirated, CMs were washed twice with PBS with Ca^{++} and Mg^{++} (Gibco™, Thermo Fisher Scientific) and incubated for 5min at 37°C with EDTA 0.5mM. After incubation, EDTA was aspirated and CMs were incubated 10-15min at 37°C with TrypLE™ Express Enzyme (1X) (Gibco™, Thermo Fisher Scientific). CM medium was added and cells were mechanically disrupted by pipetting gently with a micropipette with a 1ml tip no more than 10 times. CMs were filtered using a 40μm cell strainer (BD Bioscience) to eliminate cell clumps and washed with CM medium:EDTA 0.5mM (1:1) by centrifugation. After centrifugation CMs were resuspended by gentle pipetting with a micropipette with a 1ml tip to assure single-cell suspension in CM medium supplemented with 2μM Thiazovivin (Calbiochem) for subsequent culture or the corresponding buffer according to downstream experiments.

II.8.3 CM metabolic selection

Based on the ability of CMs to obtain energy from multiple substrates, including glucose, fatty acids and lactate, there have been several protocols developed to enrich CMs from differentiation cultures by simple medium exchange (Tohyama *et al.*, 2013). For live cell experiments where CM identity of individual cells could not be confirmed beforehand, cells were grown in glucose-depleted conditions to assure that only CMs were analyzed. CMs at day 9 of differentiation were prepared in single-cell suspension (section II.8.2) and plated at 15,000 cells per cm^2 seeding density in VTN-coated plates with CM medium supplemented with 2μM Thiazovivin (Calbiochem). 48h after seeding, medium was changed to CM selection medium consisting of RPMI 1640 Medium, no glucose (Gibco™, Thermo Fisher Scientific) and 1xB-27™ Supplement (Gibco™, Thermo Fisher Scientific) for 48h. In the final protocol, CM medium and CM selection medium were alternated to allow

CM selection and avoid CM exhaustion using the following culturing sequence: seeding, 48h CM medium, 48h CM selection medium, 48h CM medium, 96h CM selection medium, 48h CM medium, 48h CM selection medium, indefinitely CM medium.

III. Pluripotency teratoma assay

The teratoma assay was performed by EPO GmbH - Experimental Pharmacology & Oncology, Berlin, Germany. Briefly, in order to initiate the assay $1 \cdot 10^6$ cells were suspended in 50µl of PBS and thereafter mixed with 50µl of Matrigel® (Corning®). This cell suspension was then transplanted subcutaneously and under the kidney capsule into a NOG-mouse where tumor growth was documented on a weekly basis. After reaching the size of $1.5cm^3$ or 90 days after cell transplantation, the tumor was extracted and pathologically analyzed.

IV. Flow cytometry and cell sorting

Typically 10-20,000 events were acquired per sample for FACS analysis. All FACS data were analyzed using the software FlowJo® 10.3 for Mac, FlowJo, LLC. Figures displaying FACS data were further formatted using Adobe® Illustrator® CS5 Version 15.0.0 for Mac (Adobe Systems).

IV.1 Routine GFP detection by FACS

For routine GFP detection in transfected and transgenic cell lines, cells were prepared in single-cell suspension, resuspended in PBS and immediately analyzed using a FACSCalibur™ flow cytometer (BD Biosciences). Appropriate negative controls not expressing GFP and positive controls where GFP expression was confirmed by microscopy were used in every acquisition to determine the correct instrument settings and establish the gating conditions for further analysis. When GFP expression and intensity were analyzed the same day in different populations or monitored over time, the same instrument settings were kept for all the different samples and days of acquisition.

IV.2 Immunostaining and FACS analysis of cardiomyocytes

CMs were prepared in single-cell suspension (section II.8.2) and resuspended in PBS (PAA). Appropiate volume of 2% paraformaldehyde (PFA) solution was added and cells were fixed for 15min at RT with PFA at a final concentration of 1%. CMs were washed twice with PBS and aliquoted in round bottom tubes for FACS for different staining conditions, usually 250,000 cells were used for each immunostaining. After washing, cells were resuspended in 100µl of permeabilization buffer consisting of PBS with 0.25% Triton X-100

(Sigma-Aldrich) and 1% Bovine Serum Albumin (BSA, Sigma-Aldrich) containing the primary antibodies. CMs were incubated overnight at 4°C with monoclonal antibodies against TNNT2 (mouse, 1:200, Santa Cruz Biotechnology) and Nkx2.5 (rabbit, 1:1000, Cell Signaling Technology). Next day, CMs were washed three times with washing solution consisting of PBS with 0.1% Triton X-100 and incubated 1h at 4°C or 30min at RT in darkness in 100µl of permeabilization buffer containing the secondary antibodies at 1:1000 dilution: Donkey anti-Mouse IgG (H+L) Highly Cross-Adsorbed Secondary Antibody, Alexa Fluor 647 (Thermo Fisher Scientific) and Goat anti-Rabbit IgG (H+L) Cross-Adsorbed Secondary Antibody, Alexa Fluor 546 (Thermo Fisher Scientific). After incubation, cells were washed three times with washing solution, resuspended in PBS and immediately analyzed using an LSRFortessa™ flow cytometer (BD Biosciences). Cells incubated only with secondary antibodies were used as negative controls. Detailed information about used antibodies is listed in Appendix, section II. Antibodies summary table.

IV.3 Sorting of stably transgene overexpressing cell lines

Transfected cells showing stable gene expression were sorted based on their GFP expression in non-sterile conditions using a FACSAria™ cell sorter (BD Biosciences). Presorting cell preparation was performed in sterile conditions and maintained in buffer/medium supplemented with Primocin™ (InvivoGen) during the sorting procedure. Sorted cells were kept in quarantine with Primocin™ (InvivoGen) treatment for one week before changing to standard culture conditions. After that time, cell culture supernatants were analyzed and confirmed negative for *Mycoplasma* contamination prior cell storage and characterization experiments.

During sorting, cells were gated by size using Forward Scatter (FSC) and Side Scatter (SSC) width and area parameters to exclude doublets from the sorted population. Non-transfected and GFP-expressing control cell populations were used to establish the proper instrument settings and set up the gating conditions for GFP-positive cells sorting.

IV.3.1 Sorting of transgenic HEK293T

HEK293T cells were prepared in cell suspension using 0.05% trypsin-EDTA (Gibco™, Thermo Fisher Scientific) and filtered using a sterile round-bottom FACS tube with 35µm cell strainer cap. Strainer cap was exchanged to a normal cap, cells were washed by centrifugation and resuspended at ~$2 \cdot 10^6$ cells per ml in sorting buffer consisting of PBS (PAA) with 0.05mM EDTA (Invitrogen™, Thermo Fisher Scientific), 1% BSA (Sigma-Aldrich) and 100µg/ml Primocin™ (InvivoGen).

Sorting was performed as mentioned above and sorted cells were collected in a tube containing culture medium supplemented with 100µg/ml Primocin™ (InvivoGen). After sorting, cells were washed by centrifugation and plated at standard seeding density in culture medium supplemented with 100µg/ml Primocin™ (InvivoGen).

IV.3.2 Sorting of transgenic hiPSCs

hiPSCs were prepared in cell suspension with Accutase (Gibco™, Thermo Fisher Scientific) (section II.7.5) and filtered using a sterile round-bottom FACS tube with 35µm cell strainer cap. Strainer cap was exchanged to a normal cap, cells were washed by centrifugation and resuspended at ~$2{\cdot}10^6$ cells per ml in a solution consisting of 1:1 E8 medium:sorting buffer supplemented with ROCK inhibitor: 10µM Y-27632 (Calbiochem) or 2µM Thiazovivin (Calbiochem).

Sorting was performed as mentioned above and sorted cells were collected in a tube containing E8 medium supplemented with 50µg/ml Primocin™ (InvivoGen) and ROCK inhibitor: 10µM Y-27632 (Calbiochem) or 2µM Thiazovivin (Calbiochem). After sorting, cells were washed by centrifugation and plated at standard seeding density in VTN-coated plates with E8 medium supplemented with 50µg/ml Primocin™ (InvivoGen) and ROCK inhibitor: 10µM Y-27632 (Calbiochem) or 2µM Thiazovivin (Calbiochem).

V. Immunofluorescence

V.1 Immunostaining protocol

Cells were plated in VTN-coated borosilicate glass coverslips of 18mm diameter and 0.13-0.16mm thickness (Carl Roth GmbH) previously placed in 12-well plates and sterilized by exposition to UV light for at least 20min. When not indicated otherwise, washing steps were performed with the coverslip on a well of a 12-well plate with 1ml PBS during 5min in a shaker at 100rpm. Once the secondary antibody was added, incubation wet chamber and washing plate were kept in darkness by wrapping them in aluminum foil.

The first day of immunostaining, cells were washed 3 times and fixed with 4% PFA (Sigma-Aldrich) in PBS for 15min at 37°C. After fixation, cells were washed 3 times and permeabilized with 0.5% Triton X-100 (Sigma-Aldrich) in PBS during 10min at RT. After permeabilization, cells were washed twice and blocked using PBS with 3% donkey serum and 5% BSA during 1h at RT. After blocking, cells were washed once, coverslips were transferred to a incubation wet chamber and incubated with primary antibodies (Table 3 and 4) in PBS with 1%BSA overnight at 4°C. The next day, primary antibody solution was removed by absorption with a paper without touching the sample and cells were washed 3 times before the coverslips were transferred to a wet chamber and incubated with secondary antibodies (Table 3 and 4) in PBS with 1%BSA 2hs at RT. Secondary antibody solution was removed by absorption with a paper without touching the sample, and cells were incubated with 1:5000 Hoechst 33258 in PBS during 5min at RT for DNA staining. Cells were washed 3 times followed by another washing step with purified water. Finally, coverslips were mounted on glass slides using Aqua Poly/Mount (Polysciences, Inc) mounting solution. The slides were allowed to dry on a flat surface for 24h in darkness and

dry atmosphere prior their examination under the microscope. Detailed information about used antibodies is listed in Appendix, section II. Antibodies summary table.

V.2 Detection of HCN4 and pluripotency markers in hiPSCs

Subconfluent cultures of hiPSCs were split with EDTA (section II.7.4) and plated on VTN-coated coverslips, prepared as mentioned before, at normal seeding density. Cells were maintained in standard culture conditions (II.7.2) for 3-4 days until the immunostaining was performed, when hiPSC colonies displayed typical flat and condensed ESC-like morphology. hiPSCs incubated without primary antibodies and HFF, negative for pluripotency markers expression, were subjected to the same immunostaining procedure and used as negative controls for image acquisition.

Primary antibody			Secondary antibody		
Host species	Antibody	Dilution	Host species	Antibody	Dilution
Rabbit	HCN4	1:100	Donkey	anti-rabbit Cy™3	1:1000
			Donkey	anti-rabbit Alexa Fluor 647	1:1000
Goat	Nanog	1:200	Donkey	anti-goat Cy™3	1:500
			Donkey	anti-goat Alexa Fluor 555	1:1000
Mouse	Oct-3/4	1:300	Donkey	anti-mouse Alexa Fluor 647	1:1000
			Donkey	anti-mouse Alexa Fluor 555	1:1000
Mouse	TRA-1-60	1:80/1:100	Donkey	anti-mouse Alexa Fluor 647	1:1000
			Donkey	anti-mouse Alexa Fluor 555	1:1000
Mouse	TRA-1-81	1:80/1:100	Donkey	anti-mouse Alexa Fluor 647	1:1000
			Donkey	anti-mouse Alexa Fluor 555	1:1000
Goat	Sox-2 (Y-17)	1:100	Donkey	anti-goat Cy™3	1:500
			Donkey	anti-goat Alexa Fluor 555	1:1000

Table 3. Combinations of primary and secondary antibodies used for hiPSCs immunofluorescence. All the samples were stained with two different primary antibodies raised in different hosts and corresponding secondary antibodies showing different excitation/emission wavelength. Only one secondary antibody was used per primary antibody in each sample.

V.3 Detection of HCN4 and CM markers in CMs

CMs cultures at day 9 or 20 of differentiation were prepared in single-cell suspension (section II.8.2) and plated on VTN-coated coverslips, prepared as mentioned before, at 5,000-25,000 cells per cm^2 seeding density. Cells were maintained in standard culture conditions (section II.8.1) for 2-4 days prior immunostaining. CMs incubated without primary antibodies and hiPSCs, negative for CM markers expression, were subjected to the same immunostaining procedure and used as negative controls for image acquisition.

Primary antibody			Secondary antibody		
Host species	Antibody	Dilution	Host species	Antibody	Dilution
Mouse	α-Actinin (sarcomeric)	1:800/1:1000	Donkey	anti-mouse Alexa Fluor 647	1:1000
			Donkey	anti-mouse Alexa Fluor 555	1:1000
Rabbit	HCN4	1:100	Donkey	anti-rabbit Cy™3	1:1000
			Donkey	anti-rabbit Alexa Fluor 647	1:1000
Rabbit	Nkx2.5	1:800	Goat	anti-rabbit Alexa Fluor 546	1:1000
			Donkey	anti-rabbit Alexa Fluor 647	1:1000
Mouse	Troponin T-C (TNNT2)	1:200	Donkey	anti-mouse Alexa Fluor 647	1:1000
			Donkey	anti-mouse Alexa Fluor 555	1:1000

Table 4. Combinations of primary and secondary antibodies used for CMs immunofluorescence. All the samples were stained with two different primary antibodies raised in different hosts and corresponding secondary antibodies showing different excitation/emission wavelength. Only one secondary antibody was used per primary antibody in each sample.

VI. Image acquisition and analysis

VI.1 Routine image acquisition in cell culture

Routine bright field and fluorescence live cell imaging was performed using either an inverted light microscope EVOS® FL Imaging System (Invitrogen™, Thermo Fisher Scientific) with 4x, 10x and 20x magnification objectives or an inverted light microscope Leica DMi8 and Leica Application Suite (LAS) X software (Leica Mycrosystems) with 5x, 10x, 20x and 40x magnification objectives. Image acquisition was performed at RT, 22°C.

VI.2 Confocal imaging

Multi-color fluorescence confocal images of immunostained fixed samples were acquired with a Leica TCS SP5 (Leica Mycrosystems) equipped with 405 diode; Argon: 458/476/488/496/514; DPSS: 561 and HeNe: 633 laser beams and attached to an inverted epi-fluorescence microscope DMI 6600 (Leica Mycrosystems) using HC PL APO CS2 40x/NA 1.3 and HCX PL APO lambda blue 63x/NA 1.4 oil objectives. LAS AF software version 2.632 (Leica Mycrosystems) was used for acquisition.

Appropriate negative controls were used to set up laser parameters and discriminate real signal from sample autofluorescence or secondary antibodies background. Images were acquired using sequential scanning and adjusted photomultiplier tubes settings avoiding spectral overlapping between the different dyes, fluorescent proteins and fluorochromes used in each sample. Same settings were kept among different samples with same immunostaining conditions.

VI.3 Video recording

Videos of beating CMs cultures were acquired using an inverted light microscope Leica DMi8 (Leica Mycrosystems) provided with a heating plate at 37°C at 5x, 10x and 20x magnification. LAS X software (Leica Mycrosystems) was used for video acquisition (binning 2x2 and 4x4) and for video conversion to .mp4 format.

VI.4 Image processing and analysis

Microscopy images were processed using Fiji software (Schindelin *et al.*, 2012) Version 1.0 for Mac. Brightness and contrast levels (whole image) were modified for better visualization of images in printed version. Images belonging to same staining condition, from different samples and displayed in the same figure were modified equally for each adjusted parameter. All figures showing microscopy images were mounted using Adobe® InDesign® CS5 Version 7.0 for Mac (Adobe Systems) and further formatted using Adobe® Illustrator® CS5 Version 15.0.0 for Mac (Adobe Systems).

VII. Protein analysis

VII.1 Protein lysates preparation

Cells were detached using the corresponding cell suspension preparation protocol, washed in PBS or plain medium and centrifuge at 300*g* for 10min in an Eppendorf Tube® 1.5ml. Supernatant was aspirated completely and cell pellet was storage at -80°C or used immediately. Cell lysate was obtained adding RIPA buffer consisting of 50mM Tris-HCl, 150mM NaCl, 0.1% NP-40, 0.1% sodium dodecyl sulfate (SDS) and 0.1% sodium deoxycholate. One tablet of cOmplete™, Mini, EDTA-free Protease Inhibitor Cocktail (Roche) per 10ml buffer was added immediately before use. Cell pellet was gently resuspended by pipetting 100µl of complete RIPA buffer per $2{\cdot}10^6$ cells and incubated 20min on ice. After incubation, lysate was centrifuged at 20,000g at 4°C during 10min, supernatant was transferred to a new tube and stored at -80°C and pellet was discarded.

VII.2 SDS-PAGE and immunoblotting

Protein concentration of protein lysates was estimated using the Pierce™ BCA Protein Assay Kit (Thermo Scientific™, Thermo Fisher Scientific) according to manufacturer's instructions in a 96-well format and absorbance was measured using the Infinite® M200 Pro (TECAN) plate reader. 4xLaemmli Sample buffer consisting of 200mM Tris-Cl (pH 6.8), 8%(w/v) SDS, 40%(v/v) glycerol, 0.2%(w/v) bromophenol blue and 20%(v/v) fresh ß-mercaptoethanol was added to 50µg of total protein per sample to a final concentration of 1x and boiled at 96°C for 5min. 20µg of total protein per sample were loaded in a 6% (Fig 15) or 8% (Fig 9) poly-acrylamide gels, resolved in denaturing

conditions by sodium dodecyl sulfate–polyacrylamide gel electrophoresis (SDS–PAGE) and electrotransferred to Amersham Hybond-P polyvinylidene difluoride (PVDF) membranes (GE Healthcare Life Sciences) using a Trans-Blot® SD Semi-Dry Transfer Cell (Bio-Rad Laboratories). After transfer, PVDF membranes were stained with Ponceau S staining solution (0.1%(w/v) Ponceau S in 5%(v/v) acetic acid) to confirm proper protein transfer and validate equivalent protein load among different samples.

Prior assay with specific antibodies, membranes were incubated with blocking solution consisting of PBS with 0.1%(v/v) TWEEN® 20 and 5%(w/v) non-fat milk for 1h at RT in a shaker at 200rpm to reduce background signal. After blocking, membranes were incubated with 1:1000 dilution of a rabbit polyclonal antibody against HCN4 (Abcam Cat# ab69054, RRID:AB_1861080) in 1:10 blocking solution in PBS overnight at 4°C in continuous shaking. Next day, membranes were washed three times with PBS with 0.1%(v/v) TWEEN® 20 for 5min in a shaker at 200rpm and incubated 2h at RT in continuous shaking with 1:3000 dilution of an HRP-conjugated secondary antibody against rabbit IgG (H+L) (Thermo Fisher Scientific Cat# 31462, RRID:AB_228338) in 1:10 blocking solution in PBS. After incubation, membranes were washed as mentioned above and immediately developed.

Membranes were incubated with Amersham™ ECL™ Prime Western Blotting Detection Reagent (GE Healthcare) according to manufacturer's instructions and chemiluminescence was detected using a STELLA 3200 system (Raytest). Images were taken during 1 minute of exposition every 10 seconds. Image showing best relation signal vs. background was later processed (whole image) using Adobe® Photoshop® CS5 Version 12.0 x64 and further formatted using Adobe® Illustrator® CS5 Version 15.0.0 for Mac (Adobe Systems).

VIII. mRNA analysis

VIII.1 RNA isolation

Cells were detached using the corresponding cell suspension preparation protocol, washed in PBS or plain medium and centrifuge at 300*g* for 10min in an Eppendorf Tube® 1.5ml. Supernatant was aspirated completely and cell pellet was used immediately or kept at -80°C for later RNA isolation. 700µl of TRIzol™ Reagent (Invitrogen™, Thermo Fisher Scientific) was added to 1-4·10^6 cell pellet and gently mixed by pipetting until solution was completely homogeneous. Total RNA purification was performed using Direct-zol™ RNA MiniPrep kit (Zymo Research) according to manufacturer's instructions and finally eluted in RNAse free water. RNA was quantified using a NanoDrop™ spectrophotometer (Thermo Scientific™, Thermo Fisher Scientific) and storage at -80°C.

VIII.2 Reverse transcription and qPCR analysis

200-1000ng of total RNA were reverse transcribed using the High-Capacity cDNA Reverse Transcription Kit (Applied Biosystems™, Thermo Fisher Scientific) according to manufacturer's instructions. Resulting cDNA was diluted 1:10 with RNAse free water and stored as stock cDNA solution at -20°C. For PCR reactions, 3µl of 1:20 cDNA dilution per sample were mixed with 5µl of Power SYBR™ Green PCR Master Mix (Applied Biosystems™, Thermo Fisher Scientific) and 2µl of 5µM primers in a final reaction volume of 10µl. Three technical replicates per sample and primers pair were performed. PCR was run in a QuantStudio™ 6 Flex Real-Time PCR System (Applied Biosystems™, Thermo Fisher Scientific) using 384-well plate format and standard running protocol. Ct values of each sample are normalized using 18S rRNA levels (ΔCt), relatively quantified to the reference sample NT-hiPSCs (d0 of differentiation) and represented as ΔΔCt.

Target	Fw primer sequence	Rv primer sequence	Reference
18s rRNA	GTAACCCGTTGAACCCCATT	CCATCCAATCGGTAGTAGCG	Lamming *et al.*, 2003
CACNA1C	ATATGGGAAACCCAAGAAGCAGGG	TCCATTCGACAATGCTGATGCAGG	Protze *et al.*, 2017
CX31.9 (GJD3)	TGGTGGTCATGCTGATCTTC	TTGCACACGAACTCCTCTTG	Unpublished
CX40 (GJA5)	AATCTTCCTGACCACCCTGCATGT	CAGCCACAGCCAGCATAAAGACAA	Protze *et al.*, 2017
CX43 (GJA1)	GATGAGGAGTCTGCCTTTCGTTGT	AGAAGCGCACATGAGAGATTGGGA	Protze *et al.*, 2017
CX45 (GJC1)	AGAGCAGAGCCAACCCAAACCTAA	GCCAGCAACTGCAGCACATAGATT	Protze *et al.*, 2017
HCN2	AGAAGGGCATTGACTCCGAG	TAGCGGATCAGGCGTGAGA	Unpublished
HCN4	TCTTCCTCATTGTGGAGACACGCA	TGAGGATCTTCGTGAAGCGGACAA	Protze *et al.*, 2017
IRX4	AGGGCTATGGCAACTACGTG	CGAACCATCCTTGGAATCAA	Unpublished
KCNJ3	TCATCAAGATGTCCCAGCCCAAGA	CACCCGGAACATAAGCGTGAGTTT	Protze *et al.*, 2017
MYL2 (MLC2v)	TGTCCCTACCTTGTCTGTTAGCCA	ATTGGAACATGGCCTCTGGATGGA	Protze *et al.*, 2017
MYL7 (MLC2a)	GGGTGGTGAACAAGGATGAG	TGGGTGATGATGTAGCACAG	Unpublished
NKX2.5	TTTGCATTCACTCCTGCGGAGACCTA	ACTCATTGCACGCTGCATAATCGC	Protze *et al.*, 2017
SCN5A	TGCTGCTCTTCCTCGTCATGTTCA	TGTTGGCGAAGGTCTGGAAGTTGA	Protze *et al.*, 2017
SHOX2	ATCGCAAAGAGGATGCGAAAGGGA	TTCCAGGGTGAAATTGGTCCGACT	Protze *et al.*, 2017
TBX2	AACGCATGTACATCCACCCAGACA	TTGTTGGTCAGCTTCAGCTTGTGG	Protze *et al.*, 2017
TBX3	TTGAAGACCATGGAGCCCGAAGAA	CCCGCTTGTGAAACTGATCCCAAA	Protze *et al.*, 2017
TBX5	ACAAAGTGAAGGTGACGGGCCTTA	ATCTGTGATCGTCGGCAGGTACAA	Protze *et al.*, 2017
TNNT2	TTCACCAAAGATCTGCTCCTCGCT	TTATTACTGGTGTGGAGTGGGTGTGG	Protze *et al.*, 2017

Table 5. List of primers used for qPCR analysis.

IX. Genomic DNA (gDNA) analysis

IX.1 gDNA extraction

Cells were detached using the corresponding cell suspension preparation protocol, washed in PBS or plain medium and centrifuge at 300*g* for 10min in a 1.5ml Eppendorf Tube®. Supernatant was aspirated completely and cell pellet was used immediately or kept at -80°C for later gDNA extraction. gDNA extraction was performed using GeneJET Genomic DNA Purification Kit (Thermo Scientific™, Thermo Fisher Scientific) according to manufacturer's instructions.

IX.2 SNP-karyotyping and virtual karyotype analysis

gDNA isolated from the generated hiPSC clones was submitted to the MDC Stem Cell Core Facility for SNP karyotyping using the Infinium OmniExpressExome-8 Kit and the iScan system from Illumina (in cooperation with Prof. Hübner laboratory). CNV and SNP identification and visualization were performed using KaryoStudio Software v1.4 (Illumina) comparing the array results with the provided reference genome.

X. Electrophysiology

X.1 Assessment of spontaneous beating and beating rate

Single-cell CMs cultures subjected to metabolic selection (section II.8.3) were observed under an inverted light microscope Leica DMi8 (Leica Mycrosystems) provided with a heating plate at 37°C at 63x magnification. Spontaneous beating activity was determined at day 20-30 of differentiation by ocular inspection cell by cell. Similarly, beating rate was assessed visually by counting number of beats in 15 seconds and calculating to beats per minute. During this process, plates from different cell lines were analyzed separated, keeping them no longer than 15min out of the incubator to prevent temperature decrease to interfere with the measurements. Cells from at least three different differentiation experiments were analyzed.

X.2 Electrophysiological recordings

X.2.1 Cell preparation for electrophysiology

HEK293T cells were prepared in single cell suspension using 0.05% trypsin-EDTA (Gibco™, Thermo Fisher Scientific), washed by centrifugation, plated at low density (~1000 cells per cm^2) on 0.01% gelatin-coated glass coverslips kept in 60mm plates and maintained in regular culture conditions (section II.2) until the moment of analysis. I_f current recordings were performed between 18-48h after seeding.

hiPSCs were prepared in single cell suspension using Accutase (Gibco™, Thermo Fisher Scientific) (section II.7.5), washed by centrifugation, plated at low density (~1000 cells per cm^2) on VTN-coated glass coverslips kept in 60mm plates with E8 medium supplemented with 2µM Thiazovivin (Calbiochem) and maintained in regular culture conditions (section II.7.2) until the moment of analysis. I_f current recordings were performed between 18-48h after seeding.

CMs were prepared in single cell suspension (section II.8.2), washed by centrifugation and plated at low density (~1000 cells per cm^2) on VTN-coated glass coverslips kept in 60mm plates with CM medium supplemented with 2µM Thiazovivin (Calbiochem). CMs were maintained in regular culture conditions (section II.8.1) and

medium was changed every 3 days. AP and I_f current recordings were performed between 4-14 days after seeding.

X.2.2 I_f current recordings in HEK293T cells, hiPSCs and CMs

Single HEK293T cells, hiPSCs and CMs were voltage-clamped at -50mV in the whole-cell configuration and currents were acquired using a Dagan amplifier and pClamp software (Clampex 10.2). I_f current was recorded from a 3 seconds hyperpolarization pulse at potentials ranging from −60 to −120mV in 10mV steps. Borosilicate patch pipettes were prepared using a horizontal pipette puller (Model P-87, Sutter Instruments, CA) to a final resistance of 4–6 MΩ. The membrane under the patch pipette was ruptured and the cells dialyzed with pipette solutions containing (in mM): 88 K-aspartate, 60 KCl, 5 NaCl, 5 Mg-ATP, 0.5 EGTA, 0.2 $CaCl_2$ and 10 HEPES, adjusted to pH 7.2 with KOH. The extracellular bath solution contained (in mM): 137 NaCl, 5.4 KCl, 2 $CaCl_2$, 1 $MgCl_2$, 10 glucose and 10 HEPES, adjusted to pH 7.4 with NaOH. Experiments were carried out at RT, 24 °C.

X.2.3 AP recordings in CMs

Cardiac APs were recorded from single CMs. Whole-cell patch-clamp recordings were conducted, using patch pipettes with a tip resistance of 2–3MΩ, with thick-walled borosilicate pipettes (with filament; Harvard Apparatus) and fire-polished to a final resistance of 3-4MΩ. Pipettes were filled with a solution containing (in mM): 130 K-aspartate, 10 NaCl, 5 HEPES, 1 $MgCl_2$, 1.8 $CaCl_2$, 2 Mg-ATP, 0.1 GTP, 5 phosphocreatine and 5 EGTA, adjusted to pH 7.2 with KOH. The external bath solution contained (in mM): 140 NaCl, 5.4 KCl, 5 HEPES, 1 $MgCl_2$, 1.8 $CaCl_2$ and 10 glucose, adjusted to pH 7.4 with NaOH.

Currents were acquired with a HEKA EPC10 amplifier and Patchmaster software (HEKA Elektronik) at a sampling rate of 20ms and filtered at 3kHz. Spontaneous AP recordings were performed in current clamp. When cells did not spontaneously spike, cells were first hyperpolarized by injecting negative currents up to a voltage of -90mV to release inactivation of Nav channels. The hyperpolarization step was followed by increasing current injections ranging from 0 to 500pA in 50pA steps of the duration of 2 to 5 seconds. Experiments were carried out at RT, 24 °C.

X.2.4 AP analysis

Cardiac AP analysis was performed using Fitmaster software v2x90.2 for Windows (HEKA Elektronik). Maximum diastolic potential (MDP, mV), resting membrane potential (RMP, mV) and peak (mV) values were collected manually using 'measure' tool and used to calculate the AP amplitude (APA, mV), AP duration (APD), interval (s), and voltages at 90% and 50% of AP repolarization. Once these voltages were calculated, the corresponding time values were collected manually and APD90 and APD50 were obtained. Typically AP

parameters from three and at least two APs were analyzed, obtaining the average values per cell for final population analysis.

XI. Statistics

Statistic analysis and data representation were performed using GraphPad Prism 6.0c for Mac, GraphPad Software, La Jolla California USA, www.graphpad.com. Differences between the groups NT, GFP and hHCN4 were analyzed by One-way ANOVA followed by Tukey's multiple comparisons test. In experiments where data were grouped in a secondary category (voltage in current intensity experiments and day of differentiation in gene expression analysis) differences were analyzed by Two-way ANOVA followed by Tukey's multiple comparisons test. Differences were considered statistically significant when $p<0.05$. Normally, data are represented as mean ± SEM through the entire document, except when single-cell data are represented instead of average values of a population, and then mean ± SD was preferred. Data representation used in any case is indicated in the figure legend.

Results

I. Generation of overexpression constructs

I generated the construct pT2-hHCN4-GFP based on the SB-transposon system (pT2/SB100X) to integrate into the genome the overexpression cassette of the human *HCN4* gene (hHCN4) (Figure 6). All the components are cloned in a pT2 vector, which provides the IRs required for transposition. The *HCN4* CDS is followed by an Internal Ribosome Entry Site (IRES) sequence and the *GFP* reporter gene CDS, allowing the expression of both hHCN4 and GFP proteins from the same mRNA. Using IRES was preferred to hHCN4-GFP fusion protein that could interfere with the translocation to the membrane and the proper function of hHCN4. I used GFP expression to select positive cells stably expressing the transgenes by FACS and micromanipulation.

I selected CAG promoter to drive HCN4 expression due to its "double-feature". It provides robust transgene expression in undifferentiated cells and an enhanced expression in CMs (Orbán et al., 2009). On one hand, this strategy prevents the need for two tissue-specific promoters, avoiding a larger transposon cargo sequence and overall construct size that could be detrimental for both transposition and transfection efficiencies. On the other hand, it provides a separation platform for CMs upon differentiation due to the increased transcription rate in this cell type.

I also generated the control construct pT2-IRES-GFP that includes the same elements as the overexpression construct pT2-hHCN4-GFP, except for the *HCN4* CDS. Additionally, I used the pT2-GFP construct as control along the different transgenesis experiments.

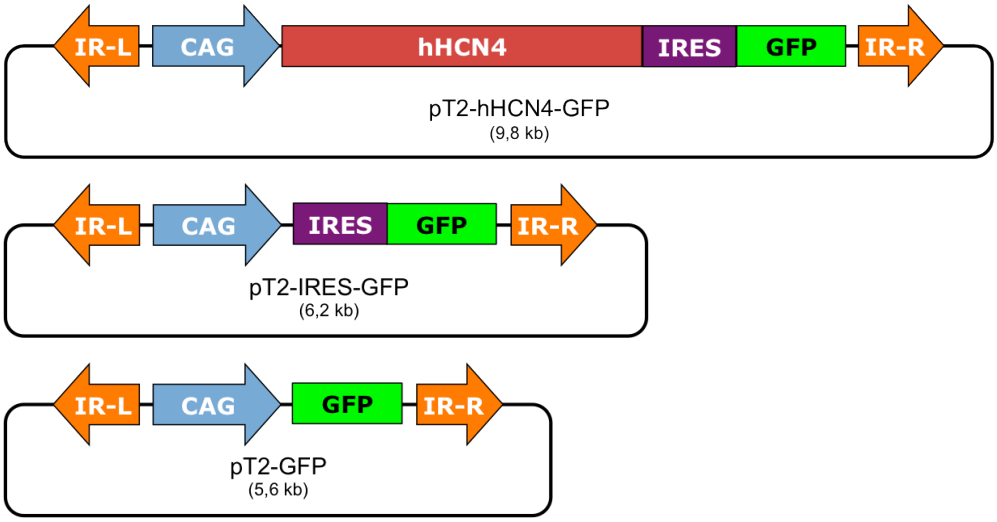

Figure 6. Schematic representation of SB-transposon based overexpression constructs. IR-L: Inverted Repeat Left, CAG: CAG promoter, hHCN4: human gene *HCN4* CDS, IRES: Internal Ribosome Entry Site, GFP: *GFP* CDS, IR-R: Inverted Repeat Right.

II. hHCN4 overexpression in HEK293T cells by SB-mediated gene transfer

I tested the overexpression construct and the working pipeline to generate hHCN4-overexpressing cell lines in HEK293T cells (hHCN4-HEK293T), before working with hiPSCs. I co-transfected HEK293T cells with the expression constructs and SB100X transposase, confirmed GFP expression by FACS and fluorescence microscopy and selected stable cell lines. Once stable cell lines were generated, I enriched the GFP positive cell population showing SB-mediated transgenesis by cell sorting. Finally, I confirmed the expression of hHCN4 by Western blot (WB) and validated the functional expression of the I_f by electrophysiology in highly enriched GFP expressing cell lines.

II.1 Generation of stable hHCN4-overexpressing HEK293T cell lines

I transfected HEK293T cells with pT2-hHCN4-GFP vector without or with the expression vector for SB100X transposase. As a positive control for transfection and GFP expression, I used the plasmid pT2-IRES-GFP. After transfection, I monitored GFP expression by FACS during one month to determine the optimal sorting time. By comparing the population transfected without or with transposase vector, I could discriminate cell populations showing GFP expression due to transient expression or SB-mediated stable transposon integration, respectively. Stable transgene expression due to random integration of the overexpression plasmid could happen at very low probability and should not be discarded.

I analyzed transfection efficiency after 48 hours. HEK293T cells transfected with pT2-hHCN4-GFP (Figure 7, red) showed slightly lower (19.18%±1.47) transfection efficiency compared with cells transfected with the positive control pT2-IRES-GFP (31.55%±2.85) (Figure 7, blue). These differences could be explained by the difference in vector size. Similarly, I could observe lower GFP intensity in cells transfected with hHCN4 overexpression construct compared to control, probably due to the lower number of plasmid molecules per cell or due to the fact that a higher size of the cistron upstream of the IRES sequence can decrease the translation efficiency of the cistron downstream.

Transposition efficiency was decreased in HEK293T cells transfected with pT2-hHCN4-GFP as compared with the control. Thus after two weeks, 22% of the cells transfected with pT2-IRES-GFP in the presence of transposase (+SB, Figure 7) showed stable GFP expression while only 1.3% of cells transfected with pT2-hHCN4-GFP and SB100X expression vector did. The transposon of the hHCN4 overexpression vector is significantly bigger (6.9kb) than the transposon of the control vector (3.2kb), which has been shown to decrease transposition efficiency. Moreover, I can not exclude that, due to size restraint during transfection, less molecules per cell would be available for transposition of the hHCN4 overexpression plasmid in comparison with the smaller control plasmid.

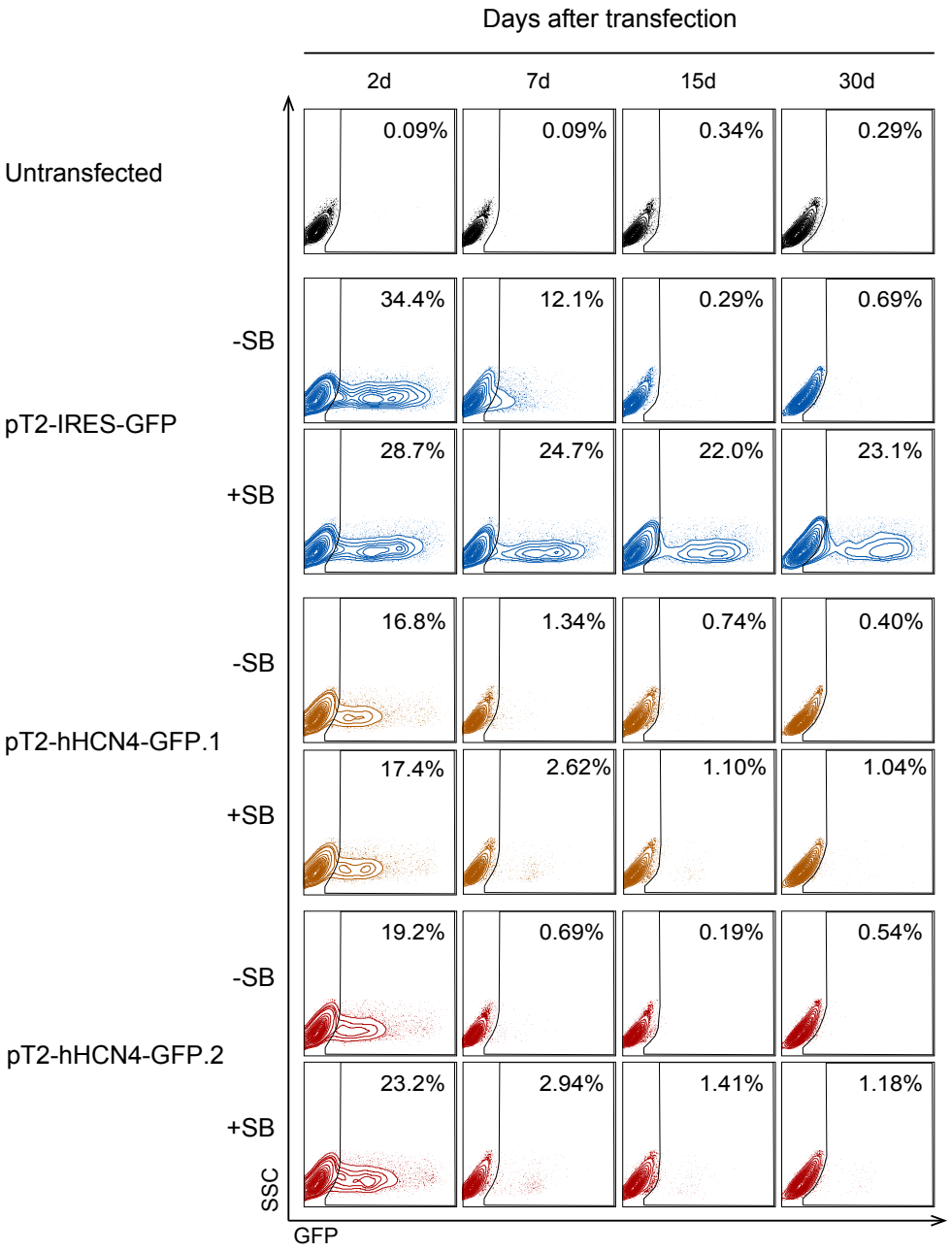

Figure 7. SB-transposition of overexpression constructs in HEK293T cells. GFP expression of transfected cells monitored by FACS 2, 7, 15 and 30 days after transfection. HEK293T were untransfected (black) or transfected with pT2-IRES-GFP (blue) or pT2-hHCN4-GFP (2 biological replicates: .1 in orange and .2 in red) in the absence (-SB) or the presence (+SB) of the SB100X expression vector. Cells showing stable expression of the overexpression cassette could be discriminated from transient events already two weeks after transfection.

One week after transfection, I could still detect GFP signal in 12.1% of the cells transfected with the positive control vector and without transposase (-SB) due to transient expression. Two weeks after transfection, only those cells transfected with transposase expressing vector (+SB) showed GFP signal (Figure 7). Therefore, I determined two weeks after transfection as the optimal time for cell sorting of HEK293T cells in order to select populations with stable transposon integration.

Next, I sorted the cells showing stable transgene expression based on reporter expression. I enriched the GFP positive population up to 52.2% and 81.8% in two different biological samples. In order to obtain a more enriched population for HCN4 expression analysis, I sorted the cells for a second time, being able to obtain populations exhibiting above 95% of GFP positive cells (Figure 8).

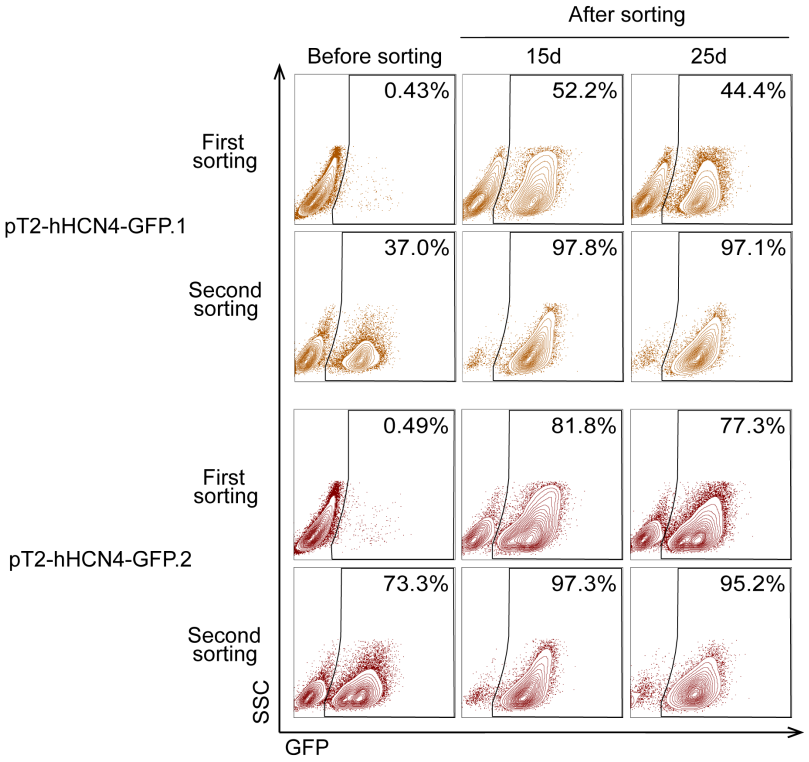

Figure 8. Sorting of HEK293T cells showing stable transposon integration. Cells transfected with pT2-hHCN4-GFP and SB100X expression plasmid were sorted based on their GFP expression. Two cell lines were generated independently. FACS plots showing GFP expression of cells before and 15 and 25 days after first and second sorting are shown. After the second sorting more than 95% of the population expressed the transgene stably.

I cultured and expanded both sorted populations and monitored GFP expression through time. Cell populations sorted only once showed a slight decrease in GFP expression through passages. pT2-hHCN4-GFP.1 GFP-positive population showed a 15% decrease 25 days after sorting (52.2% vs. 44.4%) and up to a 30% decrease 30 days after the first sorting (when the second sorting was performed, 52.2% vs. 37.0%). pT2-hHCN4-GFP.2 cell line showed more stable GFP expression and only a 10% decrease in GFP positive population 30 days after first sorting (81.8% vs. 73.3%). After the second sorting, both cell lines remained above 95% GFP positive through passages, showing only 1-2% decrease in GFP positive cells 25 days after sorting (Figure 8). Once I obtained a high percentage of GFP-expressing cells implying that most of the population underwent stable transgene integration, I used these cell lines to perform subsequent experiments for hHCN4 functional expression validation.

II.2 hHCN4-HEK293T cell lines express functional hHCN4

I generated two independent cell lines showing stable transposon integration based on their GFP expression. To validate hHCN4 expression, I performed WB of protein lysates using an antibody against HCN4 in presorted and sorted samples 90 days after transfection. I detected a band at ~150kDa, slightly higher than the predicted 129kDa for hHCN4, probably due to posttranslational modifications of the channel, which has been described to undergo glycosylation and phosphorylation of different residues. The double band at 100kDa corresponds to the expected band size documented in the antibody datasheet (human brain tested as HCN4-expressing sample). The band at 50kDa is also described in the antibody datasheet as 'unidentified band' that could arise from reported protein degradation associated to overexpression experiments. I could detect HCN4 protein only in sorted populations enriched in GFP positive cells but not in presorted samples, where only a 1-2% of cells expressed GFP due to transgene integration. This confirmed the specificity of the antibody to detect exclusively HCN4 (Figure 9A).

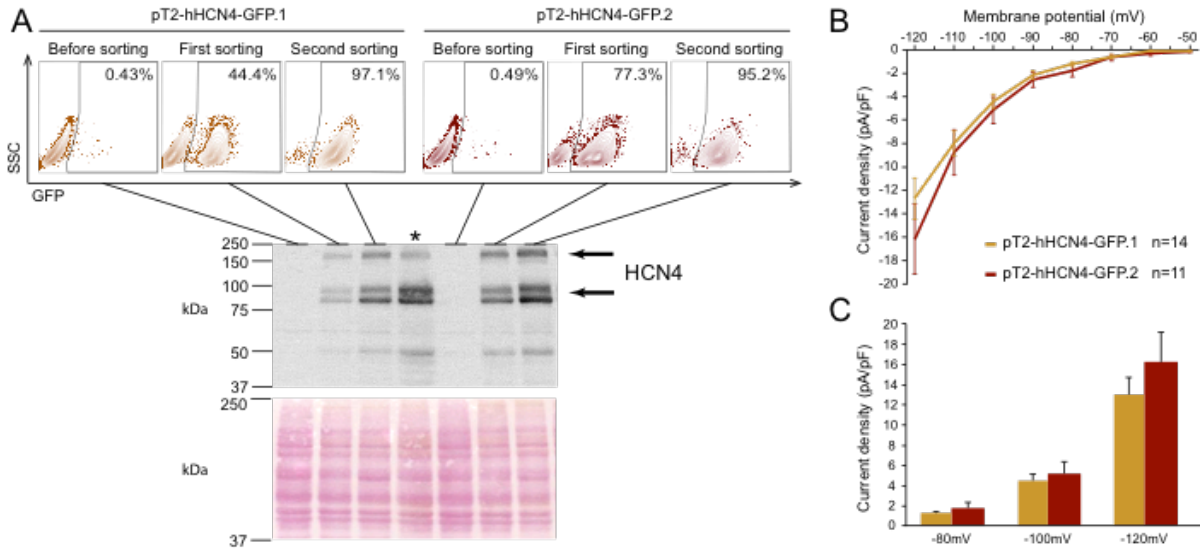

Figure 9. Functional hHCN4 expression in hHCN4-HEK293T cell lines. A) HCN4 protein expression in transfected and sorted cells. FACS plots show GFP expression in corresponding samples analyzed by WB. Presorted samples showing less than 1% GFP positive cells were used as negative control. *Positive control: HEK293T cells 48h after transient transfection with pT2-hHCN4-GFP. Ponceau staining showing equivalent protein loading of the different samples is shown below. **B)** Voltage-current relationship (IV curve) showing functional expression of I_f in two independent hHCN4-expressing stable cell lines. **C)** Average I_f intensity at different voltages. The number of cells analyzed is displayed. Data represented as mean ± SEM. hHCN4-HEK293T cell lines showed functional hHCN4 expression.

Next, we[1] analyzed the electrophysiological properties of the generated hHCN4-HEK293T cell lines. I_f was expressed in both cell lines. However, the pT2-hHCN4-GFP.2 line showed I_f activation at less negative voltages compared to

[1] In collaboration with Nathaniel Jensen in the laboratory of Prof. Dr. Martin Morad at the MedicalUniversity of South Carolina (MUSC).

pT2-hHCN4-GFP.1 line (-60mV vs. -70mV, Figure 9B) and also displayed slightly higher current intensity at every voltage tested (Figure 9C). The current displayed typical hyperpolarization activation and voltage-current intensity relationship (Figure 9B). Expressed I_f became stronger at more negative voltages and it was effectively blocked by 2mM Cs^+ (data not shown), showing the expected pharmacology and voltage dependence.

Once I validated the stable and functional overexpression of hHCN4 in HEK293T cell lines generated by SB-mediated integration of the overexpression cassette supplied by pT2-hHCN4-GFP vector, I moved forward to generate hHCN4-overexpressing hiPSC lines using the same procedure.

III. hHCN4 overexpression in hiPSCs by SB-mediated gene transfer

I generated hiPSCs by reprogramming of HFF and characterized the pluripotency and genome stability of four clones. I transfected different hiPSC lines with the overexpression constructs and generated stable cell lines by SB-transposition with SB100X. After transposition, I enriched by cell sorting the GFP-positive cell population showing SB-mediated transgenesis. Furthermore, I generated clonal populations from the sorted cells (bulk) to obtain more homogeneous overexpressing cell lines. Next, I confirmed the maintenance of pluripotency markers expression in transgenic cell lines by IF. Finally, I validated long-term expression of hHCN4 by WB and IF and the functional expression of I_f by electrophysiology in the hiPSC lines overexpressing hHCN4.

III.1 Reprogramming of human fibroblasts into hiPSCs

I generated hiPSCs by transient expression of the reprogramming factors using oriP/EBNA1 vectors, an episomal vector system derived from the Epstein-Barr virus (Okita *et al.*, 2011). Additionally, episomal reprogramming efficiency was greatly enhanced by the addition of the MEK inhibitor PD0325901, the GSK3β inhibitor CHIR99021, the TGF-β receptor inhibitor SB431542 and the ROCK inhibitor Thiazovivin (Yu *et al.*, 2011) (Figure 10A). In the final protocol, I transfected human fibroblasts with three episomal vectors containing the expression cassette for the human transcription factors OCT3/4, SOX2, KLF4, L-MYC and LIN28, as well as shRNA to suppress p53 expression, and cultured them in fibroblast medium during 7-8 days. Before reaching confluency, I reseeded the transfected fibroblasts on feeder cells and culture them in ESCs medium supplemented with the aforementioned small molecules for one week. After that time, I kept the cells in regular ESCs medium. At day 21-27 after transfection I could easily identify and isolate colonies showing ESC morphology under the scope. I expanded them on matrigel-coated plates and mTeSR medium for 5-10 passages and analyzed their pluripotency.

The generated hiPSCs grew forming compact and flat colonies composed by small cells with high nucleus/cytoplasm ratios (Figure 10B), thus displaying typical ESC morphology. The ESC morphology was maintained after more than 20 passages and less than 5% of the cells within the overall culture displayed differentiated phenotype through time.

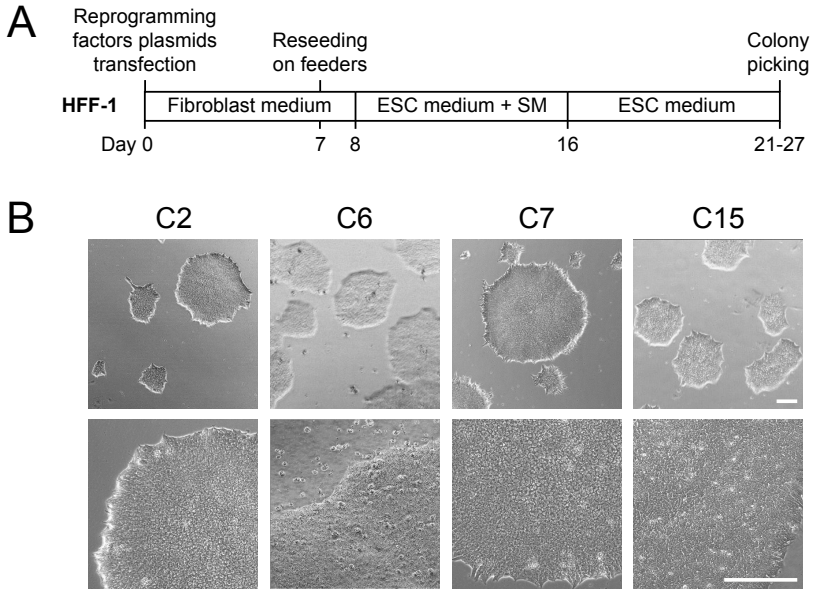

Figure 10. hiPSCs generation by reprogramming of human fibroblasts. A) Schematic timeline of the reprogramming protocol. HFF: human foreskin fibroblasts, ESCs: embryonic stem cells, SM: small molecules **B)** Bright-field images of representative cultures from generated hiPSC clones (upper row). Detail at higher magnification of one hiPSC colony from the respective clones (lower row). C2, C6, C7 and C15 indicate four different generated and established clones of hiPSCs. Scale bar 200µm. Selected hiPSC clones showed typical ESC morphology.

III.2 Characterization of generated hiPSCs

To validate the pluripotency of the established hiPSC clones, I analyzed the expression of pluripotency markers by IF staining. As control, I analyzed the hiPSC line SCVI 113 obtained from the Stanford Cardiovascular Institute (SCVI) Biobank (kindly provided by Dr. Sebastian Diecke, Stem Cell Core Facility (SCCF) at the Max Delbrück Center (MDC)). The SCVI 113 hiPSC line was generated by reprogramming peripheral blood mononuclear cells (PBMCs) using Sendai viruses carrying the reprogramming factors. Since the source cells and the reprogramming method used for the generation of this line were different from the ones I used, I decided to use in parallel this clone as external control for pluripotency characterization and generation of the hHCN4-overexpressing hiPSC lines.

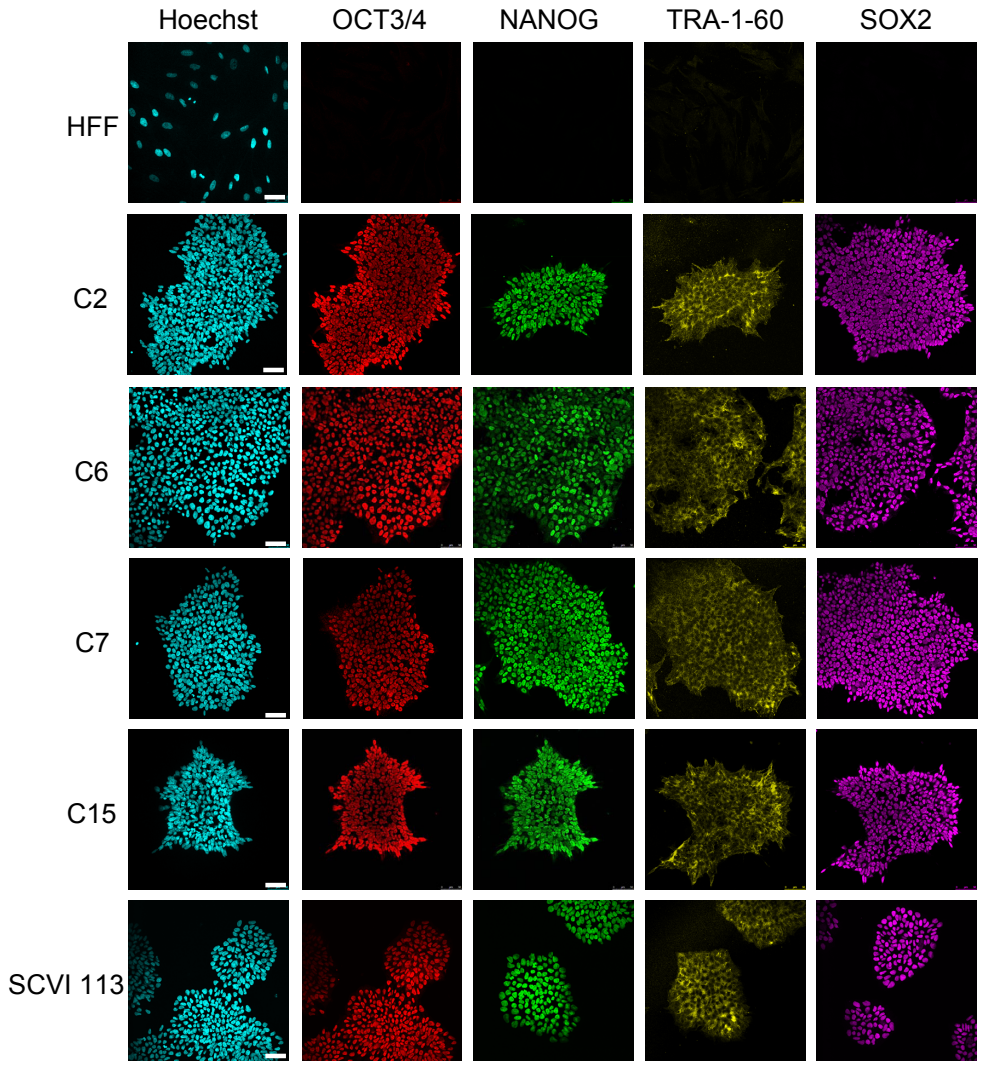

Figure 11. Pluripotency markers expression in established hiPSC clones. Representative images of IF staining of pluripotency markers in hiPSC clones. HFF: Human Foreskin Fibroblasts, parental cell line used for reprogramming and negative control used for pluripotency marker expression. DNA counterstain with Hoechst. C2, C6, C7 and C15 indicate four different generated and established clones of hiPSCs. SCVI 113, reference hiPSC clone from the SCCF, MDC. Scale bar 50µm. Generated hiPSC clones expressed pluripotency markers.

Generated hiPSCs showed positive staining for several pluripotency markers. I could detect high signal/expression of OCT3/4, NANOG and SOX2 displaying typical nuclear localization, as well as TRA-1-60 and TRA-1-81 that were expressed at the membrane of generated and reference hiPSC lines (Figure 11). Using the same staining protocol and image acquisition conditions, the parental fibroblast cell line used for the reprogramming experiment, HFF, was negative for pluripotency marker expression.

Once the expression of pluripotency markers was confirmed, we[2] further tested the ability of generated hiPSCs to differentiate into the three embryonic germ layers, *i.e.* endoderm, ectoderm and mesoderm. For this purpose, we performed a teratoma assay in immunodeficient mice. hiPSCs were injected subcutaneously and under the kidney capsule and tumor growth was monitored weekly at the injection sites. When tumors reached sufficient size (80-90 days after injection), they were collected and analyzed histopathologically. We confirmed the presence of all three germ-layers derivatives in the generated teratomas. Indeed, we identified several epithelial structures derived from endoderm, primitive mesenchyme and chondroid tissue derived from mesoderm as well as primitive neuroectodermal tissue derived from ectoderm (Figure 12). With these results, we functionally validated the pluripotent capacity of my newly established hiPSC clones.

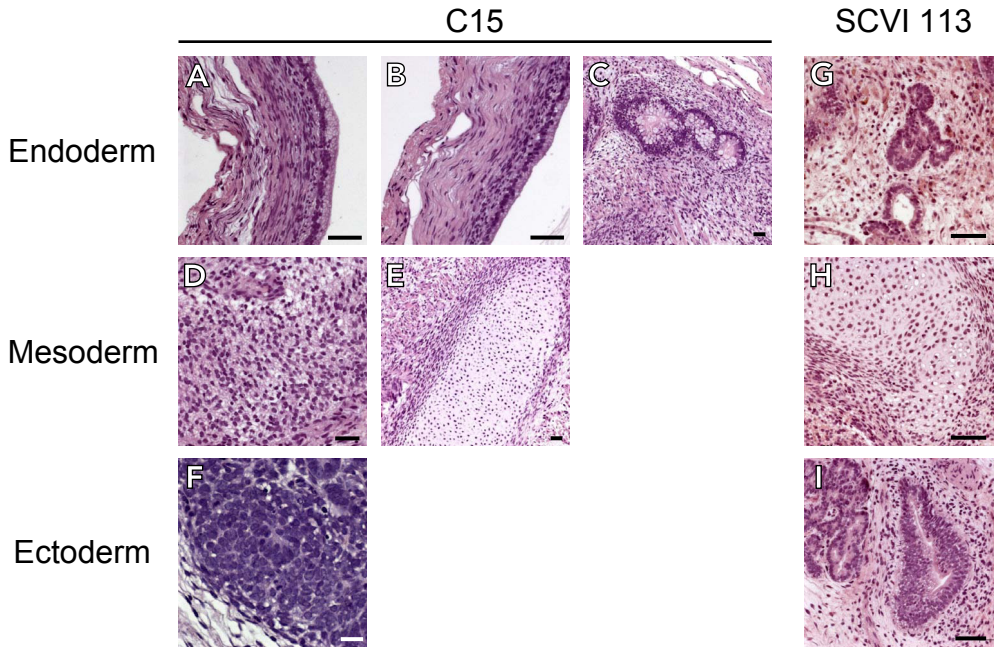

Figure 12. Histological characterization of teratomas generated after injection of hiPSCs. A-F) Hematoxylin and eosin staining of tissue structures derived from the injection of the hiPSC clone C15: A), B) cuboidal epithelium and C) vacuolated columnar epithelium derived from endoderm. D) Primitive mesenchyme and E) cartilage derived from mesoderm. F) Primitive neuroectodermal tissue derived from ectoderm. G) Gland-like structures with cuboidal epithelium derived from endoderm. **G-I)** Tissue structures derived from the injection of the hiPSC clone SCVI 113: H) cartilage derived from mesoderm. I) Primitive neuroepithelium rosette derived from ectoderm. Scale bar 50µm. hiPSC lines revealed their pluripotency by generating teratomas with histological structures derived from all three germ layers.

[2] The teratoma assay was performed by EPO GmbH - Experimental Pharmacology & Oncology, Berlin, Germany.

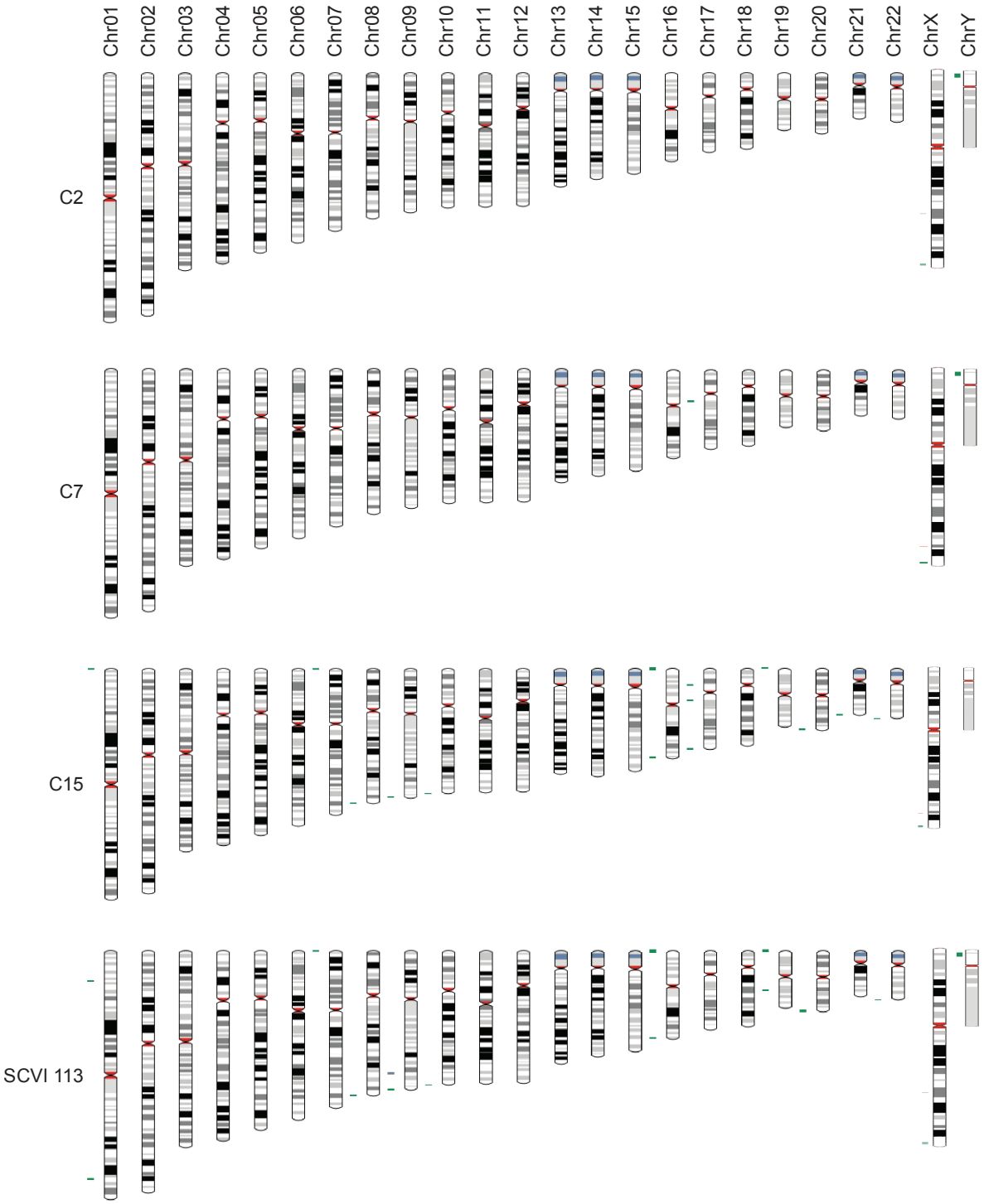

Figure 13. Virtual karyotype of generated and reference hiPSC lines. Chromosomes from clones 2, 7, 15 and SCVI113 are virtually represented simulating a classical karyotype assay. Insertions (green), deletions (red) and areas with loss of heterozygosity (grey) with respect to the genome of reference are marked on the left of each chromosome. The three hiPSC clones analyzed and the reference hiPSC line SCVI 113 showed broadly normal karyotype.

Chromosomal rearrangements and copy number variations have been frequently described upon cell reprogramming and hiPSCs derivation. In order to monitor the genomic integrity and the absence of chromosomal abnormalities in the generated hiPSC

lines, we[3] performed a karyotyping assay. Genomic DNA (gDNA) from 3 different clones was isolated and analyzed by Single-Nucleotide Polymorphism (SNP) karyotyping. The three hiPSC lines (C2, C7 and C15) showed typical karyotypes with only minor variations, mainly micro insertions. We also analyzed the reference cell line SCVI 113 and checked it for the absence of major chromosomal rearrangements. Similarly to the generated cell lines, SCVI 113 showed a normal karyotype with some micro insertions (Figure 13). Importantly, mismatches in the karyotype analysis were mainly attributed to the use of the standard control genome instead of gDNA from the parental cell lines that were used for reprogramming. The presence of the same particular micro insertions in C2 and C7 and the concordance of particular mismatches between the unrelated cell lines C15 and SCVI 113, support this hypothesis. Unfortunately, I could not have access to the parental PBMCs population of SCVI 113 hiPSC line for comparison. Moreover, the human fibroblast cell line (ATCC SCRC-1041) used for the reprogramming experiment was established from human foreskin samples pooled from two individuals, making it unsuitable as genomic reference due to the intrinsic SNP differences between the two donor genomes.

III.3 Generation of stable hHCN4-overexpressing hiPSC lines

To generate the final hHCN4-overexpressing hiPSC (hHCN4-hiPSC) lines, I selected two different hiPSC clones: C6 and C15, together with the reference cell line SCVI 113 and an established hiPSC line IMR90 C8 (kindly provided by Dr. Tomo Saric, University of Cologne). I transfected hiPSCs with a plasmid encoding SB100X and the overexpression construct pT2-hHCN4-GFP. I also transfected hiPSCs with SB100X and the pT2-GFP control vector to generate hiPSC lines overexpressing only GFP (GFP-hiPSCs) as control for SB-mediated transgene integration without hHCN4 overexpression (Figure 14A). In the final experiment, I electroporated 1.5 million cells with an equimolar amount of transposon vectors, 7µg of pT2-hHCN4-GFP and 4µg of pT2-GFP, and 10 times less SB100X expression vector (mass ratio transposase:transposon 1:10). As I already observed in HEK293T, the percentage of GFP positive cells was significantly lower in cells transfected with hHCN4 overexpression vector (2.11-23.8%, Figure 14B, Before sorting) as compared with the control plasmid (20.3-46.1%, Figure 14B, Before sorting), likely due to the difference in size of the transposon plasmid. I also observed a wide range of transfection efficiency with pT2-hHCN4-GFP between the different hiPSC lines, from 23.8% of GFP positive cells in C6 cell line to only 2% in IMR90 C8 and C15 (Figure 14B, Before sorting).

After transfection, hHCN4-hiPSC and GFP-hiPSC clones showing transposon integration were selected by cell sorting based on their GFP expression. As first approach, I sorted transfected cells 2 weeks after transfection, the optimal sorting time previously established with HEK293T cells. At that time point, only low percentage of cells transfected with the hHCN4 overexpression plasmid were GFP positive, thus requiring a large number of presorted cells in order to obtain a representative population with

[3] The SNP karyotyping was performed by the SCCF at the MDC.

transgene integration after sorting. Therefore, I decided to sort cells two days after transfection to reduce the presorted material required and to accelerate the generation of stable overexpressing cell lines (Figure 14A). After sorting, I obtained populations enriched in GFP-expressing cells above 50% with the exception of the hiPSC line C15 transfected with the hHCN4 overexpression vector (Figure 14B, lower row). When analyzed by FACS, this cell line showed both very low intensity and percentage of GFP positive cells, making the gating setup difficult. Although non-transfected parental hiPSC lines (NT-hiPSCs) negative for GFP expression were used for gating purposes, the sorted population was close to the GFP negative region. This could result in the selection of non-modified cells as reflected by the lack of enrichment in GFP positive cells. Therefore, I performed the rest of the characterization of C15 considering it as a negative control for hHCN4 expression (~~hHCN4~~).

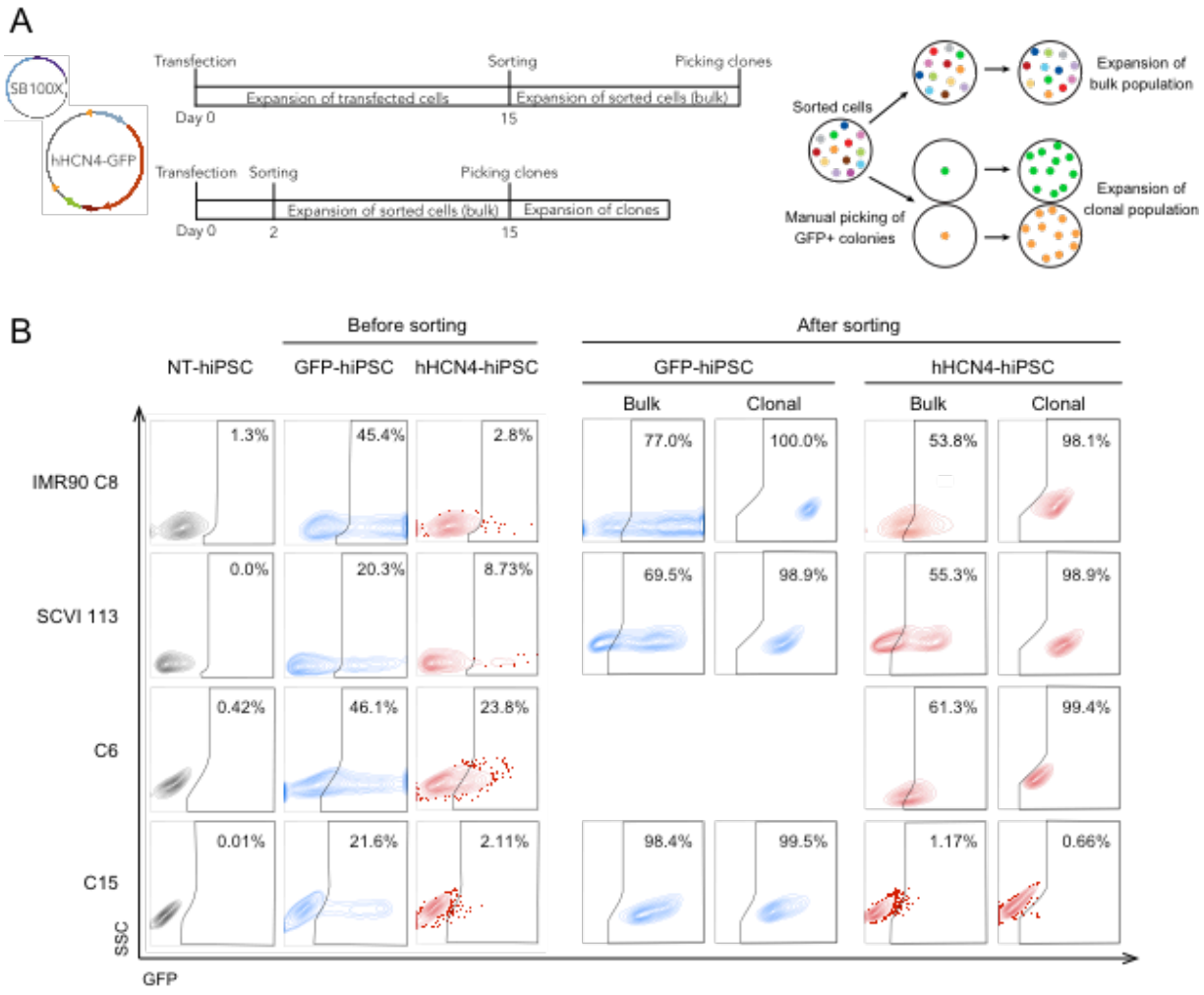

Figure 14. Generation of hiPSCs stably overexpressing hHCN4 by SB-gene transfer. A) Schematic representation of the transgenesis procedure and timeline using two different sorting strategies and the generation of bulk and clonal hHCN4 and GFP-overexpressing cell lines. **B)** GFP expression of transfected cells analyzed by FACS before sorting, after sorting (bulk population) and after clonal selection of sorted cells. Cells showing transposon integration were selected by cell sorting and further micromanipulation based on their GFP expression.

The sorted populations maintained the percentage of enrichment in GFP positive cells through passages, reflecting stable transgenesis in the majority of the cells. Next, I aimed to generate pure transgenic hiPSC lines. Culture and expansion conditions of undifferentiated hiPSCs influence the efficiency of CM differentiation protocols, being heterogeneity of the starting hiPSC population detrimental for CM yield (Mohr *et al.*, 2010; Lian *et al.*, 2013). In order to reduce variability that could interfere with CM differentiation and complicate comparative analysis between different cell lines, I decided to generate clonal cell lines from the GFP-positive sorted hiPSCs. For that purpose, after expansion and cryopreservation of the sorted bulk population, I performed limiting dilution to select colonies grown from a single cell and picked GFP-positive clones under the fluorescence microscope by micromanipulation (Figure 14A). After manual picking I expanded clonal populations and checked their GFP expression by FACS. I validated the generation of homogeneous clonal populations showing above 98% of GFP positive cells (Figure 14B, rightmost column). A GFP-negative clonal population was generated from the sorted cells from C15 and used as negative control for further characterization experiments.

For the reasons mentioned above, I used the generated clonal populations to perform the majority of the following experiments and obtain most of the data. When bulk population was used instead, or in addition to, I will refer to it as 'bulk' in the text, whereas the absence of any labeling will always indicate that clonal populations were used.

III.4 hHCN4-hiPSCs stably express hHCN4 protein and I_f while maintaining pluripotency

After sorting and manual selection of GFP-positive clones, I expanded and generated a stock of hHCN4 and GFP-overexpressing hiPSC bulk and clonal cell lines. hHCN4-hiPSC and control GFP-hiPSC lines generated by SB-transgenesis maintained ESC morphology and showed similar growing features, as compared to their corresponding NT-hiPSCs (data not shown). Once I obtained populations enriched in GFP-expressing cells and thus showing stable transgene expression through passages, I validated the expression of hHCN4 by WB and IF. I tested protein lysates of the generated hiPSC lines with an antibody against HCN4 by WB. I was able to detect the corresponding band at 150kDa only in the sorted cell lines transfected with pT2-hHCN4-GFP overexpression vector but not in the corresponding NT-hiPSC, GFP-hiPSC or C15 control lines (Figure 15).

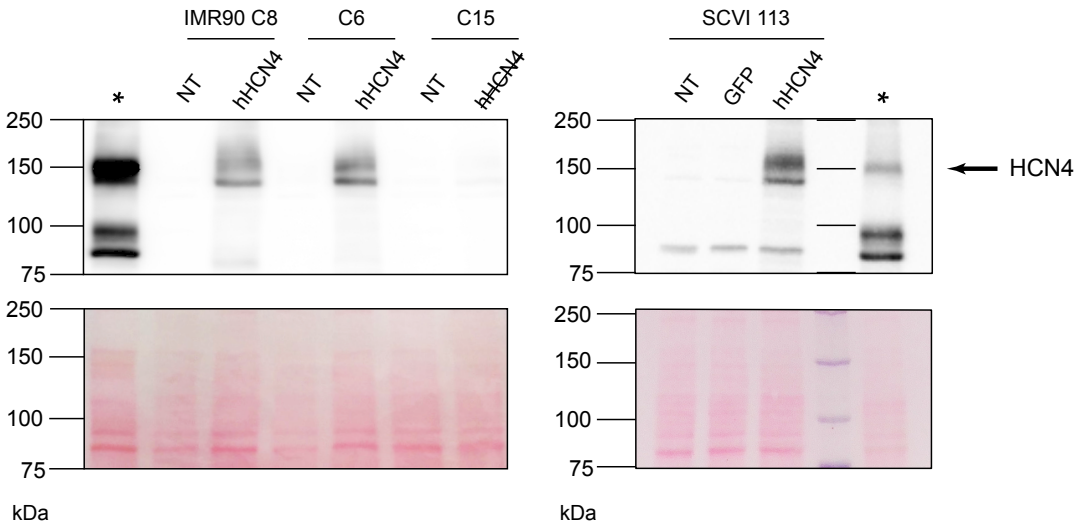

Figure 15. Analysis of HCN4 expression by WB in overexpressing and control hiPSC clones. Non-transfected (NT) and GFP-hiPSC clones were used as negative controls for HCN4 expression. *Positive control: HEK293T cells 48h after transient transfection with pT2-hHCN4-GFP. Ponceau staining showing equivalent protein loading of the different samples is shown below each WB. hiPSC clones subjected to SB-mediated transgenesis with pT2-hHCN4-GFP vector stably expressed HCN4.

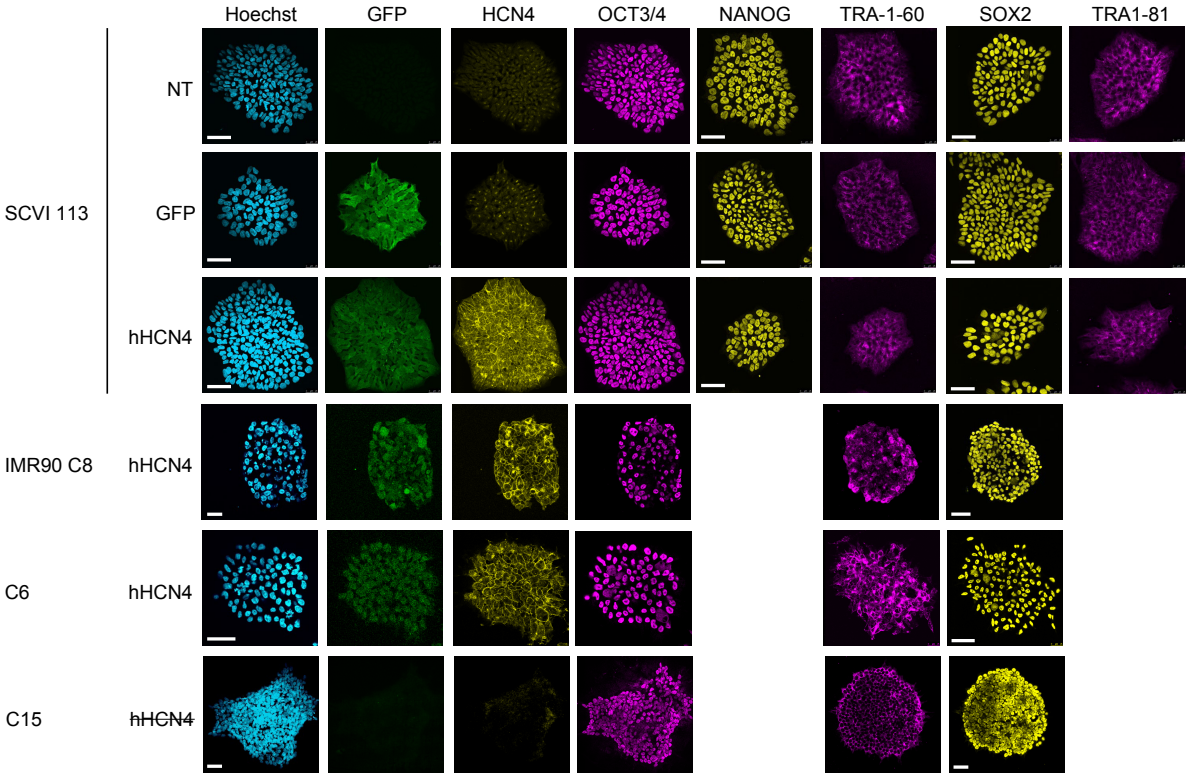

Figure 16. HCN4 expression analysis by IF in hHCN4-overexpressing and control hiPSC clones. Representative confocal images of IF staining of HCN4 and pluripotency markers (OCT3/4, NANOG, TRA-1-60, SOX2 and TRA-1-81) in control and hHCN4-overexpressing hiPSC clones. DNA counterstain with Hoechst. Scale bar 50μm. Generated hHCN4-hiPSC clones stably expressed HCN4 while maintaining pluripotency.

To confirm stable long-term expression and cellular localization of overexpressed hHCN4, I checked its expression by IF 90 days after transfection. I confirmed the correct localization of HCN4 at the cell membrane in all the hHCN4-overexpressing cell lines. HCN4 expression was not detected in GFP, NT and C15 control hiPSC lines (Figure 16). Moreover, transgenic cell lines maintained the expression of pluripotency markers, making them suitable for further differentiation and generation of overexpressing CM populations (Figure 16).

Finally, we[4] checked the functionality of the overexpressed hHCN4 protein in the hiPSC transgenic cell lines. Electrophysiological studies showed functional expression of I_f in hHCN4-hiPSCs, which activated slowly at -60 to -80mV, was blocked by Cs^+ (data not shown) and was detected in every cell of the generated clones (Figure 17A-C). The I-V curve showed the characteristic I_f voltage-current relationship with increasing current density upon higher hyperpolarization in all generated hHCN4-hiPSC lines (Figure 17B). hHCN4-hiPSCs generated with SCVI 113 parental hiPSC line showed activation at less negative voltages (-60mV vs. -80mV, Figure 17B) and stronger activation, with an average current density of 61.61±19.45pA/pF at -120mV, showing almost a ten-fold increase compared to overexpressing cell lines generated from C6 and IMR90 C8 (5.05±1.37pA/pF and 7.93±1.57pA/pF current intensity, respectively).

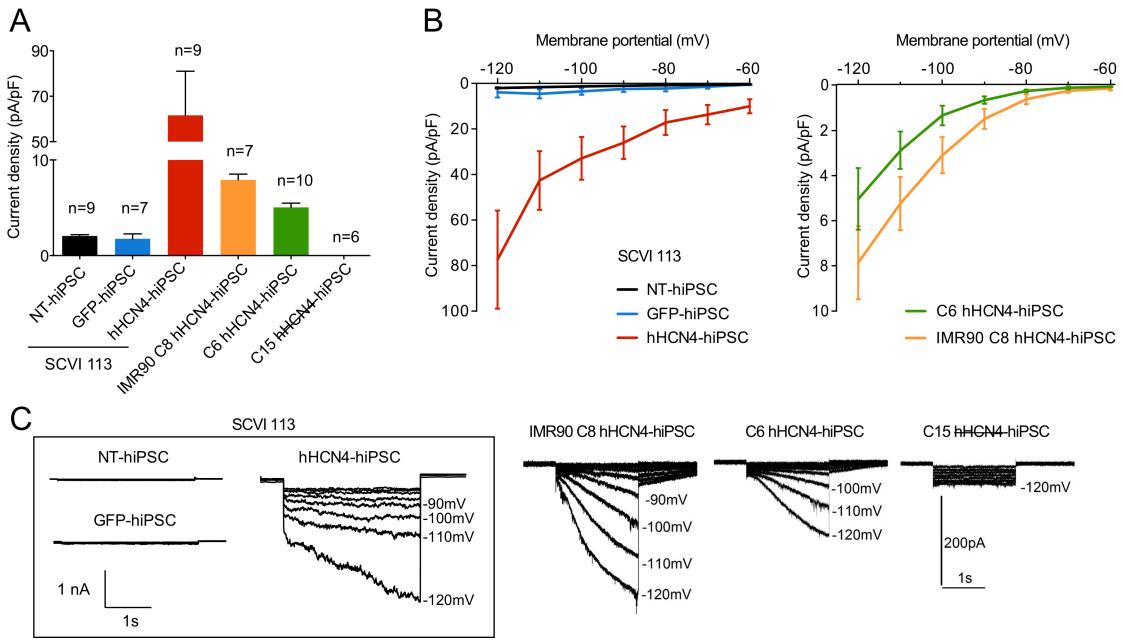

Figure 17. Electrophysiology analysis of hHCN4-hiPSCs. A) Average I_f intensity at -120mV in control and hHCN4-overexpressing cell lines. The number of cells analyzed from each cell line is indicated. **B)** Current-voltage relationship (I-V curve) of I_f in established hiPSC lines. Two graphs with scale adjusted to the different hHCN4-hiPSCs average current intensity are represented to aid data visualization. Cell number as in A; data represented as mean ± SEM. **C)** Representative traces of I_f time-course activation at different voltages (one representative cell selected). I_f was obtained during hyperpolarizing test pulses of 3 seconds between -60 and -120mV in 10mV increments from a holding potential of -40mV. Generated hHCN4-hiPSCs expressed functional hHCN4.

[4] In collaboration with Dr. Xiaohua Zhang in the laboratory of Prof. Dr. Martin Morad at the MUSC and Dr. Mirko Moroni in the laboratory of Prof. Dr. Gary R. Lewin at the MDC

IV. Characterization of cardiomyocytes derived from hHCN4-hiPSCs

Once I generated hHCN4-hiPSCs, I optimized their differentiation into CMs and validated their equivalent differentiation efficiency compared to control hiPSC lines. Next, I confirmed transgene expression throughout the differentiation process by FACS and IF and validated functional expression of I_f by electrophysiology in CMs derived from hHCN4-hiPSCs (hHCN4-hiPSC-CM). Finally, I characterized the electrophysiological properties, the morphology and the gene expression profile of hHCN4-hiPSC-CM.

IV.1 Optimization of cardiomyocyte differentiation

Several CM differentiation protocols showing both high yield of beating cells and cardiac troponin (TNNT2) positive cells after 10-20 days of differentiation are currently available. Despite the high level of efficiency and reproducibility of these protocols, a few optimization steps are necessary due to cell line-to-cell line variability and intrinsic variations in cell culture conditions. I used a monolayer directed CM differentiation protocol based in the sequential activation and inhibition of the WNT signaling pathway by the addition of small molecules (Lian *et al.*, 2012) (Figure 19A. Described in detail in Material and methods: section II.8.1, page 45). The main aspects susceptible to optimization are the hiPSCs seeding density three days prior to differentiation initiation and the concentration and duration of the treatment with CHIR99021 (GSK3 inhibitor) at day 0 of differentiation. I scored the final CM differentiation efficiency of each clone by analyzing TNNT2 expression by FACS at day 15 of differentiation (data not shown) and also by visual evaluation of beating areas from two different differentiation experiments.

First, I tested the CM differentiation ability of hiPSC clones C2, C6, C7 and C15 generated by HFF reprogramming with episomal vectors. For that purpose, I designed an optimization experiment where I tested three different hiPSC seeding densities treated during two different incubation times, keeping a constant CHIR99021 concentration of 6μM. In the final experiment, I plated hiPSCs at 20,000, 25,000 and 30,000 cells per cm^2 and treated them in duplicates with 6μM CHIR99021 during 24 or 48h (Figure 18A). With the exception of C6, all tested hiPSC clones differentiated into CM following most of the tested protocols. Among all the conditions tested, differentiation using 20,000 cells per cm^2 and 24h treatment with 6μM CHIR99021 was, on average, the most efficient for clones C2, C7 and C15 (Figure 18A).

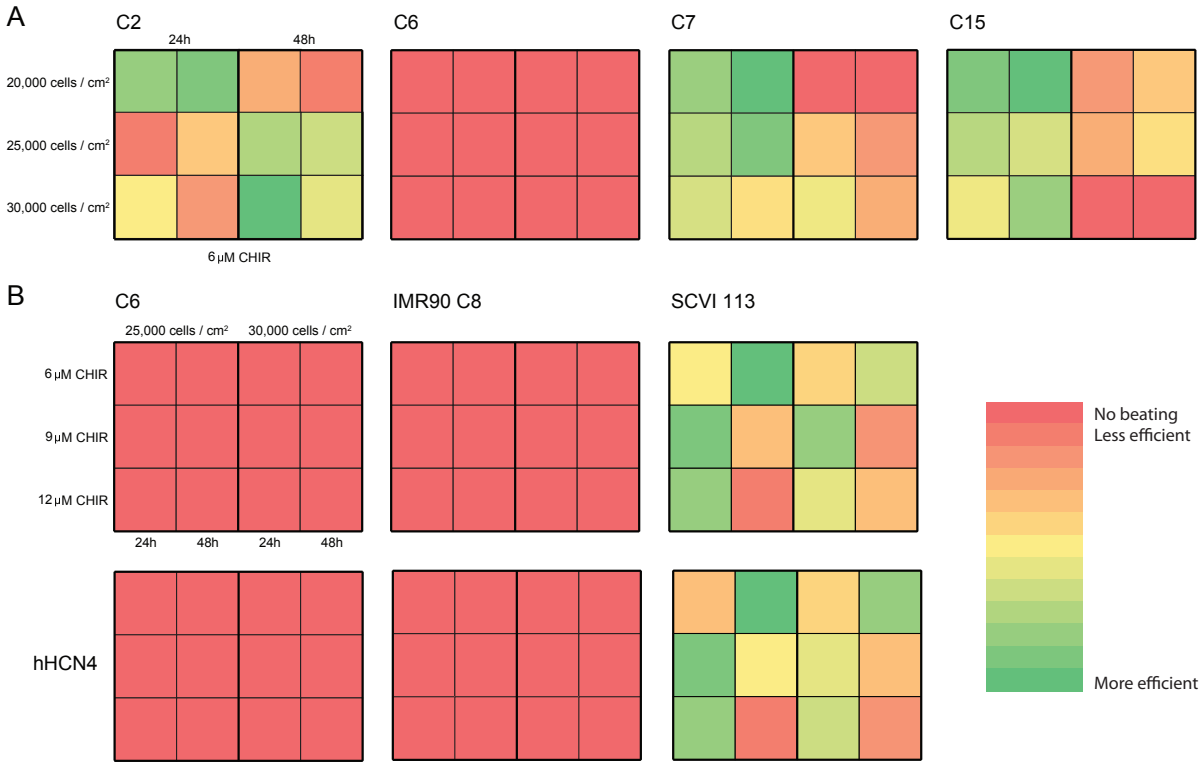

Figure 18. Assessment of optimal CM differentiation protocol. Scheme of a 12 well plate design for the CM differentiation optimization experiments of **A)** generated hiPSC clones by HFF reprogramming and **B)** SB-mediated transgenic hHCN4-hiPSCs and their respective parental hiPSC lines. Color code shows most (green), intermediate (orange, yellow) or less (red) efficient differentiation conditions using the average score of two optimization experiments calculated by size of beating areas and TNNT2-expressing cells percentage at day 15 of differentiation. Conditions where no beating was observed are labeled in dark red. C6 and IMR90 C8 hiPSC lines did not differentiate into CM using any of the tested conditions.

Next, I decided to assess the differentiation conditions that would lead to less variability in CM yield using hHCN4-overexpressing and their parental non-modified hiPSC lines. For this optimization experiments, I tested two different hiPSC seeding densities using three concentrations and two different durations of CHIR99021 treatment. I plated hiPSCs at 25,000 and 30,000 cells per cm^2 and treated them with 6, 9 and 12µM CHIR99021 for 24 or 48h (Figure 18B). Among all the CM differentiation protocols tested for NT and hHCN4-overexpressing hiPSC lines from parental clones C6 and IMR90 C8, none of them displayed beating clusters (Figure 18B). Due to this limitation, these clones were excluded from further experiments.

Both non-modified and hHCN4-overexpressing cell lines from the parental clone SCVI 113 efficiently differentiated into CM with most of the differentiation conditions tested. Moreover, nearly the same conditions yielded the highest differentiation efficiencies in both cell lines, indicating that SB-mediated transgenesis procedure did not alter differentiation ability of SCVI 113 hiPSC line and transgene expression did not

interfere with the differentiation process. Among all the conditions tested, differentiation using 25,000 cells per cm^2 and 48h treatment with 6µM CHIR99021 was, on average, the most efficient for non-modified and hHCN4-overexpressing hiPSC lines (Figure 18B). In light of these results, I decided to continue the characterization of hHCN4-hiPSC-CM using the hHCN4-hiPSC line generated with the reference hiPSC line SCVI 113. Both non-transfected (NT-hiPSCs) parental cell line and the transgenic cell line generated by SB and pT2-GFP vector (GFP-hiPSCs) were used as controls.

Once I identified the most efficient CM differentiation conditions for SCVI 113, I tested again four different conditions in 6 well plate format (the final format used for all experiments) to validate the most reproducible protocol for all NT, GFP and hHCN4-overexpressing bulk and clonal hiPSC lines after scaling-up. I plated hiPSCs at 25,000 cells per cm^2 and treated them with 6 and 9µM CHIR99021 during 24h. Surprisingly, bulk hHCN4-hiPSCs efficiently differentiated into CM showing comparable efficiency to the clonal population (data not shown). The highest yield of CM at day 15 of differentiation was achieved by seeding hiPSCs at 25,000 cells per cm^2 and 24h treatment with 6µM CHIR99021. Therefore, I adopted these conditions for further differentiation experiments.

IV.2 hHCN4-hiPSCs efficiently differentiate into cardiomyocytes

Once I established the optimal conditions for CM differentiation of NT, GFP and hHCN4-hiPSC lines generated from the parental hiPSC line SCVI 113 (Figure 19A), I characterized the resulting CM populations from control and hHCN4-overexpressing cell lines. Robust beating was observed in CM cultures derived from all cell lines from day 7 to 10 of differentiation. I characterized the expression of CM specific markers by IF and validated the expression of TNNT2 and NKX2-5 in all cell lines already after 9 days of differentiation (Figure 19B). Moreover, when observed at high magnification, the presence of structured myofilaments giving the typical striated pattern in CMs could be clearly observed in hiPSC-CMs generated from all cell lines (Figure 19B, detail).

To quantify the CM differentiation efficiency I also analyzed the expression of TNNT2 and NKX2-5 by FACS (Figure 20A). At day 9 of differentiation, a high percentage of the population was TNNT2 positive. No significant differences between hiPSC-CMs derived from NT (77.8±3.1%), GFP (77.6±11.3%) or hHCN4-hiPSCs (79.0±7.2%) were observed (Figure 20B). Likewise, the majority of the cells were NKX2-5 positive at day 9 of differentiation and no differences were found between NT (68.1±9,4%), GFP (65.4±9,2%) and hHCN4 (64.0±10.7%) cell lines (Figure 20A, B). Thus, I concluded that hHCN4-hiPSCs can differentiate into CMs with similar levels of efficiency than control cell lines.

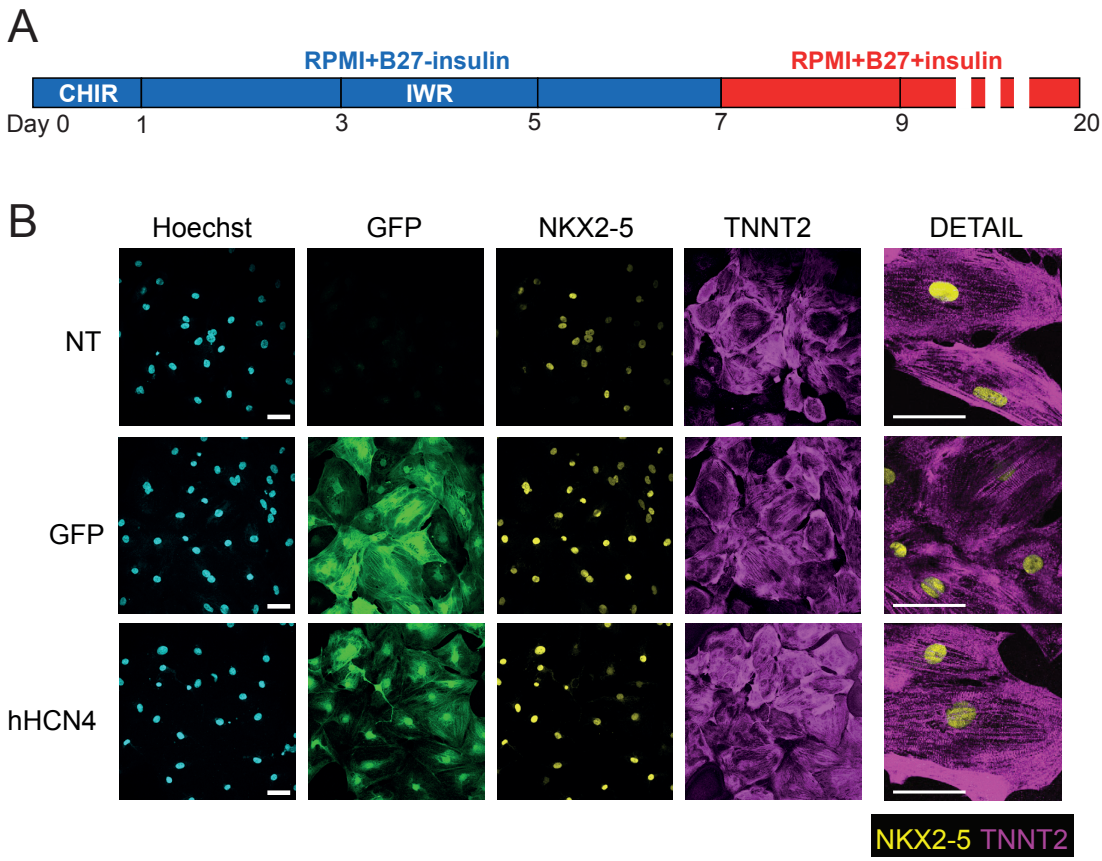

Figure 19. CM differentiation of hHCN4-overexpressing and control hiPSC lines. A) Schematic timeline representation of the final optimized CM differentiation protocol. **B)** Representative confocal images of CM derived from hHCN4-overexpressing and control cell lines at day 9 of differentiation (beating cultures). Expression of cardiac specific markers (TNNT2 and NKX2-5) was confirmed in all the generated hiPSC-CMs by immunostaining. DNA counterstain with Hoechst. Detail images at higher magnification (rightmost column) show the typical striated pattern of well-organized myofibrils. Scale bar 50μm. hHCN4-hiPSCs efficiently differentiated into CMs.

Despite the traditional role of NKX2-5 as master regulator of CM development, several publications have recently identified the SA nodal cells progenitor population as a cardiac mesodermal population characterized by the lack of NKX2-5 expression. Moreover, it has been shown that upon differentiation, pacemaker-like cells remained negative for NKX2-5 expression while expressing other CM-specific (TNNT2) and SA nodal cells markers (Birket et al., 2015; Protze et al., 2017). For this reason, I further investigated the expression of NKX2-5 within the TNNT2-expressing population of generated CM at day 9 of differentiation. However, the majority of TNNT2-expressing cells were also expressing NKX2-5 in all cell lines, NT (77,19±7,39%), GFP (86,47±5,18%), hHCN4 (75,90±11,73%) and no significant differences could be found between them (Figure 20C).

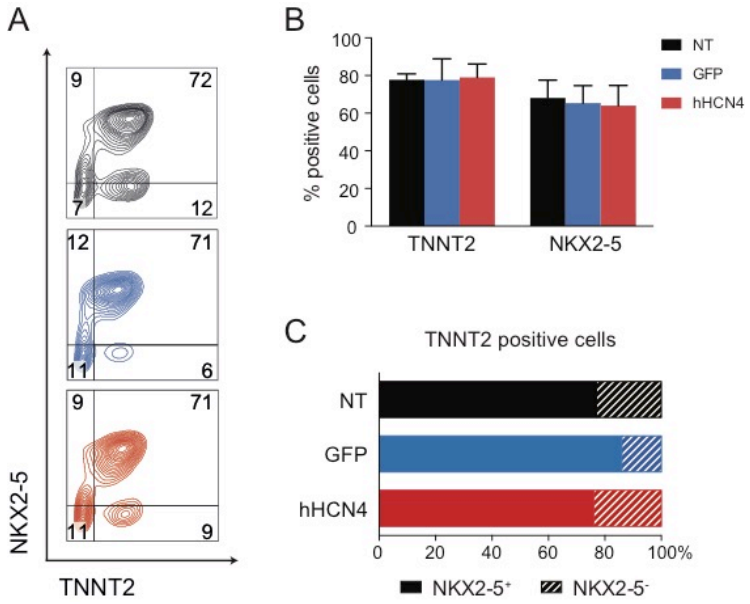

Figure 20. CM differentiation efficiency of hHCN4-overexpressing and control hiPSC lines. A) Representative FACS plots displaying TNNT2 and NKX2-5 staining of NT (black), GFP (blue) and hHCN4-hiPSC-CM (red). **B)** CM differentiation efficiency at day 9 of differentiation quantified by FACS and shown as the percentage of TNNT2 and NKX2-5 positive cells. Data represented as mean ± SEM of three differentiation experiments. No significant differences were found between different hiPSC-CMs. **C)** Percentage of positive and negative NKX2-5 cell populations within TNNT2 expressing hiPSC-CMs at day 9 of differentiation. Average values of three differentiation experiments are shown. No significant differences were found between hiPSC-CMs. All hiPSC lines showed an equivalent yield of CM upon differentiation, as judged by TNNT2/NKX2-5 expression.

IV.3 hHCN4-hiPSC-CM stably overexpress hHCN4 protein and display I_f

Once I tested the CM differentiation ability of SB-mediated transgenic GFP and hHCN4-hiPSC lines and validated equivalent CM differentiation efficiency with the corresponding non-modified NT-hiPSC line, I studied transgene expression throughout the CM differentiation process. As a first approach, I analyzed GFP expression from day 0 to day 25 of CM differentiation by FACS. GFP and hHCN4 cell lines remained more than 95% of GFP-expressing cells throughout the entire differentiation process (Figure 21A). At every time point measured, the GFP-overexpressing control cell line showed higher GFP mean intensity than the hHCN4-overexpressing cell line. This difference could be due to: i) a less efficient IRES-mediated translation provided by pT2-hHCN4-GFP integrated transposon (Figure 6); ii) differences in copy number; or iii) different integration sites of the transgene cassette in the different cell lines.

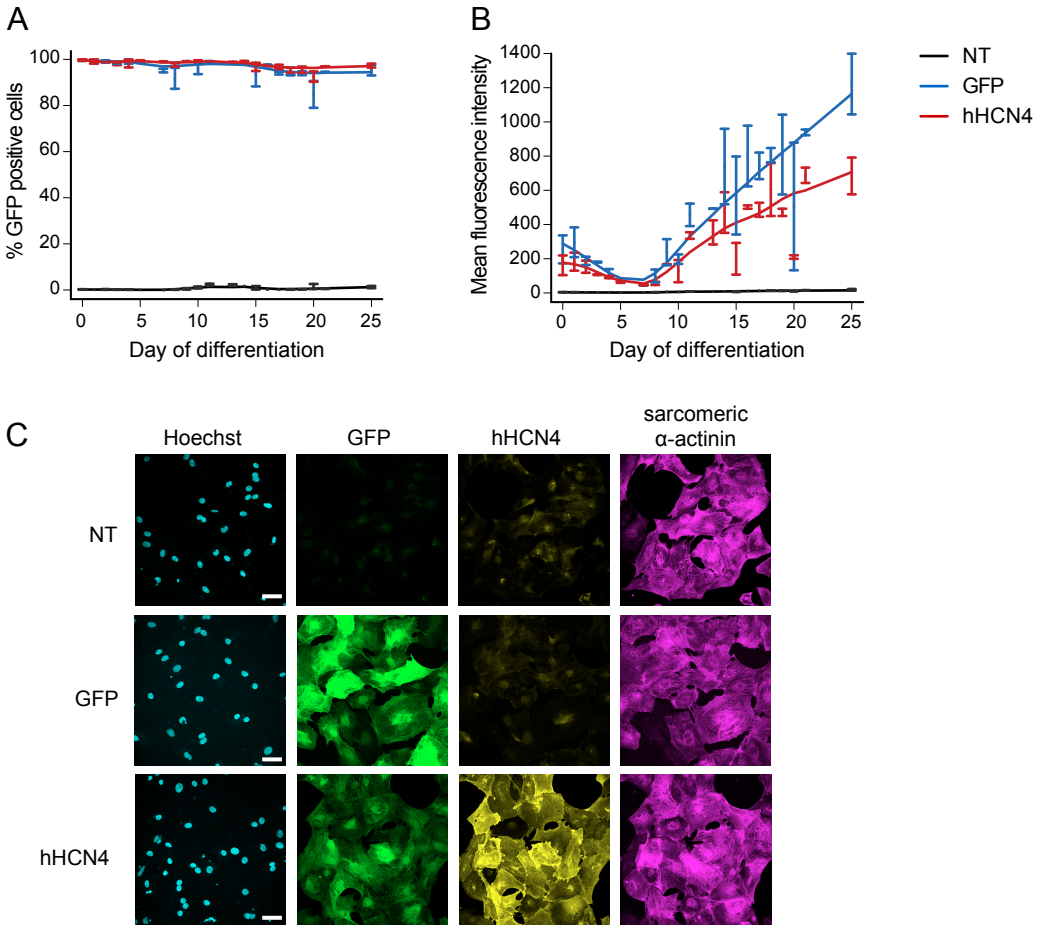

Figure 21. Transgene expression during CM differentiation. A) Percentage of GFP-positive cells and **B)** mean fluorescence intensity of NT, GFP and hHCN4 cell populations analyzed by FACS at different days of CM differentiation. Data represented as mean ± SD of two differentiation experiments. **C)** Representative confocal images of IF staining of HCN4 and sarcomeric α-actinin in CM derived from hHCN4-overexpressing and control cell lines at day 9 of differentiation (beating cultures). DNA counterstain with Hoechst. Scale bar 50µm. Overexpressing cell lines maintained transgene expression through CM differentiation and hHCN4-hiPSC-CM clones showed stable HCN4 overexpression.

Interestingly, both GFP and HCN4 showed the same trend in GFP expression during CM differentiation. GFP mean intensity decayed slightly from day 3 to 7 of differentiation as compared to hiPSCs (day 0 of differentiation), and increased markedly every day from day 8 until day 25 of differentiation, when the highest fluorescence intensity was measured (Figure 21B). This tendency in transgene expression was expected because of the CAG promoter gene expression regulation: previous studies have shown that transgene expression under CAG promoter is significantly higher in CM population compared to other cell types, including hiPSCs and ESCs (Orbán *et al.*, 2009).

Next, I studied HCN4 expression in generated CM by IF. CMs differentiated from hHCN4-hiPSCs showed clear overexpression of HCN4 compared to those generated from NT and GFP-hiPSC control cell lines at day 9 (Figure 21, 25) and 20 (Figure 25) of differentiation. HCN4 expression was not limited to the cell membrane, since some signal

was detected in the cytoplasm. Interestingly, GFP and HCN4 expression levels did not correlate in hHCN4-hiPSC-CM.

To quantify and validate functional overexpression of HCN4, we[5] measured I_f in generated hiPSC-CMs. In agreement with protein expression data, hHCN4-hiPSC-CM showed increased I_f intensity compared with control hiPSC-CMs. hHCN4-hiPSC-CM showed significantly higher I_f density, exhibiting up to 4-fold increase when measured at -100mV (5.65±0.76pA/pF) in comparison with NT (1.40±0.37pA/pF) and GFP-hiPSC-CM (1.67±0.14pA/pF) (Figure 22A). I_f properties of hHCN4-hiPSC-CM displayed the characteristic voltage-activation dependence (Figure 22C, Basal), as well as typical I-V relationship, activating from -60mV and increasing current intensity at higher levels of hyperpolarization (Figure 22B, Basal). Moreover, we recorded I_f before and after treatment with 1µM isoproterenol, a ß-adrenergic receptor agonist. Upon ß-adrenergic stimulation, hHCN4-hiPSC-CM showed increased current densities (Figure 22B and C, Isoproterenol), confirming adequate pharmacological regulation of the overexpressed hHCN4.

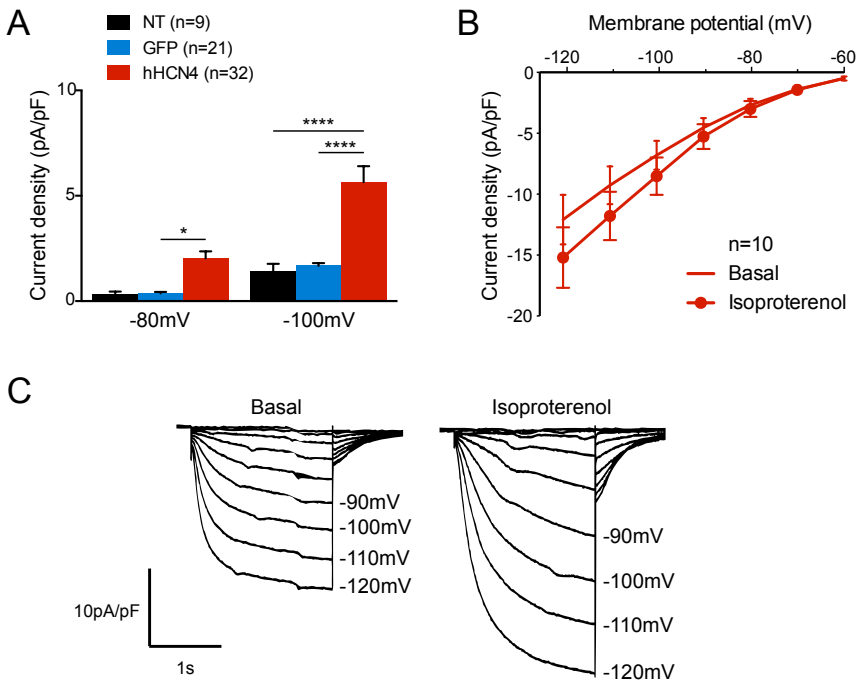

Figure 22. I_f expression characterization in hHCN4-hiPSC-CM. Analysis of single cell hiPSC-CMs at day 20 of differentiation. **A)** Average I_f intensity at -80mV and -100mV in control and hHCN4-hiPSC-CM. Data represented as mean ± SEM, *p<0,05, ****p<0,0001. The number of cells analyzed in each cell line is indicated. **B)** Current-voltage relationship (I-V curve) and **C)** representative traces of I_f time-course activation at different voltages (one representative cell) expressed by hHCN4-hiPSC-CM in basal conditions and upon 1µM isoproterenol treatment. Generated hHCN4-hiPSC-CM showed functional hHCN4 overexpression with the typical pharmacological regulation.

[5] In collaboration with Dr. Xiaohua Zhang in the laboratory of Prof. Dr. Martin Morad at the MUSC.

IV.4 hHCN4-hiPSC-CM show increased beating rate and similar action potential properties than control hiPSC-CMs

Electrophysiology of nodal CM is significantly different to that in working CM. The ability to generate spontaneous APs without external stimuli is a main characteristic of pacemaker cells (Morris & Kalman, 2014). To test whether hHCN4 overexpression through CM differentiation would affect spontaneous activity, I analyzed single cell cultures of hiPSC-CMs at day 20 of differentiation and assessed the percentage of spontaneously beating cells in the culture. Typically, around 20% of the analyzed cells displayed spontaneous beating activity, and no significant differences in this proportion were observed between control and hHCN4-hiPSC-CM (Figure 23A). Next, I decided to analyze the beating rate of spontaneously beating cells derived from the three cell lines. hiPSC-CMs derived from both control cell lines displayed a slow beating frequency which was below the levels of resting adult human heart rate (50-90bpm), probably influenced by dissociation and culture conditions. Interestingly, under similar conditions, hHCN4-hiPSC-CM displayed a significantly higher beating rate (72.48±31.59bpm) compared with NT (40.54±18.31bpm) and GFP-hiPSC-CM (34.36±19.74bpm) (Figure 23B), in agreement with previous studies carried out in HCN4-overexpressing and SA nodal-like CM (Saito *et al.*, 2015; Protze *et al.*, 2017).

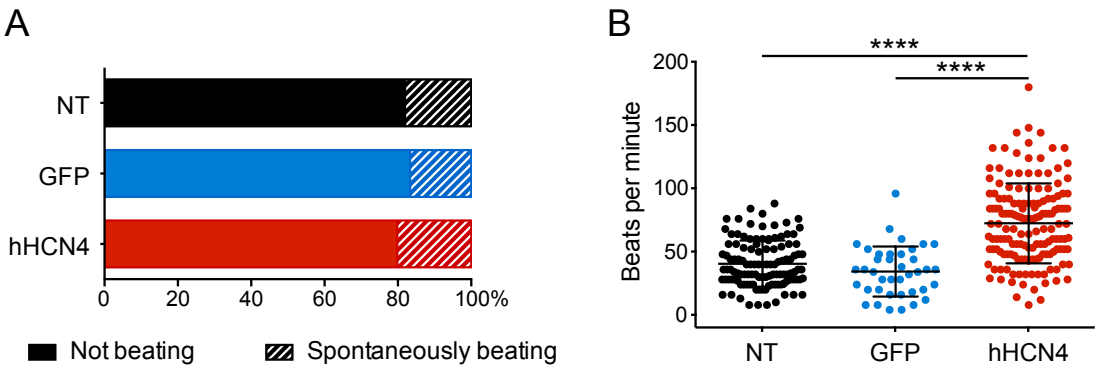

Figure 23. Spontaneous beating analysis in generated hiPSC-CMs. Analysis of single cell hiPSC-CMs at day 20 of differentiation. **A)** Average percentage of not beating vs. spontaneously beating hiPSC-CMs from control and overexpressing cell lines from three differentiation experiments. **B)** Quantification of spontaneous beating rate in NT (n=116), GFP (n=39) and hHCN4-hiPSC-CM (n=155) from three (GFP) and five (NT, hHCN4) differentiation experiments. Data represented as mean ± SD, ****p<0,0001. hHCN4-hiPSC-CM showed higher beating rate that control hiPSC-CMs.

Using the described CM differentiation protocol, the resulting hiPSC-CMs cultures are typically a mixture of ventricular, atrial and nodal CM. Another distinguishing feature between pacemaker and working CM is the profile of the generated APs. In order to determine the impact of hHCN4 overexpression in AP properties, we[6] analyzed several parameters of spontaneous and triggered APs from single cell hiPSC-CMs derived from

the different cell lines at day 20 in two differentiation experiments (Figure 24A). Average values of analyzed AP parameters are summarized in the table showed at Figure 24B. Overall, no significant differences were found between control and hHCN4-hiPSC-CM regarding their AP properties. Although pacemaker cells display a higher maximum diastolic potential (MDP, ~60mV) as compared to that of atrial and ventricular CM (~90mV), the average MDP in hiPSC-CMs generated from the three cell lines was closer to those displayed by pacemaker cells (Figure 24B, MDP). Likewise, although peak voltage tends to be lower in pacemaker cells, control and overexpressing hiPSC-CMs displayed similar values (Figure 24B, Peak).

A

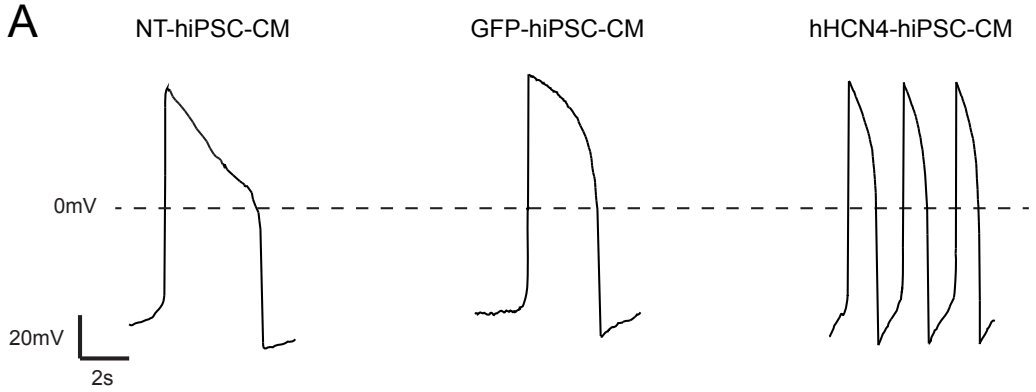

B

	MDP (mV)	Peak (mV)	Interval (s)	APA (mV)	APD90 (s)	APD50 (s)
NT-hiPSC-CM (n=10)	-60.71 ± 5.42	66.81 ± 20.03	4.68 ± 1.44	98.07 ± 8.02	1.96 ± 1.12	1.79 ± 1.03
GFP-hiPSC-CM (n= 9)	-56.55 ± 11.16	67.58 ± 32.60	4.58 ± 2.09	77.31 ± 21.95	1.28 ± 1.40	1.11 ± 1.32
HCN4-hiPSC-CM (n=16)	-60.77 ± 7.8	69.72 ± 30.60	3.72 ± 2.15	93.25 ± 18.72	0.84 ± 0.54	0.68 ± 0.53

Figure 24. AP analysis of generated hiPSC-CMs. Analysis of single cell hiPSC-CMs at day 20 of differentiation. **A)** Representative traces of recorded APs under current clamp of single cell hiPSC-CMs at day 20 of differentiation of NT, GFP and hHCN4-hiPSC-CM. Data represented as mean ± SD. **B)** Summary table of analyzed AP parameters. MDP, maximum diastolic potential; Peak, peak voltage; Interval, beat rate interval; APA, AP amplitude; APD90, APD50, AP duration at 90% and 50% of repolarization. No significant differences in AP properties were found between control and hHCN4-hiPSC-CM.

Taking a closer look at the distribution of single-cell APs, I observed more variability in AP values recorded in NT and GFP-hiPSC-CM than in hHCN4-hiPSC-CM (Figure 25). Although these differences were not statistically significant, GFP-hiPSC-CM (77.31±21.95mV) presented smaller APA values (a typical feature of pacemaker cells), as compared with NT (98.07±8.02mV) or hHCN4-hiPSC-CM (93.25±18.72mV) (Figure 24B). When I analyzed in detail single-cell AP parameters (Figure 25), an abnormal clustering of data in two different groups was observed. This could suggest some degree of technical

[6] In collaboration with Dr. Mirko Moroni in the laboratory of Prof. Dr. Gary R. Lewin at the MDC.

bias (*i.e.* a higher percentage of triggered vs. spontaneous APs were analyzed in the GFP-hiPSC-CM population) that could be normalized by analyzing a larger sample size.

Next, I studied in detail APs duration parameters. Similar to pacemaker cells, hHCN4-hiPSC-CM showed, in average, faster repolarization. This resulted in shorter AP duration at 90% and 50% of repolarization (Figure 24B, APD90, APD50) as compared with control hiPSC-CMs. I also analyzed single values distribution of APD90 and APD50 parameters, and I confirmed that hHCN4-hiPSC-CM presented a clear enrichment in cells with shorter AP duration in comparison with control hiPSC-CMs (Figure 25). Nevertheless, analysis of a larger number of cells derived from different differentiation experiments would help to further clarify the influence of hHCN4 overexpression on AP parameters.

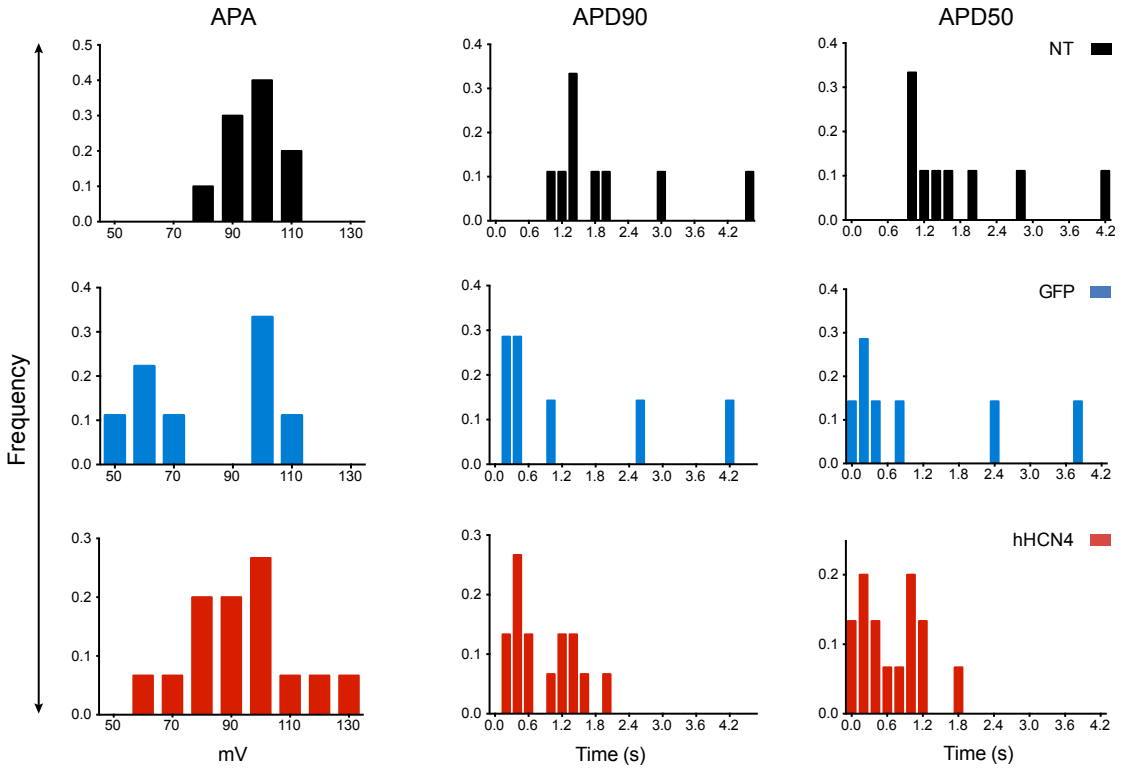

Figure 25. AP analysis of generated hiPSC-CMs (continuation). Frequency distribution of AP parameters obtained from single cell NT (black, n=10), GFP (blue, n=9) and hHCN4-hiPSC-CM (red, n=16) at day 20 of differentiation. APA, AP amplitude; APD90, APD50, AP duration at 90% and 50% of repolarization. hHCN4-hiPSC-CM showed tendency to have shorter AP duration.

IV.5 hHCN4-hiPSC-CM are enriched in cells with pacemaker-like morphology

It is well known that SA nodal cells show particular morphological characteristics that are substantially different to those displayed by ventricular and atrial CM. Working CMs have larger area and well developed myofibrils, in contrast to pacemaker cells that are smaller, have a large surface-volume ratio, and show disperse myofilaments (James *et al.*, 1966). In addition, SA nodal cells have been traditionally classified in 'spindle' cells when

showing an elongated shape, or 'spider' cells when they present several extensions (J. Wu et al., 2001). In order to investigate the proportion of pacemaker CM, I decided to analyze the morphological features of the generated hiPSC-CMs.

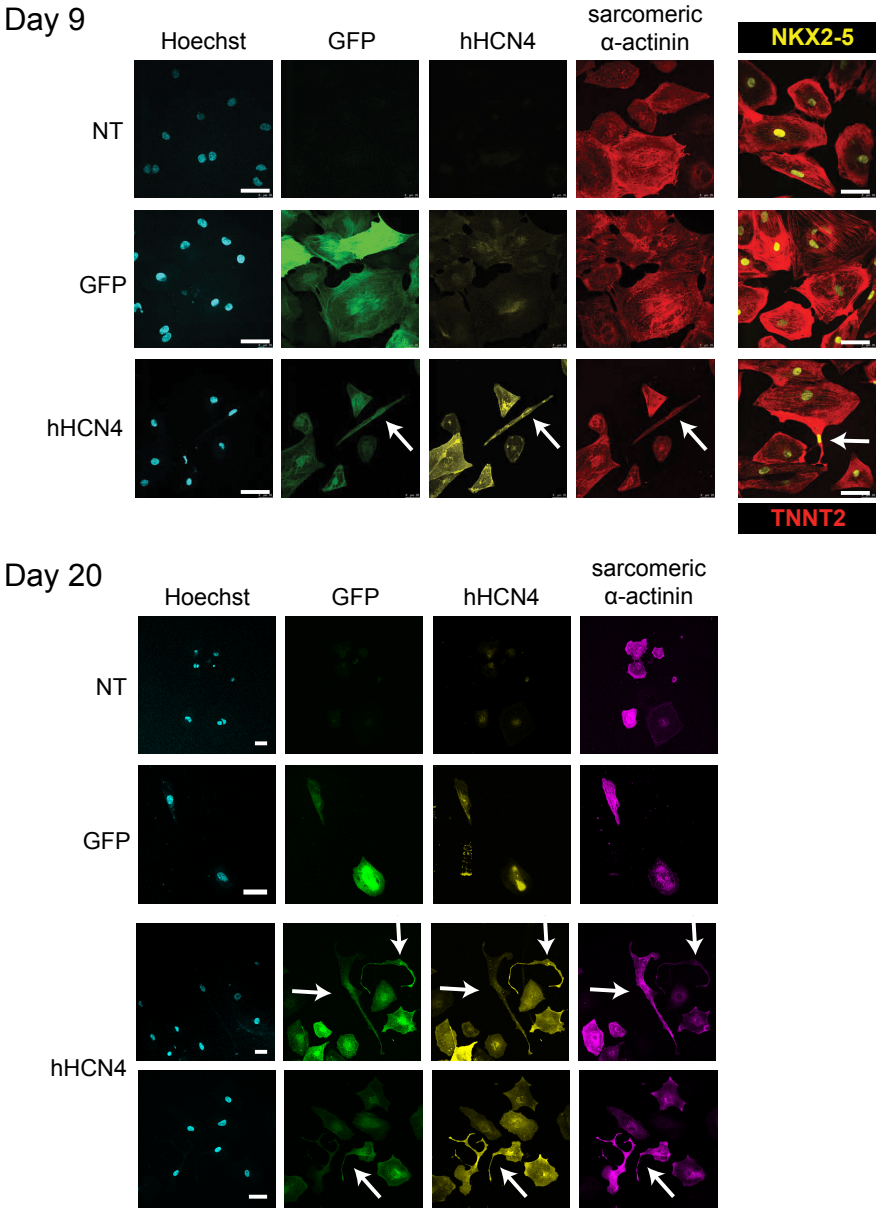

Figure 26. Morphological characterization of generated hiPSC-CMs. Representative confocal images of IF staining of HCN4, sarcomeric α-actinin, TNNT2 and NKX2-5 in hHCN4-overexpressing and control hiPSC-CMs at day 9 and 20 of differentiation. DNA counterstain with Hoechst. White arrows mark CM with pacemaker-like morphology. Scale bar 50µm. Spindle and spider cell types were identified in hiPSC-hHCN4-CM cultures.

During routine maintenance, I was able to identify spindle and spider cells in single-cell cultures of hHCN4-hiPSC-CM scattered between immature CM with typical polygonal shape (data not shown). To confirm the CM identity of these cells, I stained single-cell hiPSC-CMs preparations at day 9 and 20 of differentiation with the CM specific marker TNNT2 and sarcomeric α-actinin. I recognized CM displaying spindle or spider

morphology in hiPSC-CMs derived from all cell lines at day 9 and 20 of differentiation (Figure 26). However, these cell types appeared to be particularly frequent in hHCN4-hiPSC-CM.

I further quantified CM with spindle or spider cell morphology within single-cell hiPSC-CM cultures. CM displaying neither spindle nor spider morphology were labeled as 'other'. As expected, at day 9 most of hiPSC-CMs showed the usual geometric morphology in NT (96.21±2.68%, mean±SD), GFP (96.02±4.32%) and hHCN4-hiPSC-CM (83.48±5.71%). Interestingly, the percentage of these cells decreased at day 20 of differentiation, although they remained the most frequent cell type in NT (88.14±7.14%), GFP (86.67±13.33%) and hHCN4-hiPSC-CM (77.02±15.26%) (Figure 27A). hHCN4-hiPSC-CM showed a clear enrichment in pacemaker-like cells both at day 9 and 20 of differentiation. At day 9 of differentiation, approximately 4% of the control hiPSC-CMs displayed pacemaker-like morphology. Within this cell type, spindle cells were more frequent than spider cells (12.27±1.16% vs. 4.25±1.01%) in hHCN4-hiPSC-CM and both morphologies were enriched compared to control hiPSC-CMs. At day 20 of differentiation, pacemaker-like cells in control hiPSC-CMs displayed spindle and spider morphologies in similar proportions, consisting each in approximately 6% of the total population. On the contrary, spider cells were more frequent than spindle cells (14.57±12.01% vs. 8.41±4.97%) in hHCN4-hiPSC-CM. (Figure 27A). When analyzed in detail, spindle and spider cells showed a similar range of hHCN4 staining intensity, suggesting that the level of expression of hHCN4 is not directly correlated with the display of specific morphologies (Figure 26).

It is widely accepted that membrane capacitance correlates with cell size. Moreover, studies in CM have concluded that membrane capacitance is a reliable measurement to estimate cell volume in this particular cell type (Satoh *et al.*, 1996). In order to investigate cell size distribution of hiPSC-CMs derived from the three different cell lines, I quantified and compared capacitance data from hiPSC-CMs whole-cell patch clamp experiments. hHCN4-hiPSC-CM showed on average smaller cell volume, resulting in lower capacitance values (34.73±18.45pF), compared with NT (42.34±31.24pF) and GFP-hiPSC-CM (50.49±23.50pF) (Figure 27B). hHCN4-hiPSC-CM were significantly smaller when compared to GFP-hiPSC-CM control, which also showed an increased cell size when compared to NT-hiPSC-CM.

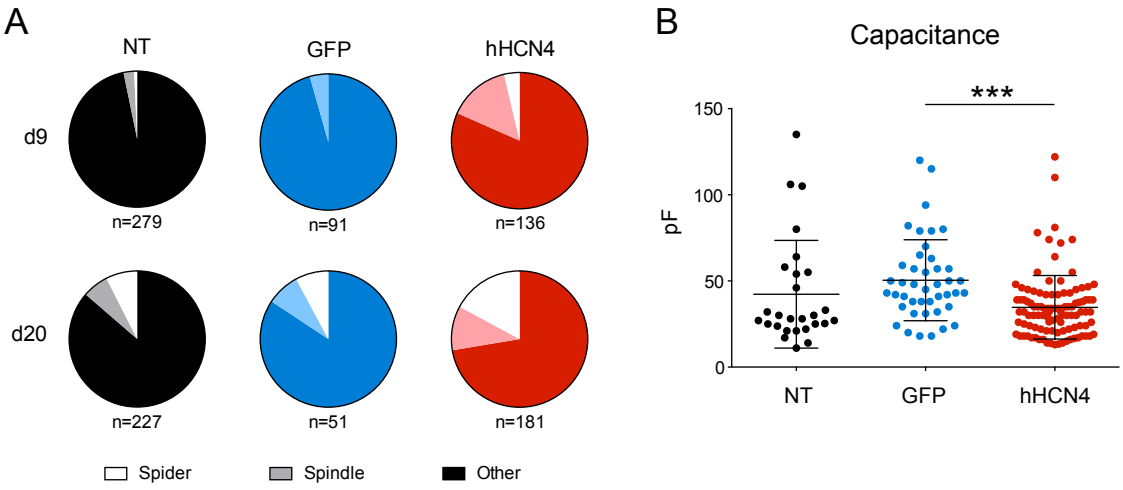

Figure 27. Cell type distribution and capacitance quantification in generated hiPSC-CMs. A) Pie charts showing percentages of spider (white), spindle (light color) and other (dark color) cell types in hiPSC-CMs at day 9 and 20 of differentiation. Data represented as the average value of at least two differentiation experiments. The number of cells analyzed per condition is indicated below each chart. **B)** Average cell capacitance values from at least three differentiation experiments of NT (n=24), GFP (n=43) and hHCN4-hiPSC-CM (n=102) at day 20 of differentiation. Data represented as mean ± SD, ***p<0.005. hHCN4-overexpressing cultures were enriched in CM with pacemaker-like morphology and showed a tendency to be smaller in size compared with control hiPSC-CMs.

IV.6 hHCN4-hiPSC-CM show a similar gene expression profile than control hiPSC-CMs

Pacemaker CM specific features are the consequence of a tightly regulated gene expression program resulting in a specific profile of ion channels, among other proteins, that have been used as molecular markers for SA nodal cells. To test whether overexpression of hHCN4 would influence gene expression in differentiated CM, I analyzed the expression of different CM genes by qPCR, including those differentially expressed in pacemaker CM compared with atrial and ventricular CM.

I analyzed gene expression of hiPSCs (day 0 of differentiation) and hiPSC-CMs at day 9 and 20 of differentiation of hHCN4-overexpressing and control cell lines (Figure 21). The expression of pan-CM markers (Figure 28A) was significantly increased in both day 9 and day 20 CM and was consistent among the different cell lines, confirming the equal capacity and efficiency of CM differentiation in all analyzed cell lines. As expected, *HCN4* expression was significantly higher in hHCN4-overexpressing cell lines compared to controls at all time points tested (Figure 28B, first panel). hHCN4-hiPSC-CM showed a 2.5-fold increase in *HCN4* expression both at day 9 (8.9±0.6ΔΔCt) and day 20 (9.6±0.7ΔΔCt) compared to NT (3.2±0.9ΔΔCt at day 9 and 4.0±0.5ΔΔCt at day 20) and GFP-hiPSC-CM (3.2±1.2ΔΔCt at day 9 and 4.6±1.0ΔΔCt at day 20). I did not find differences in the expression of another member of the HCN family, *HCN2*, which showed very low

expression levels in all cell lines at the analyzed time points (Figure 28B). In addition, I also analyzed the levels of expression of several ion channels related to pacemaker function. An increased expression of *KCNJ3* and a decreased expression of *SCN5A* have been described in pacemaker cells when compared to atrial or ventricular CMs. However, I could not find significant differences in the expression of these genes in hHCN4 vs. control hiPSC-CMs (Figure 28B).

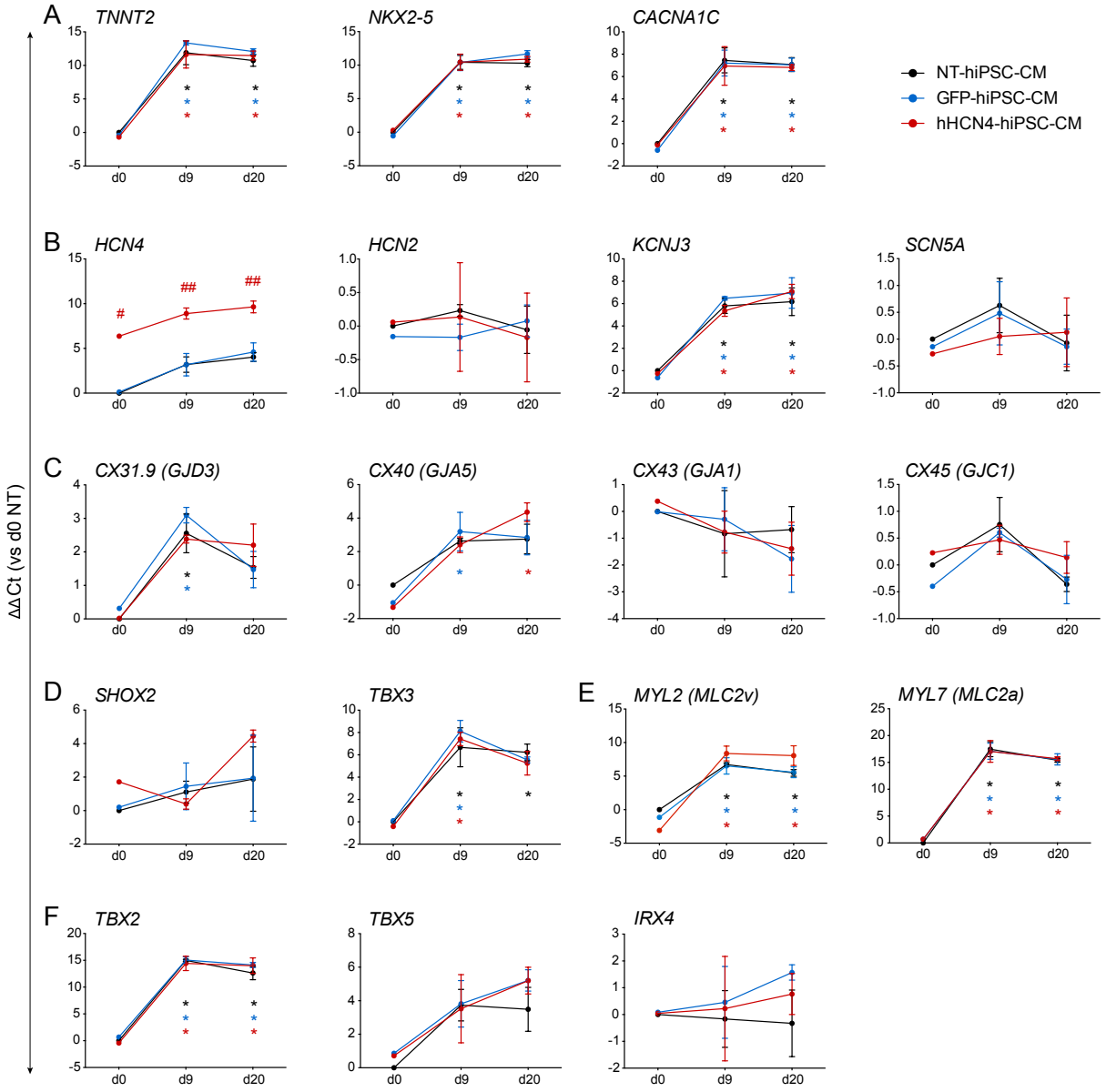

Figure 28. Gene expression profile of hHCN4-hiPSC-CM during differentiation. Gene expression was analyzed at day 0 (d0, hiPSCs), 9 (d9) and 20 (d20) of CM differentiation by qPCR. Graphs show the expression levels of **(A)** pan-CM, **(B)** ion channels, **(C)** connexins, **(D)** SAN transcription factors, **(E)** myosins and **(F)** working CMs transcription factors genes, normalized to 18S rRNA. Data represented as mean ± SEM of three biological replicates. #p<0.05 vs. NT and GFP; ##p<0.005 vs. NT and GFP; *p<0.05 vs. d0. No significant differences were found between NT vs. GFP and d9 vs. d20 for any of the analyzed genes. hiPSC-CMs derived from hHCN4-hiPSCs showed a similar gene expression profile to those derived from NT or GF-hiPSCs.

The Cx expression profile in working CM and specialized CM of the CCS and the SAN has been shown to be fundamentally different and highly correlated with the primary contractile (fast AP conduction) or electrical (slower and synchronized AP conduction) function of these cells. *CX43* is the main Cx expressed in working CM while its expression is reduced and almost absent in pacemaker CM, where *CX40* and *CX45* are typically expressed. Similarly, it has been suggested that *CX31.9* is expressed in the human SAN by analogy with the expression of its homologous *Cx30.2* in the mouse SAN. Although there seemed to be a higher expression of *CX40* (4.4±0.6ΔΔCt in hHCN4 vs. 2.8±0.9ΔΔCt in NT and 2,8±1.0ΔΔCt GFP-hiPSC-CM) and *CX31.9* (2.2±0.6ΔΔCt in hHCN4 vs. 1.5±0.3ΔΔCt in NT and 1.5±0.5ΔΔCt GFP-hiPSC-CM) in hHCN4-hiPSC-CM at day 20 of differentiation, no significant differences were found among the different cell lines in terms of Cx expression (Figure 28C).

Finally, to complete the molecular characterization of hHCN4-hiPSC-CM, I analyzed the expression of several transcription factors involved in heart development, which are mainly expressed in atrial and ventricular CM (Figure 28F) or specifically expressed in SA nodal cells (Figure 28D). I did not find significant differences between the different cell lines in different days of CM differentiation. Moreover, gene expression analysis of atrial (*MYL7*) and ventricular (*MYL2*) specific myosin light chain did not show any significant differences between hHCN4-overexpressing and control cell lines (Figure 28E).

Overall, overexpression of *HCN4* did not affect the expression of the analyzed genes involved in CM function and development. Gene expression analysis was performed at day 9 (already beating cultures) and 20 (mature CM) of differentiation. Differences derived from HCN4 expression arising at earlier time points or attenuated upon additional CM differentiation/maturation cannot be excluded.

Discussion

Cardiovascular diseases remained the leading cause of morbidity and mortality worldwide over the past decade. The number of patients with cardiovascular diseases increases every year due to the aging of human population. In 2015, ~83.5 million people in Europe[7] and ~27.6 million people in the United States were diagnosed with cardiovascular disease. By 2035, this number is predicted to rise to more than 130 million patients only in the United States (Benjamin et al., 2018; Timmis et al., 2018).

The cause or consequence of many cardiovascular diseases is the irreversible loss of CMs. The adult heart has very limited regenerative capacity, most of adult CMs are not proliferative and although cardiac stem cells have been described within the cardiac tissue, their differentiation capacity is insufficient to compensate the CM loss associated to heart diseases (Bearzi et al., 2007; Beltrami et al., 2003). After cellular damage, dead CMs are replaced by fibroblasts, promoting the formation of scar areas that display abnormal electrophysiological and contractile properties. The presence of this altered tissue within the myocardium lead to cardiac remodeling that often induces heart failure and additional cell damage (Burridge et al., 2012).

Available treatments are mainly palliative and do not prevent disease progression, which ultimately leads to heart failure and leaves transplantation as last option. Unfortunately, existing sources for cardiac transplantation are restricted by lack of donor organs and cells. Due to these limitations, transplantation of more accessible non-cardiac cells including skeletal muscle cells, bone marrow-derived cells and MSCs has been tested in patients with different heart conditions. These studies reported just minor improvement in cardiac function that was attributed to paracrine effect, making evident the need for new approaches to generate de novo CMs (Burridge et al., 2012; Hastings et al., 2014). The establishment of hESCs (Thomson et al., 1998) and hiPSCs (Takahashi et al., 2007) coupled with the development of efficient and reproducible CM differentiation protocols under defined conditions, has made possible the generation of human CMs on a clinically relevant scale, and to consider feasible the use of hPSC-CMs for regenerative therapies (Burridge et al., 2014; Karakikes et al., 2014; Lian et al., 2012, 2013).

Although considerable efforts have been made to improve available CM differentiation protocols, an unsolved issue is the heterogeneity of the resulting CM population that includes cardiac cells with ventricular, atrial and nodal features (J. Zhang et al., 2009). The development of directed differentiation protocols to generate the different subtypes of CMs is essential for regenerative medicine, as different heart diseases requires CMs with specific electrophysiological and contractile properties. Working CMs are required to provide the contractile force in atria and ventricles and would be necessary to repair affected myocardium after ischemic injury. Instead, pacemaker CMs would be

[7]Cardiovascular Disease Statistics of the European Society of Cardiology member countries, including European, non-European former Russian Republics, East Mediterranean and North African countries.

needed to restore damaged components of the CCS involved in different types of arrhythmias.

Normal heart function relies on the generation and propagation of electrical impulses by the specialized CMs of the CCS. Under several pathologic conditions and during aging, the CCS undergoes irreversible degeneration that can result in lethal cardiac arrhythmias, including SND, and atrial or ventricular fibrillation. Available antiarrhythmic drug therapy is not suitable for long-term treatment of these heart rhythm disorders and ultimately the implantation of an electronic pacemaker is required. Every year, more than 200,000 and 500,000 electronic pacemaker implantations are performed in the United States and Europe respectively. Only in Germany, the most active European country, more than 100,000 devices were placed during 2016 (Benjamin et al., 2018; Raatikainen et al., 2017). Although electronic devices have been improved for more than five decades, they still have limitations such as inadequate autonomic response, limited battery life, risk of infections, and adverse cardiac remodeling. These issues may be overcome by the development of biological pacemakers (Boink et al., 2012; Rosen et al., 2004).

Several strategies have been investigated in the last years to develop gene and cell therapy methods to restore pacing activity in damaged hearts. A variety of approaches involving gene delivery of ion channels or transcription factors involved in SAN function and development by viral vectors or in combinations with different cellular platforms have been already tested to generate a candidate biological pacemaker. Although initial results are encouraging, the general outcome of these studies is partial recovery of the heart rate that does not achieve complete physiological demands and do not persist longer than few weeks. Importantly, the vast majority of these approaches have been developed in animal models and still not translated to human cells (Husse & Franz, 2016; Saito et al., 2018). For these reasons, we decided to develop a combined cell and gene therapy strategy, where the non-viral integrating transposon system SB, already proven safe and efficient for gene delivery in clinical applications, is used to overexpress the ion channel hHCN4 in hiPSCs as a platform for differentiation of pacemaker CMs.

I. From human fibroblasts to hHCN4-hiPSC-CM: workflow validation

One important goal of this project was to develop a workflow that would resemble and accomplish critical steps of hHCN4-hiPSC-CM generation for future clinical applications. For this matter, I established a working pipeline from hiPSCs establishment by fibroblast reprogramming to hHCN4-overexpressing CMs generation.

To generate hiPSCs, I undertook a classical procedure in which I transfected fibroblasts with expression vectors for the 'reprogramming factors' (i.e. POU5F1 (OCT3/4), SOX2, KLF4, LIN28 and MYC) and used a cocktail of small molecules to enhance reprogramming efficiency (Okita et al., 2011; Yu et al., 2011). The initial protocol involved

seeding the transfected fibroblasts onto inactivated MEFs to promote maturation and stabilization of the reprogrammed cells after the initial proliferation phase (Figure 10A). For clinical applications, however, the use of free of animal-derived products is preferred. For this reason, although I continued using and characterizing the firstly generated hiPSC clones, I established in parallel a feeder-free reprogramming protocol using a totally defined culture media (Yu et al., 2011) that resulted in reprogramming efficiencies comparable to the original one (data not shown). Additionally, I used Matrigel (undefined extracellular matrix produced by a mouse sarcoma cell line) as coating surface for the initial culture steps of hiPSCs. Although I further adapted hiPSCs culture to xeno-free conditions combining VTN-coating and E8 medium without major difficulties, I did not test this culture setup in newly generated hiPSCs clones.

I performed the conventional experiments to validate pluripotency and genome stability of the generated hiPSCs clones (Takahashi et al., 2007; Thomson et al., 1998). The majority of the tested clones expressed pluripotency markers (Figure 11), showed normal karyotype (Figure 13) and efficiently differentiated into cell types from the three germ layers (Figure 12), including CMs (Figure 18). However, one hiPSC clone (C6) displayed impaired differentiation capacity towards CMs (Figure 18). These data highlighted the importance of fully characterize derived hiPSC clones prior further use, especially for clinical applications. Although here I used the teratoma assay to validate pluripotent ability of the generated hiPSC clones, this technique is tedious and involves animal experimentation. In addition, teratoma formation requires typically several weeks, lengthening the already time-consuming process of hiPSC generation (Gropp et al., 2012; Ratcliffe et al., 2011). To overcome these limitations, a microarray system named 'PluriTest' has been developed. It is based on the comparison of transcripts from newly generated hiPSC clones with the gene expression profile of a large database of cell samples known to be pluripotent (Müller et al., 2011). An interesting alternative could be to validate pluripotency of hiPSC clones with PluriTest and combine it with the required CM differentiation optimization step (described in detail in Discussion: section III.1, page 94) to accelerate the process from hiPSCs to functional hHCN4-hiPSC-CM generation.

In parallel to hiPSCs generation, I designed and constructed the pT2-hHCN4-GFP vector to generate stable hHCN4-overexpressing cell lines by SB-mediated genomic integration (Figure 6). After transfection into the target cells, this construct should provide: i) GFP expression for selection of transgenic cells, ii) a template sequence for the integration of the overexpression cassette into the genome by coexpression with SB100X transposase, and iii) functional expression of hHCN4, I_f. All these features were first tested and validated in HEK293T cells. As expected, HEK293T cells transfected with pT2-hHCN4-GFP in combination with the SB100X expression vector expressed GFP (Figure 7-9), allowing their purification by cell sorting. Moreover, the transposon was

successfully integrated into the genome of sorted cells, as revealed by the sustained expression of the transgenes (Figure 8, 9) and the functional expression of hHCN4 (Figure 9).

Next, I generated hHCN4-hiPSC by co-transfecting hiPSCs with pT2-hHCN4-GFP and a SB100X expression vector. Although initial transfection efficiencies were low, cell subpopulations of cells expressing the reporter could be easily sorted and enriched only 48h after transfection. After cell sorting, most of the population maintained GFP expression demonstrating an efficient and relatively fast SB-mediated integration of the overexpression cassette into the genome (Figure 14). After the initial purification by cell sorting, I easily derived and maintained hHCN4-hiPSC clonal populations, making them an ideal cellular platform to produce hHCN4-hiPSC-CM (described in detail in Discussion: section II, page 93)

When using DNA vectors for gene expression, segments of the plasmid could randomly integrate in the genome of target cells. Although probability of such events are very low, this risk could be avoided using mRNA to provide expression of the protein of interest. Thus, reprogramming factors and SB100X expression could be supplied by mRNA molecules for future clinical applications. For obvious reasons, the transposon carrying the hHCN4 expression cassette has to be provided as DNA molecule. However, it can be engineered in minicircles (Holstein et al., 2018; Monjezi et al., 2017) or pFAR (Marie et al., 2010; Pastor et al., 2018) to decrease the overall DNA amount delivered into the target cells and avoid additional risks associated with the random integration of bacterial or antibiotic resistance sequences present in the original transposon plasmid.

For clinical applications, the final transgene overexpression cassette should not include any exogenous reporter gene. As alternative to the original selection strategy, transgenic cells could be sorted by using a tagged transposase or by supplying the reporter gene as an independent expression cassette in the transposase expression vector or outside the IRs in the transposon vector (Mezzadra et al., 2016). However, these indirect selection methods require accurate and extensive validation of transposon integration in the purified populations. Nevertheless, preclinical studies to validate functional pacing of hHCN4-hiPSC-CM in relevant animal models are still required. For this purpose, GFP expression in transplanted cells would be extremely useful to identify engrafted hHCN4-hiPSC-CM and further analyze their effect within the host cardiac tissue.

Finally, I efficiently differentiated hHCN4-hiPSC-CM from hHCN4-hiPSCs using available CM differentiation protocols (Lian et al., 2012, 2013) including minor optimization steps (described in detail in Discussion: section III.1, page 94). Although this protocol is highly efficient and reproducible, the differentiation medium is not fully defined, and some reagents (e.g. B27 supplement) contain animal-derived components. Thus, a chemically defined CM differentiation protocol would be preferred for further clinical applications (Burridge et al., 2014).

In summary, I established an optimal workflow for hHCN4-hiPSC-CM generation by SB-mediated transgenesis. Nevertheless, once the initial pipeline has been validated, aforementioned improvements could be addressed for future preclinical studies. The final project plan would include:

- Feeder-free reprogramming procedure using non-integrating non-viral episomal vectors or mRNA combined with defined culture media supplemented with small molecules, followed by hiPSCs expansion in xeno-free conditions using VTN-coating and E8 medium.
- Cotransfection of hiPSCs with an optimized pT2-hHCN4-GFP vector and SB100X expression vector or mRNA, followed by cell sorting of GFP-expressing cells 48h hours after transfection.
- Expansion of sorted hHCN4-hiPSCs in xeno-free conditions and generation of pure transgenic cell populations:
    - Bulk hHCN4-hiPSC line generation by additional cell sorting of GFP-expressing cells.
    - Clonal hHCN4-hiPSC line generation by limiting dilution.
- Differentiation of hHCN4-hiPSCs using a fully chemically defined protocol to generate hHCN4-hiPSC-CM.

II. Sustained functional hHCN4 expression in hiPSCs by SB-mediated gene transfer

After I selected hHCN4-hiPSC lines based on the expression of the GFP reporter gene, I confirmed the functional expression of hHCN4 in these cell lines (Figure 15-17). As intended, hHCN4-hiPSC lines showed a robust expression of HCN4 protein (Figure 15, 16) and displayed the corresponding I_f current that showed the appropriate voltage-dependent and time course activation (Figure 17).

Although SB has a safe integration profile close to random, like every gene delivery method involving DNA integration into the genome, there is a chance that the transposon integrates into genes or regulatory elements causing transcriptional deregulation and genotoxicity (Hudecek et al., 2017). Thus, I kept in continuous culture hHCN4-hiPSCs and their corresponding control cell lines to analyze their proliferation and spontaneous differentiation rates. Transgenic cell lines did not show any abnormalities in comparison with their equivalent non-modified hiPSC lines and expressed pluripotency markers at comparable levels after more than one month in culture (Figure 16). In parallel, I also detected robust hHCN4 expression at the plasma membrane in all hHCN4-hiPSC lines, confirming stable long-term expression provided by SB transposition. These data indicate that neither SB-mediated transgenesis nor hHCN4 expression interfered with the normal

proliferation and pluripotency properties of the genetically engineered hHCN4-hiPSC lines, making them suitable for differentiation applications.

III. Efficient generation of hHCN4-overexpressing cardiomyocytes

III.1 Optimal cardiomyocyte differentiation conditions

Currently available CM differentiation protocols are very efficient and highly reproducible, but can show variable performance using different hiPSC lines and therefore still require minor optimization steps. Additionally, the quality and optimal conditions of starter hiPSCs cultures are crucial for the final CM yield (Mohr et al., 2010; Lian et al., 2013). For those reasons, I designed and performed several optimization experiments to test the CM differentiation capacity and efficiency of the generated hiPSC clones and the hiPSC lines used for transgenesis with SB (Figure 18). Surprisingly, IMR90 C8, an established and well characterized hiPSC line, failed to differentiate into CMs. Although hiPSCs are characterized by their self-renewal capacity and in theory can be indefinitely passaged, they have been shown to accumulate genetic aberrations upon continued culture (Laurent et al., 2010). Differentiation and transgenesis experiments with the IMR90 C8 hiPSC line were performed with cells above passage 60. In addition, maintenance cultures occasionally displayed spontaneous differentiation, suggesting possible abnormalities in their pluripotent state that could explain their failure to differentiate. Similarly, the newly derived hiPSC clone C6 did not differentiate into CMs. It has been shown that, after the reprogramming process, some hiPSC clones displayed ESC-like morphology and express pluripotency markers but they retain limited differentiation capacity. These 'differentiation defective' clones are usually biased towards differentiation into certain cell lineages and remain undifferentiated or differentiate into different cell types when subjected to directed differentiation protocols (Koyanagi-Aoi et al., 2013; Ohnuki et al., 2014). Regardless of the underlying cause, the defective CM differentiation capacity of these two cell lines made them unsuitable for the project and therefore they were discarded for further experiments. Additional genomic characterization and pluripotency analysis of these hiPSC lines were not performed, as it was considered out of the scope of this project.

Three clones (C2, C7 and C15) derived from the HFF reprogramming experiment, as well as the reference hiPSC line SCVI 113, efficiently differentiated into CMs under several of the tested conditions (Figure 18A). Interestingly, although the most efficient condition for all the different clones was the same for all the different clones, intrinsic differences in CM differentiation efficiency could be observed between them. While certain conditions resulted very efficient for differentiation of C2 (e.g. 30.000 cells/cm^2 and 48h of 6μM CHIR treatment), C7 differentiated poorly and C15 did not differentiate at all. These results highlight the variability between hiPSC lines, and stress out the need for a differentiation

optimization step before comparative experiments are carried out. Surprisingly, when I assessed the differentiation efficiency of non-modified vs. clonal and bulk hHCN4-overexpressing SCVI 113 hiPSC lines, the different conditions tested reported comparable outcomes in both cell lines (Figure 18B, data not shown). These data, together with the aforementioned pluripotency marker expression, confirmed that hHCN4 overexpression and the overall SB-mediated transgenesis procedure in hiPSCs do not affect their self-renewal and pluripotency capacities.

Initially, I decided not to work with bulk populations to avoid possible differentiation barriers that have been associated with the heterogeneity of the initial hiPSCs culture (Mohr et al., 2010; Lian et al., 2013). Moreover, the broad transgene expression levels could make difficult to interpret the effect of hHCN4 overexpression in CMs. However, unexpectedly, bulk hHCN4-hiPSCs efficiently differentiated into CMs, generating comparable yields when compared to the corresponding clonal cell line (data not shown). Although I only analyzed partially the phenotype of CMs derived from bulk hiPSC lines due to time constraints, additional analysis of these cells and their subpopulations could be useful to understand both the minimal expression requirements and the real effect of heterogeneous expression levels in hHCN4-hiPSCs within the proposed strategy. Further functional validation of hHCN4-hiPSC-CM derived from bulk populations would accelerate the overall process by avoiding the manual and time-consuming workflow associated with the generation of clonal cell lines, and might be considered for future clinical applications.

III.2 hHCN4 expression does not interfere with cardiomyocyte differentiation

An important goal for gene-cell therapy approaches is the sustained expression of the therapeutic transgene in the target cell types. Human CMs and cardiac progenitors are difficult to obtain and manipulate. The use of hPSCs has overcome this limitation, since they provide an unlimited source of human CMs upon differentiation. Moreover, their ability to proliferate indefinitely and grow clonally, make them a perfect cell platform for gene engineering in order to generate transgenic effector cells (Oikonomopoulos et al., 2018).

In murine models, Hcn4 has been shown to be essential for proper cardiac function and pacemaker AP generation during embryonic development and adulthood (Baruscotti et al., 2011; Herrmann et al., 2007; Stieber et al., 2003). Moreover, several reporter mice have shown very dynamic expression of *Hcn4* in distinct progenitors and cell populations at different developmental stages. Earliest Hcn4-expressing cells mark first heart field (FHF) progenitors, giving rise exclusively to myocardial lineage in the left ventricle and part of the atria. During later stages, Hcn4 expression is restricted to CMs, with high expression in the CCS and lower expression in the left ventricle and atria. At final stages of development and during adulthood, Hcn4 expression is limited to CCS components, SVC and coronary sinus. This implies *de novo* expression of Hcn4 also in cells derived from

multipotent second heart field (SHF) progenitors that give rise to CMs, smooth muscle and endothelial cells. Thus, during mouse development there is a temporally regulated allocation of Hcn4-expressing cells derived from both FHF and SHF contributing to several cardiac tissues (Liang et al., 2015).

While Hcn4 expression has been extensively studied in mice, HCN4 expression dynamics during human heart development remain unknown. To date, only one study has investigated HCN4-expressing cells during CM differentiation from hESCs. The authors purified HCN4-expressing cells at early stages of differentiation when FHF and SHF progenitors were already detected. $HCN4^+$ cells comprised only a 2% of the differentiating culture, expressed high levels of *TBX5* and *NKX2-5* and showed preferential differentiation potential towards CMs (97% $TNNT2^+$ cells). These data suggest that, similarly to mouse, $HCN4^+$ cells at early development stages mark FHF progenitors (Später et al., 2013). The expression profile of HCN4 at later differentiation stages remains unclear. Since I used a constitutive promoter to drive the expression of hHCN4, its expression throughout the entire process could potentially interfere with CM differentiation. However, hHCN4-hiPSCs differentiated into CMs and showed comparable efficiency to control hiPSC lines (Figure 20A, B). Moreover, I detected transgene expression in nearly all the overexpressing cell population throughout the entire differentiation process (Figure 21, 26, 28B leftmost panel), demonstrating that SB-mediated gene integration provides both safe and sustained expression of the transgene in multiple cell platforms and through complex biological processes without undergoing transgene silencing. Additionally, when I monitored GFP expression in detail, I observed a marked increased expression towards later differentiation time points that was similar in hHCN4-hiPSCs and control GFP-hiPSCs (Figure 21A). This was expected, since CAG promoter has been shown to provide increased transcriptional rate in CMs compared with other cell types, including hPSCs (Orbán et al., 2009). Interestingly, this expression trend was independent of the different integration profile of both transgenic hiPSC lines. Since SB integrates the transposon cassette randomly and there are $2{\cdot}10^8$ potential integration sites (TA dinucleotides) in the human genome (Izvák et al., 2002; Ivics et al., 1997), clonal populations derived from different transposition experiments would integrate the transposon into different genomic locations at high probability. Nevertheless, further studies in integration site profiling and copy number determination in transgenic hiPSC lines would provide deeper insight about the optimal conditions for robust transgenic expression and ultimate therapeutic effect.

III.3 Sustained functional hHCN4 overexpression in hiPSC-CMs

As described for hHCN4-overexpressing cell lines, differentiated hHCN4-hiPSC-CM also displayed a robust hHCN4 overexpression profile in comparison with control hiPSC-CMs (Figure 21, 26, 28B leftmost panel). The main aim of the project was to provide high density of I_f to hiPSC-CMs as an insulation mechanism. Since hiPSC-CMs already

express low levels of HCN4 and I_f, quantitative electrophysiology analysis was necessary to validate the expected functional overexpression. Indeed, hHCN4-hiPSC-CM showed larger I_f density at every voltage measured, reaching up to 4-fold increase when measured at -100mV when compared to control hiPSC-CMs (Figure 22A). I_f current mediated by hHCN4 overexpression displayed typical voltage-dependent activation and, just like in SA nodal cells, activated slowly at -60mV and became larger with increasing levels of hyperpolarization (Figure 22B, C, Basal). In addition, this current showed adequate response to ß-adrenergic stimulation by isoproterenol that resulted in enhanced current densities compared with basal conditions (Figure 22B, C). Taken together, these results show that I achieved functional hHCN4 overexpression in spontaneously beating hiPSC-CMs. Moreover, I validated a large I_f density susceptible of autonomic regulation in hHCN4-hiPSC-CM, generating a cell substrate with theoretically enough mechanisms to pace the heart and regulate its beating rate.

IV. hHCN4 overexpression is not enough to confer complete pacemaker identity to hiPSC-CMs

The different types of CMs are categorized by their anatomical localization in the heart chambers, atrial and ventricular phenotype, and the SA/AVN, nodal phenotype. In addition, CM classification reflects as well differences in the main function of these CM subtypes. While working CMs, comprising atrial and ventricular CMs, are responsible for the contraction of the cardiac muscle, those of the CCS are specialized in AP generation and propagation. These distinct functions are reflected in their electrophysiological properties and gene expression. Thus phenotypic differences can be used to identify subtypes of CMs within the contractile cell populations derived by *in vitro* differentiation protocols (Kane & Terracciano, 2017). Once I established an effective method to generate hiPSC-CMs with solid I_f current expression, I tested whether these cells would resemble other particular features of pacemaker CMs.

To characterize possible changes in hHCN4-hiPSC-CM, I compared their gene expression profile with that of control hiPSC-CMs. Except for the aforementioned increased expression of *HCN4*, I did not observe apparent variations in gene expression between hHCN4-overexpressing and control hiPSC-CMs. These data agree with previous studies (Saito et al., 2015), and suggest that hHCN4 overexpression does not influence the transcriptional profile of hiPSC-CMs during or upon differentiation. However, I determined transcript levels in already beating cultures at day 9 and 20 of differentiation (Figure 28). Since HCN4 has been shown to be differentially expressed in FHF and SHF progenitors (Später et al., 2013), transcriptional changes induced by hHCN4 overexpression at early time-points of CM differentiation, during cardiac mesodermal induction and heart field development, could be masked at later stages and would be missed in this study.

AP morphology has been traditionally used to classify hPSC-CM into ventricular, atrial or nodal-like CMs. The specific electrophysiological characteristics of this cells result in distinguishable and measurable AP properties (Ma et al., 2011; Satoh, 2003). I analyzed several parameters in APs recorded from hiPSC-CMs and did not find significant differences between hHCN4 overexpressing and control cells. hiPSC-CMs from all cell lines showed high MDP (~-60mV) and low peak (~70mV) that are typically associated to nodal CMs. These values could be explained by the low level of maturation of hiPSC-CMs typically achieved by currently available differentiation protocols, highlighted by the presence of spontaneous beating activity in analyzed cells derived from all hiPSC lines. However, in agreement with spontaneous beating analysis, the AP interval tended to be smaller in hHCN4-hiPSC-CM (i.e., these cells showed an increased beating frequency, Figure 24). Although some differences could be observed between hiPSC-CMs generated from different cell lines, the low sample size analyzed did not provide enough statistical power.

A large number of studies have used AP morphology to characterize hiPSC-CMs into different subtypes. However, detailed information about the used criteria is not always clear and threshold values considered for that categorization varies considerably between different studies (Briek et al., 2015; Ma et al., 2011; Satoh, 2003). These observations, together with the limitations associated to the low throughput data acquisition provided by patch-clamp experiments, have generated skepticism in the field. Several studies have suggested that AP parameters in hiPSC-CMs are dependent of the cell density and should be interpret with caution particularly in single cell preparations (Du et al., 2015; Kane et al., 2016).

IV.1 hHCN4-hiPSC-CM display increased beating rate and enrichment in CMs with pacemaker-like morphology

I compared several characteristics of CMs derived from either control or hHCN4-hiPSC lines and found two main distinct features: hHCN4-hiPSC-CM displayed an increased beating rate both in monolayers cultures (data not shown) and as single cells (Figure 23B), and they showed an enrichment of cells displaying pacemaker-like morphology in single cell preparations (Figure 26, 27).

Previous studies have investigated HCN4 overexpression in different cell substrates as candidate for biological pacemaker generation (Boink et al., 2008; J. Cai et al., 2007; Feng et al., 2016; Saito et al., 2015, 2018; X. Yang et al., 2008). However, these studies are difficult to compare since they are performed using animal cells or models and the features analyzed (e.g. beating rate or morphology) for HCN4-overexpressing cells characterization differ from one study to another. Nevertheless, when analyzed, increased beating rate was also observed in monolayers and single cell myocytes upon lentiviral-mediated hHCN4 overexpression in NRVM when compared to non-transduced cells (Boink et al., 2008).

Similarly, when rabbit HCN4 was overexpressed in mESC-CMs they displayed significantly higher beating rates compared to control mESC-CMs. Our results agree with these data and, although the underlying mechanism for this phenomenon is unclear, denote an association between HCN4 overexpression and higher beating rate in a variety of setups. Interestingly, in recent works where SAN-like cells have been derived from hPSC by optimization of developmental staged CM differentiation protocols, increased beating rate was also observed in these cells compared with ventricular-like CMs generated in parallel. In addition, gene expression analysis of SAN-like cells revealed high expression of *HCN4* and *HCN1*. In these study, the authors associated the increased beating frequency with the immature nature of SAN-like CMs differentiated *in vitro* and the absence of vagal stimulation (Birket et al., 2015; Protze et al., 2017).

The faster beating rate observed *in vitro* in hHCN4-hiPSC-CM cultures could represent a limitation *in vivo*, since they could induce arrhythmia after transplantation into the heart. However, it is intriguing that this phenomena is consistently observed in cardiac cells showing high levels of HCN4, whether its expression is provided by an overexpression cassette or not. It has been suggested that this effect could be due to the combined effect of HCN4 overexpression and additional electrophysiological characteristics of the immature CMs used (i.e. NRVM, mESC-CMs and hPSC-CMs). A possible strategy to overcome this limitation would be to increase CMs maturation by modifying differentiation conditions, e.g. using small molecules, micropatterning or electromechanical stimulation (Cimetta et al., 2009; Ronaldson-Bouchard et al., 2018). It would be interesting to test whether hHCN4-hiPSC-CM cells alone would be able to drive the heart at physiological rates once they are properly coupled in the host myocardium after transplantation into the heart of animals with basal heart rates similar to humans (e.g. pigs) and appropriate sympathetic and parasympathetic innervation.

In opposition with beating rate, morphology studies were not performed in any of the studies investigating HCN4-overexpression. Nevertheless, CMs displaying pacemaker-like morphology have been identified in mouse CMs derived from Tbx3-overexpressing mESCs in combination with Myh6-promoter-selection (Rimmbach et al., 2015), upon Tbx18 expression in NRVM (Kapoor et al., 2013) and in a recent study in which hPSCs were differentiated into pacemaker-like CMs using FBS-enriched media (Schweizer et al., 2017). Although these reports describe CMs with typical pacemaker morphology, the quantification of this particular cell population within the overall differentiation culture was not assessed. However, cell area and capacitance of Tbx18-NRVM were studied and were shown to decrease compared to control NRVM (Kapoor et al., 2013). These data are consistent with the lower capacitance values observed in hHCN4-hiPSC-CM in comparison with GFP-hiPSC-CM (Figure 27B).

Morphology data should be interpreted with caution since CMs shape is susceptible to change by substrate patterning. Thus, the use of certain matrices during differentiation

and culture can influence the final morphology displayed by hiPSC-CMs (Mengsteab et al., 2016, Yechikov et al., 2016). To avoid this bias, I compared the morphology of hHCN4-overexpressing and control hiPSC-CMs that have been differentiated, cultured and stained using identical conditions.

IV.2 Influence of the differentiation method in pacemaker CM yield

The establishment of cardiac differentiation from hPSCs has increased our understanding of the human cardiac development. Previous studies in developmental biology have served as foundation to elucidate and control the molecular mechanisms underlying CM differentiation and ultimately develop efficient protocols to generate different cardiac cell types. Human cardiogenesis is tightly regulated by the spatial and temporal expression of transcription factors and the activation/inhibition of specific signaling pathways. Thus, human CM differentiation requires modulation of TGFß (BMP/activin), WNT and FGF pathways (Burridge et al., 2012; Mummery et al., 2012).

Whether the CM differentiation protocol is established with the minimum possible steps (Burridge et al., 2014; Lian et al., 2012, 2013) or recapitulates the different developmental stages of human cardiogenesis (Kattman et al., 2011; L. Yang et al., 2008), the typical outcome is a mixed population of CMs resembling subtype proportions found in the heart (Ma et al., 2011; J. Zhang et al., 2009). Most of these methods are biased towards a ventricular phenotype, the most abundant cell type in the heart. CMs displaying atrial features are modestly represented, and nodal CM are typically less than 10% of the differentiated cell population and often absent (Karakikes et al., 2014).

Recent studies have identified specific progenitor cells responsible for the generation of the different cell types constituting the human cardiac tissue. In the first of these studies, the authors were able to recreate early heart field development and characterized NKX2-5^{-} (SHF) and NKX2-5^{+} (FHF) progenitors by modulation of FGF and BMP expression. Moreover, they further derived terminally differentiated NKX2-5^{-} pacemaker-like and NKX2.5^{+} ventricular-like CMs (Birket et al., 2015). In agreement with these observations, Protze and collaborators also identified a NKX2-5^{-} population as the SA nodal cell progenitor population after cardiac mesodermal induction. In addition, the differentiation of hPSC into NKX2-5^{-} pacemaker-like cells was optimized by addition of RA and inhibition of the TGFß and FGF signaling pathways (Protze et al., 2017). In a parallel study, the authors identified the progenitor population that specifically derived atrial and ventricular CMs, and generated cultures enriched in these CM subtypes by balancing RA expression (Lee et al., 2017). Importantly, all these studies concluded that generation of the proper progenitor after initial cardiac mesodermal induction is critical for lineage commitment and further cell specification into different classes of CM.

Since I have been using a directed protocol for cardiac differentiation, developmental stages are not sequentially completed, which results in a strong bias towards NKX2-5^{+} cells generation. These cells already represent the majority of the culture from day 5 onwards during differentiation and resemble FHF-like progenitors, which have exclusively myogenic capacity and differentiate mainly into working CMs (Birket et al., 2015; Lian et al., 2012, 2013). Similarly, when I analyzed differentiation cultures at day 9, cell populations derived from all hiPSC lines were ~65% NKX2-5^{+} (Figure 20). Indeed, the directed differentiation protocol is based in the modulation of the WNT signaling pathway, while appropriate lineage commitment to FHF or SHF-like progenitors has been shown to be modulated additionally by TGFß and FGF pathways (Birket et al., 2015; Protze et al., 2017).

SAN-like cells are generated from a SHF-like progenitor that does not express NKX2-5, and they remain NKX2-5^{-} once differentiated (Birket et al., 2015; Protze et al., 2017). The directed differentiated protocol I used, provides a strong lineage commitment towards FHF (NKX2-5^{+}). In addition, HCN4 expression is expected to be different in FHF and SHF-like progenitors, and also to be dynamic during the process of cardiac lineage commitment. Thus, it is possible that the effects of HCN4 overexpression are attenuated in CMs derived by the differentiation protocol I have used. Therefore, generation of pacemaker-like CMs could be optimized by the combination of a differentiation protocol that allows the generation of NKX2-5^{-} cardiac progenitors coupled with HCN4 overexpression. In addition, it has been shown that Hcn4-expressing FHF cells contribute only to few cells in the murine SAN, while most of the SA nodal cells are derived from the SHF and initiate Hcn4 expression at later stages (Liang et al., 2015). Thus, it would be interesting to investigate the final composition of the CM population upon controlled HCN4 expression at different stages of differentiation by 'pulse-chase' experiments.

V. Summary and future perspectives

I successfully designed and established a working pipeline from reprogramming of fibroblast into hiPSCs to the generation of hHCN4-hiPSC-CM, using the SB transposon system as gene delivery method. I achieved stable and long-term expression of functional hHCN4 in both hHCN4-hiPSCs and hHCN4-hiPSC-CM, providing a therapeutically relevant cell platform to develop tissue-based biological pacemaker approaches. Although the obtained hHCN4-hiPSC-CM did not show major differences when compared to control hiPSC-CMs, we hypothesize that the large I_f density expressed by already spontaneously beating CMs would confer them insulation from the surrounding hyperpolarized cells in the cardiac tissue, and allow them to lead the beating. This hypothesis would require to be tested by verifying the pacing ability of hHCN4-hiPSC-CM in co-culture with monolayers of ventricular-like hiPSC-CMs. Ideally, aggregates of hHCN4-hiPSC-CM placed onto CM

monolayers would be able to couple electrically and modulate their beat rate. Once pacing is achieved *in vitro*, the next step would be to investigate viability, safety and long-term performance of hHCN4-hiPSC-CM in large animal models.

The SAN is a highly specialized and complex tissue structure characterized by a marked heterogeneity in cell composition, electrophysiological properties and gene expression. Thus, understanding and recapitulating SAN function requires elucidating and mirroring the cellular properties of single pacemaker CMs and also understanding the specific distribution and electrical coupling between these cells throughout the SAN and with the surrounding atrium at the paranodal area. Moreover, many other cell types have been described within the SAN. For all these reasons, in order to generate sustained pacing activity, it would be desirable to resemble, at least partially, the complex architecture and cellular composition of the SAN by tissue engineering.

Since hiPSC-CMs have yet to be tested in clinical trials, the ability of these cells to engraft and deliver therapeutic effect in hearts subjected to aging and disease remains unclear. Although some biological pacemaker strategies have been tested in preclinical setups, these studies, at their best, used large-animal bradycardia models inducing acute SAN malfunction. However, it is known that SND or AF induce certain level of cardiac remodeling. Thus, it remains open whether SAN-like cells derived from hiPSCs would perform efficiently in those circumstances.

During the last decade, the investigation of different gene- and cell-based approaches to develop a biological pacemaker has produced encouraging results. The advances in PSC biology and cardiac differentiation methods have made possible to consider the generation of patient-specific therapies designed to repair damaged SAN function by tissue-based pacemakers. However, one of the main challenges faced by these methods is to achieve at least similar performance and success rate as the current technology, i.e. electronic pacemakers. Bioengineered pacemakers have to meet high standards to be considered an alternative to the already robust therapeutic effect delivered by electronic devices.

The complete development of this technology could allow, not only to treat, but also to repair damaged tissue involved in heart rhythm disorders pathology. Ideally, having complete information about the molecular mechanisms underlying SAN development, function and disease, it would be possible to design personalized therapies to restore the specific molecular mechanism underlying arrhythmogenic events in individual patients.

References

Ambrosi, C. M., Fedorov, V. V., Schuessler, R. B., Rollins, A. M., & Efimov, I. R. (2012). Quantification of fiber orientation in the canine atrial pacemaker complex using optical coherence tomography. *Journal of Biomedical Optics*, *17*(7), 071309.

Anumonwo, J. M., Wang, H. Z., Trabka-Janik, E., Dunham, B., Veenstra, R. D., Delmar, M., & Jalife, J. (1992). Gap junctional channels in adult mammalian sinus nodal cells. Immunolocalization and electrophysiology. *Circulation Research,71*(2), 229-239.

Avior, Y., Sagi, I., & Benvenisty, N. (2016). Pluripotent stem cells in disease modelling and drug discovery. *Nature Reviews Molecular Cell Biology,17*(3), 170-182.

Ayabe, H., Anada, T., Kamoya, T., Sato, T., Kimura, M., Yoshizawa, E., … Taniguchi, H. (2018). Optimal Hypoxia Regulates Human iPSC-Derived Liver Bud Differentiation through Intercellular TGFB Signaling. *Stem Cell Reports*, *11*(2), 306–316.

Baig, S. M., Koschak, A., Lieb, A., Gebhart, M., Dafinger, C., Nürnberg, G., . . . Bolz, H. J. (2010). Loss of Cav1.3 (CACNA1D) function in a human channelopathy with bradycardia and congenital deafness. *Nature Neuroscience,14*(1), 77-84. doi:10.1038/nn.2694

Bakker, M. L., Boink, G. J., Boukens, B. J., Verkerk, A. O., Boogaard, M. V., Haan, A. D., . . . Christoffels, V. M. (2012). T-box transcription factor TBX3 reprogrammes mature cardiac myocytes into pacemaker-like cells. *Cardiovascular Research,94*(3), 439-449. doi:10.1093/cvr/cvs120

Baruscotti, M., & Robinson, R. B. (2007). Electrophysiology and pacemaker function of the developing sinoatrial node. American Journal of Physiology-Heart and Circulatory Physiology, 293(5).

Baruscotti, M., Barbuti, A., & Bucchi, A. (2010). The cardiac pacemaker current. *Journal of Molecular and Cellular Cardiology,48*(1), 55-64.

Baruscotti, M., Bucchi, A., Viscomi, C., Mandelli, G., Consalez, G., Gnecchi-Rusconi, T., … DiFrancesco, D. (2011). Deep bradycardia and heart block caused by inducible cardiac-specific knockout of the pacemaker channel gene *Hcn4*. *Proceedings of the National Academy of Sciences of the United States of America*, *108*(4), 1705–1710.

Baruscotti, M., Bucchi, A., Milanesi, R., Paina, M., Barbuti, A., Gnecchi-Ruscone, T., . . . Difrancesco, D. (2015). A gain-of-function mutation in the cardiac pacemaker HCN4 channel increasing cAMP sensitivity is associated with familial Inappropriate Sinus Tachycardia. *European Heart Journal,38*(4), 280-288.

Baruscotti, M., Bianco, E., Bucchi, A., & Difrancesco, D. (2016). Current understanding of the pathophysiological mechanisms responsible for inappropriate sinus tachycardia: Role of the If "funny" current. *Journal of Interventional Cardiac Electrophysiology,46*(1), 19-28.

Baus, J., Liu, L., Heggestad, A. D., Sanz, S., & Fletcher, B. S. (2005). Hyperactive Transposase Mutants of the Sleeping Beauty Transposon. *Molecular Therapy,12*(6), 1148-1156.

Bearzi, C., Rota, M., Hosoda, T., Tillmanns, J., Nascimbene, A., De Angelis, A., … Anversa, P. (2007). Human cardiac stem cells. *Proceedings of the National Academy of Sciences of the United States of America*, *104*(35), 14068–14073.

Beltrami, A. P., Barlucchi, L., Torella, D., Baker, M., Limana, F., Chimenti, S., . . . Anversa, P. (2003). Adult Cardiac Stem Cells Are Multipotent and Support Myocardial Regeneration. *Cell,114*(6), 763-776.

Benati, D., Cocchiarella, F., & Recchia, A. (2018). An Efficient In Vitro Transposition Method by a Transcriptionally Regulated Sleeping Beauty System Packaged into an Integration Defective Lentiviral Vector. *Journal of Visualized Experiments,*(131).

Benjamin, E. J., Virani, S. S., Callaway, C. W., Chamberlain, A. M., Chang, A. R., Cheng, S., . . . Muntner, P. (2018). Heart Disease and Stroke Statistics—2018 Update: A Report From the American Heart Association. *Circulation,137*(12).

Biel, M., Schneider A.& Wahl C. (2002). Cardiac HCN Channels Structure, Function, and Modulation. *Trends in Cardiovascular Medicine,12*(5), 206-213.

Biel, M. (2009). Cyclic Nucleotide-regulated Cation Channels. *The Journal of Biological Chemistry*, *284*(14), 9017–9021.

Birket, M. J., Ribeiro, M. C., Verkerk, A. O., Ward, D., Leitoguinho, A. R., Hartogh, S. C., . . . Mummery, C. L. (2015). Expansion and patterning of cardiovascular progenitors derived from human pluripotent stem cells. *Nature Biotechnology,33*(9), 970-979.

Bodega, B., & Orlando, V. (2014). Repetitive elements dynamics in cell identity programming, maintenance and disease. *Current Opinion in Cell Biology,31*, 67-73.

Boehme, P., Zhang, W., Solanki, M., Ehrke-Schulz, E., & Ehrhardt, A. (2016). A High-Capacity Adenoviral Hybrid Vector System Utilizing the Hyperactive Sleeping Beauty Transposase SB100X for Enhanced Integration. *Molecular Therapy. Nucleic Acids*, *5*(7), e337–.

Bogdanov, K. Y., Vinogradova, T. M., & Lakatta, E. G. (2001). Sinoatrial Nodal Cell Ryanodine Receptor and Na -Ca2 Exchanger : Molecular Partners in Pacemaker Regulation. *Circulation Research,88*(12), 1254-1258.

Boink, G. J., Verkerk, A. O., Amersfoorth, S. C., Tasseron, S. J., Rijt, R. V., Bakker, D., . . . Tan, H. L. (2008). Engineering physiologically controlled pacemaker cells with lentiviral HCN4 gene transfer. *The Journal of Gene Medicine,10*(5), 487-497.

Boink, G. J., Duan, L., Nearing, B. D., Shlapakova, I. N., Sosunov, E. A., Anyukhovsky, E. P., . . . Rosen, M. R. (2013). HCN2/SkM1 Gene Transfer Into Canine Left Bundle Branch Induces Stable, Autonomically Responsive Biological Pacing at Physiological Heart Rates. *Journal of the American College of Cardiology,61*(11), 1192-1201.

Boyett, M. (2000). The sinoatrial node, a heterogeneous pacemaker structure. *Cardiovascular Research,47*(4), 658-687.

Boyett, M. R. (2009). 'And the beat goes on' The cardiac conduction system: The wiring system of the heart. *Experimental Physiology,94*(10), 1035-1049.

Brioschi, C., Micheloni, S., Tellez, J. O., Pisoni, G., Longhi, R., Moroni, P., . . . Baruscotti, M. (2009). Distribution of the pacemaker HCN4 channel mRNA and protein in the rabbit sinoatrial node. *Journal of Molecular and Cellular Cardiology,47*(2), 221-227.

Brown, H. F., Difrancesco, D., & Noble, S. J. (1979). How does adrenaline accelerate the heart? *Nature,280*(5719), 235-236.

Brown, H., & Difrancesco, D. (1980). Voltage-clamp investigations of membrane currents underlying pace-maker activity in rabbit sino-atrial node. *The Journal of Physiology,308*(1), 331-351.

Bruzauskaite, I., Bironaite, D., Bagdonas, E., Skeberdis, V. A., Denkovskij, J., Tamulevicius, T., . . . Bernotiene, E. (2016). Relevance of HCN2-expressing human mesenchymal stem cells for the generation of biological pacemakers. *Stem Cell Research & Therapy,7*(1).

Bucchi, A., Plotnikov, A. N., Shlapakova, I., Danilo, P., Kryukova, Y., Qu, J., . . . Rosen, M. R. (2006). Wild-Type and Mutant HCN Channels in a Tandem Biological-Electronic Cardiac Pacemaker. *Circulation,114*(10), 992-999.

Burridge PW, Keller G, Gold JD, Wu JC. Production of De Novo Cardiomyocytes: Human Pluripotent Stem Cell Differentiation and Direct Reprogramming. *Cell Stem Cell.* 2012;10(1):16-28. doi:10.1016/j.stem.2011.12.013.

Burridge, P. W., Matsa, E., Shukla, P., Lin, Z. C., Churko, J. M., Ebert, A. D., … Wu, J. C. (2014). Chemically Defined and Small Molecule-Based Generation of Human Cardiomyocytes. *Nature Methods*, *11*(8), 855–860.

Cai, D., Winslow, R., & Noble, D. (1994). Effects of gap junction conductance on dynamics of sinoatrial node cells: Two-cell and large-scale network models. *IEEE Transactions on Biomedical Engineering,41*(3), 217-231.

Cai, J., Yi, F., Li, Y., Yang, X., Song, J., Jiang, X., . . . Wang, W. (2007). Adenoviral gene transfer of HCN4 creates a genetic pacemaker in pigs with complete atrioventricular block. *Life Sciences,80*(19), 1746-1753.

Chandler, N. J., Greener, I. D., Tellez, J. O., Inada, S., Musa, H., Molenaar, P., . . . Dobrzynski, H. (2009). Molecular Architecture of the Human Sinus Node: Insights Into the Function of the Cardiac Pacemaker. *Circulation,119*(12), 1562-1575.

Chandler, N., Aslanidi, O., Buckley, D., Inada, S., Birchall, S., Atkinson, A., . . . Dobrzynski, H. (2011). Computer Three-Dimensional Anatomical Reconstruction of the Human Sinus Node

and a Novel Paranodal Area. *The Anatomical Record: Advances in Integrative Anatomy and Evolutionary Biology,294*(6), 970-979.

Chauveau, S., Anyukhovsky, E. P., Ben-Ari, M., Naor, S., Jiang, Y., Danilo, P., . . . Rosen, M. R. (2017). Induced Pluripotent Stem Cell–Derived Cardiomyocytes Provide In Vivo Biological Pacemaker Function. *Circulation: Arrhythmia and Electrophysiology,10*(5).

Choi, Y. S., Dusting, G. J., Stubbs, S., Arunothayaraj, S., Han, X. L., Collas, P., … Dilley, R. J. (2010). Differentiation of human adipose-derived stem cells into beating cardiomyocytes. *Journal of Cellular and Molecular Medicine*, *14*(4), 878–889.

Chong, J. J. H., Yang, X., Don, C. W., Minami, E., Liu, Y.-W., Weyers, J. J., … Murry, C. E. (2014). Human Embryonic Stem Cell-Derived Cardiomyocytes Regenerate Non-Human Primate Hearts. *Nature*, *510*(7504), 273–277.

Choudhury, M., Boyett, M. R., & Morris, G. M. (2015). Biology of the Sinus Node and its Disease. *Arrhythmia & Electrophysiology Review*, *4*(1), 28–34.

Christoffels, V. M., & Moorman, A. F. (2009). Development of the Cardiac Conduction System: Why Are Some Regions of the Heart More Arrhythmogenic Than Others? *Circulation: Arrhythmia and Electrophysiology,2*(2), 195-207.

Cimetta, E., Pizzato, S., Bollini, S., Serena, E., Coppi, P. D., & Elvassore, N. (2008). Production of arrays of cardiac and skeletal muscle myofibers by micropatterning techniques on a soft substrate. *Biomedical Microdevices,11*(2), 389-400.

Csepe, T. A., Zhao, J., Hansen, B. J., Li, N., Sul, L. V., Lim, P., … Fedorov, V. V. (2016). Human Sinoatrial Node Structure: 3D Microanatomy of Sinoatrial Conduction Pathways. *Progress in Biophysics and Molecular Biology*, *120*(1-3), 164–178.

Dakkak W, Doukky R. Rhythm, Sick Sinus Syndrome. [Updated 2017 Nov 27]. In: StatPearls [Internet]. Treasure Island (FL): StatPearls Publishing; 2018 Jan-. Available from: https://www.ncbi.nlm.nih.gov/books/NBK470599/

Darr, H. (2006). Overexpression of NANOG in human ES cells enables feeder-free growth while inducing primitive ectoderm features. *Development,133*(6), 1193-1201.

Davies, M. J., & Pomerance, A. (1972). Quantitative study of ageing changes in the human sinoatrial node and internodal tracts. *Heart,34*(2), 150-152.

Davis, L. M., Rodefeld, M. E., Green, K., Beyer, E. C., & Saffitz, J. E. (1995). Gap Junction Protein Phenotypes of the Human Heart and Conduction System. *Journal of Cardiovascular Electrophysiology,6*(10), 813-822.

Denning, C., Borgdorff, V., Crutchley, J., Firth, K. S. A., George, V., Kalra, S., … Young, L. E. (2016). Cardiomyocytes from human pluripotent stem cells: From laboratory curiosity to industrial biomedical platform. *Biochimica et Biophysica Acta*, *1863*(7Part B), 1728–1748.

Deshmukh, R. S., Kovács, K. A., & Dinnyés, A. (2012). Drug Discovery Models and Toxicity Testing Using Embryonic and Induced Pluripotent Stem-Cell-Derived Cardiac and Neuronal Cells. *Stem Cells International*, *2012*, 379569.

Difrancesco, D., & Ojeda, C. (1980). Properties of the current if in the sino-atrial node of the rabbit compared with those of the current iK, in Purkinje fibres. *The Journal of Physiology,308*(1), 353-367.

Difrancesco, D. (1985). The cardiac hyperpolarizing-activated current, if. origins and developments. *Progress in Biophysics and Molecular Biology,46*(3), 163-183.

Difrancesco, D., & Tortora, P. (1991). Direct activation of cardiac pacemaker channels by intracellular cyclic AMP. *Nature,351*(6322), 145-147.

Dimos, J. T., Rodolfa, K. T., Niakan, K. K., Weisenthal, L. M., Mitsumoto, H., Chung, W., . . . Eggan, K. (2008). Induced Pluripotent Stem Cells Generated from Patients with ALS Can Be Differentiated into Motor Neurons. *Science,321*(5893), 1218-1221.

Dobrzynski, H. (2005). Computer Three-Dimensional Reconstruction of the Sinoatrial Node. *Circulation,111*(7), 846-854.

Dobrzynski, H., Boyett, M. R., & Anderson, R. H. (2007). New Insights Into Pacemaker Activity: Promoting Understanding of Sick Sinus Syndrome. *Circulation,115*(14), 1921-1932.

Du, D. T. M., Hellen, N., Kane, C., & Terracciano, C. M. N. (2015). Action Potential Morphology of Human Induced Pluripotent Stem Cell-Derived Cardiomyocytes Does Not Predict Cardiac Chamber Specificity and Is Dependent on Cell Density. *Biophysical Journal*, *108*(1), 1–4.

Edelberg, J. M., Aird, W. C., & Rosenberg, R. D. (1998). Enhancement of murine cardiac chronotropy by the molecular transfer of the human beta2 adrenergic receptor cDNA. *Journal of Clinical Investigation*, *101*(2), 337–343.

Edelberg, J., Huang, D., Josephson, M., & Rosenberg, R. (2001). Molecular enhancement of porcine cardiac chronotropy. *Heart*, *86*(5), 559–562.

Escobar, H., Schöwel, V., Spuler, S., Marg, A., & Izsvák, Z. (2016). Full-length Dysferlin Transfer by the Hyperactive *Sleeping Beauty* Transposase Restores Dysferlin-deficient Muscle. *Molecular Therapy. Nucleic Acids*, *5*(1), e277–.

Espinoza-Lewis, R. A., Yu, L., He, F., Liu, H., Tang, R., Shi, J., … Chen, Y. (2009). *Shox2* is essential for the differentiation of cardiac pacemaker cells by repressing *Nkx2-5*. *Developmental Biology*, *327*(2), 376–385.

Fedorov, V. V., Hucker, W. J., Dobrzynski, H., Rosenshtraukh, L. V., & Efimov, I. R. (2006). Postganglionic nerve stimulation induces temporal inhibition of excitability in rabbit sinoatrial node. *American Journal of Physiology-Heart and Circulatory Physiology,291*(2).

Fedorov, V. V., Glukhov, A. V., Chang, R., Kostecki, G., Aferol, H., Hucker, W. J., … Efimov, I. R. (2010). Optical mapping of the isolated coronary-perfused human sinus node. *Journal of the American College of Cardiology*, *56*(17), 1386–1394.

Feng, Y., Luo, S., Yang, P., & Song, Z. (2016). Electric pulse current stimulation increases electrophysiological properties of I_f current reconstructed in mHCN4-transfected canine mesenchymal stem cells. *Experimental and Therapeutic Medicine*, *11*(4), 1323–1329.

Fernández-Avilés, F., Sanz-Ruiz, R., Climent, A. M., Badimon, L., Bolli, R., Charron, D., … Ylä-Herttuala, S. (2017). Global position paper on cardiovascular regenerative medicine. *European Heart Journal*, *38*(33), 2532–2546.

Ferrer, M. I. (1973). The Sick Sinus Syndrome. *Circulation,47*(3), 635-641.

Fonoudi, H., & Bosman, A. (2017). Turning Potential Into Action: Using Pluripotent Stem Cells to Understand Heart Development and Function in Health and Disease. *Stem Cells Translational Medicine*, *6*(6), 1452–1457.

Freeman, B. T., Kouris, N. A., & Ogle, B. M. (2015). Tracking Fusion of Human Mesenchymal Stem Cells After Transplantation to the Heart. *Stem Cells Translational Medicine*, *4*(6), 685–694.

Geurts AM, Yang Y, Clark KJ, Liu G, Cui Z, Dupuy AJ, … Hackett PB. (2003) Gene transfer into genomes of human cells by the sleeping beauty transposon system. *Molecular Therapy*. 8(1),108-17.

Giadone, R. M., Rosarda, J. D., Akepati, P. R., Thomas, A. C., Boldbaatar, B., James, M. F., . . . Murphy, G. J. (2018). A library of ATTR amyloidosis patient-specific induced pluripotent stem cells for disease modelling and in vitro testing of novel therapeutics. *Amyloid,*1-8.

Giudice, A., & Trounson, A. (2008). Genetic Modification of Human Embryonic Stem Cells for Derivation of Target Cells. *Cell Stem Cell,2*(5), 422-433.

Gropp, M., Shilo, V., Vainer, G., Gov, M., Gil, Y., Khaner, H., … Reubinoff, B. E. (2012). Standardization of the Teratoma Assay for Analysis of Pluripotency of Human ES Cells and Biosafety of Their Differentiated Progeny. *PLoS ONE*, *7*(9), e45532.

Hartogh, S. C., & Passier, R. (2015). Concise Review: Fluorescent Reporters in Human Pluripotent Stem Cells: Contributions to Cardiac Differentiation and Their Applications in Cardiac Disease and Toxicity. *Stem Cells,34*(1), 13-26.

Harzheim, D., Pfeiffer, K. H., Fabritz, L., Kremmer, E., Buch, T., Waisman, A., … Seifert, R. (2008). Cardiac pacemaker function of HCN4 channels in mice is confined to embryonic development and requires cyclic AMP. The EMBO Journal, 27(4), 692–703.

Hashem, S. I., & Claycomb, W. C. (2013). Genetic isolation of stem cell-derived pacemaker-nodal cardiac myocytes. *Molecular and Cellular Biochemistry,383*(1-2), 161-171.

Hashem, S. I., Lam, M. L., Mihardja, S. S., White, S. M., Lee, R. J., & Claycomb, W. C. (2013). Shox2 Regulates the Pacemaker Gene Program in Embryoid Bodies. *Stem Cells and Development,22*(21), 2915-2926.

Hastings, C. L., Roche, E. T., Ruiz-Hernandez, E., Schenke-Layland, K., Walsh, C. J., & Duffy, G. P. (2015). Drug and cell delivery for cardiac regeneration. *Advanced Drug Delivery Reviews,84*, 85-106.

Hausl, M. A., Zhang, W., Muther, N., Rauschhuber, C., Franck, H. G., Merricks, E. P., . . . Ehrhardt, A. (2010). Hyperactive sleeping beauty transposase enables persistent phenotypic correction in mice and a canine model for hemophilia B. *Molecular Therapy, 18*(11), 1896-1906.

Hayoz, S., Tiwari, P. B., Piszczek, G., Üren, A., & Brelidze, T. I. (2017). Investigating cyclic nucleotide and cyclic dinucleotide binding to HCN channels by surface plasmon resonance. *Plos One,12*(9).

Herrmann, S., Stieber, J., Stöckl, G., Hofmann, F., & Ludwig, A. (2007). HCN4 provides a 'depolarization reserve' and is not required for heart rate acceleration in mice. *The EMBO Journal,26*(21), 4423-4432.

Hodge, R., Narayanavari, S. A., Izsvák, Z., & Ivics, Z. (2017). Wide Awake and Ready to Move: 20 Years of Non-Viral Therapeutic Genome Engineering with the Sleeping Beauty Transposon System. *Human Gene Therapy,28*(10), 842-855.

Holstein, M., Mesa-Nuñez, C., Miskey, C., Almarza, E., Poletti, V., Schmeer, M., . . . Ivics, Z. (2018). Efficient Non-viral Gene Delivery into Human Hematopoietic Stem Cells by Minicircle Sleeping Beauty Transposon Vectors. *Molecular Therapy,26*(4), 1137-1153.

Hoogaars, W., Tessari A., Moorman A.F., de Boer P.A., Hagoort J., Soufan A.T., Campione M., Christoffels V.M. (2004). The transcriptional repressor Tbx3 delineates the developing central conduction system of the heart. *Cardiovascular Research,62*(3), 489-499.

Hoogaars, W. M. H., Engel, A., Brons, J. F., Verkerk, A. O., de Lange, F. J., Wong, L. Y. E., … Christoffels, V. M. (2007). Tbx3 controls the sinoatrial node gene program and imposes pacemaker function on the atria. *Genes & Development*, *21*(9), 1098–1112.

Hornberger, L. K., & Sahn, D. J. (2007). Rhythm abnormalities of the fetus. *Heart*, 93(10), 1294-1300.

Hou, P., Li, Y., Zhang, X., Liu, C., Guan, J., Li, H., . . . Deng, H. (2013). Pluripotent Stem Cells Induced from Mouse Somatic Cells by Small-Molecule Compounds. *Science,341*(6146), 651-654.

Hu, Y., Dawkins, J. F., Cho, H. C., Marban, E., & Cingolani, E. (2014). Biological pacemaker created by minimally invasive somatic reprogramming in pigs with complete heart block. *Science Translational Medicine,6*(245).

Hudecek, M., Izsvák, Z., Johnen, S., Renner, M., Thumann, G. & Ivics, Z. (2017) Going non-viral: the *Sleeping Beauty* transposon system breaks on through to the clinical side. *Critical Reviews in Biochemistry and Molecular Biology* 52:4, pages 355-380.

Husse, B., & Franz, W. (2016). Generation of cardiac pacemaker cells by programming and differentiation. *Biochimica Et Biophysica Acta (BBA) - Molecular Cell Research,1863*(7), 1948-1952.

Ieda, M., Fu, J.-D., Delgado-Olguin, P., Vedantham, V., Hayashi, Y., Bruneau, B. G., & Srivastava, D. (2010). Direct Reprogramming of Fibroblasts into Functional Cardiomyocytes by Defined Factors. *Cell*, *142*(3), 375–386.

Ionta, V., Liang, W., Kim, E. H., Rafie, R., Giacomello, A., Marbán, E., & Cho, H. C. (2015). *SHOX2* Overexpression Favors Differentiation of Embryonic Stem Cells into Cardiac Pacemaker Cells, Improving Biological Pacing Ability. *Stem Cell Reports*, *4*(1), 129–142.

Ishii, T. M., Takano, M., Xie, L., Noma, A., & Ohmori, H. (1999). Molecular Characterization of the Hyperpolarization-activated Cation Channel in Rabbit Heart Sinoatrial Node. *Journal of Biological Chemistry,274*(18), 12835-12839.

Ivics, Z., Izsvak, Z., Minter, A., & Hackett, P. B. (1996). Identification of functional domains and evolution of Tc1-like transposable elements. *Proceedings of the National Academy of Sciences,93*(10), 5008-5013.

Ivics, Z., Hackett, P. B., Plasterk, R. H., & Izsvák, Z. (1997). Molecular Reconstruction of Sleeping Beauty, a Tc1-like Transposon from Fish, and Its Transposition in Human Cells. *Cell,91*(4), 501-510.

Ivics, Z., Li, M. A., Mátés, L., Boeke, J. D., Bradley, A., & Izsvák, Z. (2009). Transposon-mediated Genome Manipulations in Vertebrates. *Nature Methods*, *6*(6), 415–422.

Izsvák, Z., Khare, D., Behlke, J., Heinemann, U., Plasterk, R. H., & Ivics, Z. (2002). Involvement of a Bifunctional, Paired-like DNA-binding Domain and a Transpositional Enhancer inSleeping BeautyTransposition. *Journal of Biological Chemistry,277*(37), 34581-34588.

James, T. N., Sherf, L., Fine, G., & Morales, A. R. (1966). Comparative Ultrastructure of the Sinus Node in Man and Dog. *Circulation,34*(1), 139-163.

Jin, M., Cuntai, Z., Shen, H., Guoqiang, W., & Xiaoqing, Q. (2010). Use of rats mesenchymal stem cells modified with mHCN2 gene to create biologic pacemakers. *Journal of Huazhong University of Science and Technology [Medical Sciences],30*(4), 447-452.

Jun, C., Zhihui, Z., Lu, W., Yaoming, N., Lei, W., Yao, Q., & Zhiyuan, S. (2012). Canine bone marrow mesenchymal stromal cells with lentiviral mHCN4 gene transfer create cardiac pacemakers. *Cytotherapy,14*(5), 529-539.

Kane, C., Du, D. T. M., Hellen, N., & Terracciano, C. M. (2016). The Fallacy of Assigning Chamber Specificity to iPSC Cardiac Myocytes from Action Potential Morphology. *Biophysical Journal*, *110*(1), 281–283.

Kane, C., & Terracciano, C. M. N. (2017). Concise Review: Criteria for Chamber□Specific Categorization of Human Cardiac Myocytes Derived from Pluripotent Stem Cells. *Stem Cells (Dayton, Ohio)*, *35*(8), 1881–1897.

Kapoor, N., Liang, W., Marbán, E., & Cho, H. C. (2012). Direct conversion of quiescent cardiomyocytes to pacemaker cells by expression of Tbx18. *Nature Biotechnology,31*(1), 54-62.

Karakikes, I., Senyei, G. D., Hansen, J., Kong, C.-W., Azeloglu, E. U., Stillitano, F., … Hajjar, R. J. (2014). Small Molecule-Mediated Directed Differentiation of Human Embryonic Stem Cells Toward Ventricular Cardiomyocytes. *Stem Cells Translational Medicine*, *3*(1), 18–31.

Katter, K., Geurts, A. M., Hoffmann, O., Mátés, L., Landa, V., Hiripi, L., . . . Izsvák, Z. (2013). Transposon-mediated transgenesis, transgenic rescue, and tissue-specific gene expression in rodents and rabbits. *The FASEB Journal,27*(3), 930-941.

Kattman, S. J., Witty, A. D., Gagliardi, M., Dubois, N. C., Niapour, M., Hotta, A., . . . Keller, G. (2011). Stage-Specific Optimization of Activin/Nodal and BMP Signaling Promotes Cardiac Differentiation of Mouse and Human Pluripotent Stem Cell Lines. *Cell Stem Cell,8*(2), 228-240.

Kebriaei, P., Huls, H., Singh, H., Olivares, S., Figliola, M., Kumar, P. R., … Champlin, R. E. (2013). First Clinical Trials Employing Sleeping Beauty Gene Transfer System and Artificial Antigen Presenting Cells To Generate and Infuse T Cells Expressing CD19-Specific Chimeric Antigen Receptor. *Blood*, 122(21), 166.

Kebriaei, P., Singh, H., Huls, M. H., Figliola, M. J., Bassett, R., Olivares, S., … Cooper, L. J. N. (2016). Phase I trials using *Sleeping Beauty* to generate CD19-specific CAR T cells. *The Journal of Clinical Investigation*, *126*(9), 3363–3376.

Kehat, I., Kenyagin-Karsenti, D., Snir, M., Segev, H., Amit, M., Gepstein, A., … Gepstein, L. (2001). Human embryonic stem cells can differentiate into myocytes with structural and functional properties of cardiomyocytes. *Journal of Clinical Investigation*, *108*(3), 407–414.

Kehat, I., Khimovich, L., Caspi, O., Gepstein, A., Shofti, R., Arbel, G., . . . Gepstein, L. (2004). Electromechanical integration of cardiomyocytes derived from human embryonic stem cells. *Nature Biotechnology,22*(10), 1282-1289.

Keith, A., & Flack, M. (1907). The Form and Nature of the Muscular Connections between the Primary Divisions of the Vertebrate Heart. *Journal of Anatomy and Physiology*, *41*(Pt 3), 172–189.

Keller, G. (2005). Embryonic stem cell differentiation: Emergence of a new era in biology and medicine. *Genes & Development,19*(10), 1129-1155.

Keung, W., Boheler, K. R., & Li, R. A. (2014). Developmental cues for the maturation of metabolic, electrophysiological and calcium handling properties of human pluripotent stem cell-derived cardiomyocytes. *Stem Cell Research & Therapy*, *5*(1), 17.

Kim, D., Kim, C.-H., Moon, J.-I., Chung, Y.-G., Chang, M.-Y., Han, B.-S., … Kim, K.-S. (2009). Generation of Human Induced Pluripotent Stem Cells by Direct Delivery of Reprogramming Proteins. *Cell Stem Cell*, *4*(6), 472–476.

Kim, J. H., Wang, M., Lee, J., Park, H., Han, C., Hong, H. S., . . . Woo, D. (2017). Prediction of hepatotoxicity for drugs using human pluripotent stem cell-derived hepatocytes. *Cell Biology and Toxicology,34*(1), 51-64.

Klabunde, R. (2012). *Cardiovascular / physiology concepts*. Philadelphia, PA: Wolters Kluwer Health.

Kleger, A., Seufferlein, T., Malan, D., Tischendorf, M., Storch, A., Wolheim, A., . . . Liebau, S. (2010). Modulation of Calcium-Activated Potassium Channels Induces Cardiogenesis of Pluripotent Stem Cells and Enrichment of Pacemaker-Like Cells. *Circulation,122*(18), 1823-1836.

Koyanagi-Aoi, M., Ohnuki, M., Takahashi, K., Okita, K., Noma, H., Sawamura, Y., … Yamanaka, S. (2013). Differentiation-defective phenotypes revealed by large-scale analyses of human pluripotent stem cells. *Proceedings of the National Academy of Sciences of the United States of America*, *110*(51), 20569–20574.

Kreitner, D. (1981) Existence of two distinct kinds of pacemaker cells in isolated pieces of the rabbit sinus node. *Journal of Physiology. 312*, 37P-38P.

Kreuzberg, M. M., Liebermann, M., Segschneider, S., Dobrowolski, R., Dobrzynski, H., Kaba, R., . . . Willecke, K. (2009). Human connexin31.9, unlike its orthologous protein connexin30.2 in the mouse, is not detectable in the human cardiac conduction system. *Journal of Molecular and Cellular Cardiology,46*(4), 553-559.

Kuga, K., Yamaguchi, I., Sugishita, Y., & Ito, I. (1988). Assessment by autonomic blockade of age-related changes of the sinus node function and autonomic regulation in sick sinus syndrome. *The American Journal of Cardiology,61*(4), 361-366.

Kuga, K., Yamaguchi, I., & Sugishita, Y. (1993). Age-relaterd changes of sinus node function and autonomic regulation in subjects without sinus node disease: Assessment by pharmacologic autonomic blockade. *Japanese Circulation Journal,57*(8), 760-768.

Laflamme, M. A., Chen, K. Y., Naumova, A. V., Muskheli, V., Fugate, J. A., Dupras, S. K., . . . Murry, C. E. (2007). Cardiomyocytes derived from human embryonic stem cells in pro-survival factors enhance function of infarcted rat hearts. *Nature Biotechnology,25*(9), 1015-1024.

Lander, E. S., Linton, L. M., Birren, B., Nusbaum, C., Zody, M. C., Baldwin, J., . . . International Human Genome Sequencing, Consortium. (2001). Initial sequencing and analysis of the human genome. *Nature, 409*(6822), 860-921.

Laurent, L. C., Ulitsky, I., Slavin, I., Tran, H., Schork, A., Morey, R., … Loring, J. F. (2011). Dynamic Changes in the Copy Number of Pluripotency and Cell Proliferation Genes in Human ES and iPS Cells during Reprogramming and Time in Culture. *Cell Stem Cell*, *8*(1), 106–118.

Lavon, N., Yanuka, O., & Benvenisty, N. (2006). The Effect of Overexpression of Pdx1 and Foxa2 on the Differentiation of Human Embryonic Stem Cells into Pancreatic Cells. *Stem Cells,24*(8), 1923-1930. doi:10.1634/stemcells.2005-0397

Lee, J., Liu, J., Lin, S., Harn, H., & Chiou, T. (2018). Advances in Patient-Specific Induced Pluripotent Stem Cells Shed Light on Drug Discovery for Amyotrophic Lateral Sclerosis. *Cell Transplantation,*096368971878515.

Lee, J. H., Protze, S. I., Laksman, Z., Backx, P. H., & Keller, G. M. (2017). Human Pluripotent Stem Cell-Derived Atrial and Ventricular Cardiomyocytes Develop from Distinct Mesoderm Populations. *Cell Stem Cell,21*(2).

Li, M., Kanda, Y., Ashihara, T., Sasano, T., Nakai, Y., Kodama, M., . . . Kurokawa, J. (2017). Overexpression of KCNJ2 in induced pluripotent stem cell-derived cardiomyocytes for the assessment of QT-prolonging drugs. *Journal of Pharmacological Sciences,134*(2), 75-85.

Lian, X., Hsiao, C., Wilson, G., Zhu, K., Hazeltine, L. B., Azarin, S. M., … Palecek, S. P. (2012). Robust cardiomyocyte differentiation from human pluripotent stem cells via temporal modulation of canonical Wnt signaling. *Proceedings of the National Academy of Sciences of the United States of America*, *109*(27), E1848–E1857.

Lian, X., Zhang, J., Azarin, S. M., Zhu, K., Hazeltine, L. B., Bao, X., … Palecek, S. P. (2013). Directed cardiomyocyte differentiation from human pluripotent stem cells by modulating Wnt/β-catenin signaling under fully defined conditions. *Nature Protocols*, *8*(1), 162–175.

Liang, X., Evans, S. M., & Sun, Y. (2015). Insights into Cardiac Conduction System Formation Provided by HCN4 Expression. *Trends in Cardiovascular Medicine*, *25*(1), 1–9.

Liu, J., Dobrzynski, H., Yanni, J., Boyett, M. R., & Lei, M. (2007). Organisation of the mouse sinoatrial node: Structure and expression of HCN channels. *Cardiovascular Research,73*(4), 729-738.

Lou, Q., Hansen, B. J., Fedorenko, O., Csepe, T. A., Kalyanasundaram, A., Li, N., … Fedorov, V. V. (2014). Upregulation of Adenosine A1 Receptors Facilitates Sinoatrial Node Dysfunction in Chronic Canine Heart Failure by Exacerbating Nodal Conduction Abnormalities Revealed by Novel Dual-Sided Intramural Optical Mapping. *Circulation*, *130*(4), 315–324.

Lu, W., Yaoming, N., Boli, R., Jun, C., Changhai, Z., Yang, Z., & Zhiyuan, S. (2013). MHCN4 Genetically Modified Canine Mesenchymal Stem Cells Provide Biological Pacemaking Function in Complete Dogs with Atrioventricular Block. *Pacing and Clinical Electrophysiology,36*(9), 1138-1149.

Luo, W., Shih, Y., Hung, C., Lo, K., Chiang, C., Lo, W., . . . Hu, Y. (2011). Development of the hybrid Sleeping Beauty-baculovirus vector for sustained gene expression and cancer therapy. *Gene Therapy,19*(8), 844-851.

Lyashkov, A. E., Behar, J., Lakatta, E. G., Yaniv, Y., & Maltsev, V. A. (2018). Positive Feedback Mechanisms among Local Ca Releases, NCX, and I CaL Ignite Pacemaker Action Potentials. *Biophysical Journal,114*(5), 1176-1189.

Ma, J., Guo, L., Fiene, S. J., Anson, B. D., Thomson, J. A., Kamp, T. J., … January, C. T. (2011). High purity human-induced pluripotent stem cell-derived cardiomyocytes: electrophysiological properties of action potentials and ionic currents. *American Journal of Physiology - Heart and Circulatory Physiology*, *301*(5), H2006–H2017.

Madhavan, M., Mulpuru, S. K., Mcleod, C. J., Cha, Y., & Friedman, P. A. (2017). Advances and Future Directions in Cardiac Pacemakers. *Journal of the American College of Cardiology,69*(2), 211-235.

Magdy, T., Schuldt, A. J., Wu, J. C., Bernstein, D., & Burridge, P. W. (2018). Human Induced Pluripotent Stem Cell (hiPSC)-Derived Cells to Assess Drug Cardiotoxicity: Opportunities and Problems. *Annual Review of Pharmacology and Toxicology,58*(1), 83-103.

Maltsev, V. A., & Lakatta, E. G. (2009). Synergism of coupled subsarcolemmal Ca2 clocks and sarcolemmal voltage clocks confers robust and flexible pacemaker function in a novel pacemaker cell model. *American Journal of Physiology-Heart and Circulatory Physiology,296*(3).

Maltsev, V. A., & Lakatta, E. G. (2013). Numerical models based on a minimal set of sarcolemmal electrogenic proteins and an intracellular Ca2 clock generate robust, flexible, and energy-efficient cardiac pacemaking. *Journal of Molecular and Cellular Cardiology,59*, 181-195.

Mandai, M., Watanabe, A., Kurimoto, Y., Hirami, Y., Morinaga, C., Daimon, T., . . . Takahashi, M. (2017). Autologous Induced Stem-Cell–Derived Retinal Cells for Macular Degeneration. *New England Journal of Medicine,376*(11), 1038-1046.

Marie, C., Vandermeulen, G., Quiviger, M., Richard, M., Préat, V., & Scherman, D. (2010). PFARs, Plasmids free of antibiotic resistance markers, display high-level transgene expression in muscle, skin and tumour cells. *The Journal of Gene Medicine,12*(4), 323-332.

Mates, L., Chuah, M. K., Belay, E., Jerchow, B., Manoj, N., Acosta-Sanchez, A., . . . Izsvak, Z. (2009). Molecular evolution of a novel hyperactive Sleeping Beauty transposase enables robust stable gene transfer in vertebrates. *Nature Genetics, 41*(6), 753-761.

Maylie, J., Morad, M., & Weiss, J. (1981). A study of pace-maker potential in rabbit sino-atrial node: Measurement of potassium activity under voltage-clamp conditions. *The Journal of Physiology,311*(1), 161-178.

Mengsteab, P. Y., Uto, K., Smith, A. S. T., Frankel, S., Fisher, E., Nawas, Z., … Kim, D.-H. (2016). Spatiotemporal Control of Cardiac Anisotropy Using Dynamic Nanotopographic Cues. *Biomaterials*, *86*, 1–10.

Mezzadra, R., Hollenstein, A., Gomez-Eerland, R., & Schumacher, T. N. (2016). A Traceless Selection: Counter-selection System That Allows Efficient Generation of Transposon and CRISPR-modified T-cell Products. *Molecular Therapy. Nucleic Acids*, *5*(3), e298–.

Miake, J., Marbán, E., & Nuss, H. B. (2002). Gene therapy: Biological pacemaker created by gene transfer. *Nature,419*(6903), 132-133.

Mierop, L. V., & Gessner, I. H. (1970). The morphologic development of the sinoatrial node in the mouse. *The American Journal of Cardiology,25*(2), 204-212.

Mitrofanova, L. B., Gorshkov, A. N., Konovalov, P. V., & Krylova, J. S. (2018). Telocytes in the human sinoatrial node. *Journal of Cellular and Molecular Medicine*, *22*(1), 521–532.

Mohr, J. C., Zhang, J., Azarin, S. M., Soerens, A. G., de Pablo, J. J., Thomson, J. A., … Kamp, T. J. (2010). The Microwell Control of Embryoid Body Size in order to Regulate Cardiac Differentiation of Human Embryonic Stem Cells. *Biomaterials*, *31*(7), 1885.

Monfredi, O., Dobrzynski, H., Mondal, T., Boyett, M. R., & Morris, G. M. (2010). The Anatomy and Physiology of the Sinoatrial Node-A Contemporary Review. *Pacing and Clinical Electrophysiology,33*(11), 1392-1406.

Monjezi, R., Miskey, C., Gogishvili, T., Schleef, M., Schmeer, M., Einsele, H., . . . Hudecek, M. (2016). Enhanced CAR T-cell engineering using non-viral Sleeping Beauty transposition from minicircle vectors. *Leukemia,31*(1), 186-194.

Morad, M., & Zhang, X. (2017). Mechanisms of spontaneous pacing: Sinoatrial nodal cells, neonatal cardiomyocytes, and human stem cell derived cardiomyocytes. *Canadian Journal of Physiology and Pharmacology*, 95(10), 1100-1107.

Morris, G. M., & Kalman, J. M. (2014). Fibrosis, Electrics and Genetics. *Circulation Journal,78*(6), 1272-1282.

Much, B., Wahl-Schott, C., Zong, X., Schneider, A., Baumann, L., Moosmang, S., . . . Biel, M. (2003). Role of Subunit Heteromerization andN-Linked Glycosylation in the Formation of Functional Hyperpolarization-activated Cyclic Nucleotide-gated Channels. *Journal of Biological Chemistry,278*(44), 43781-43786.

Müller, F.-J., Schuldt, B. M., Williams, R., Mason, D., Altun, G., Papapetrou, E., … Loring, J. F. (2011). A bioinformatic assay for pluripotency in human cells. *Nature Methods*, 8(4), 315–317.

Mulpuru, S. K., Madhavan, M., Mcleod, C. J., Cha, Y., & Friedman, P. A. (2017). Cardiac Pacemakers: Function, Troubleshooting, and Management. *Journal of the American College of Cardiology,69*(2), 189-210.

Mummery, C. L., Zhang, J., Ng, E. S., Elliott, D. A., Elefanty, A. G., & Kamp, T. J. (2012). Differentiation of Human ES and iPS Cells to Cardiomyocytes: A Methods Overview. *Circulation Research*, *111*(3), 344–358.

Muñoz-López, M., & García-Pérez, J. L. (2010). DNA Transposons: Nature and Applications in Genomics. *Current Genomics*, *11*(2), 115–128.

Nam, Y.-J., Song, K., Luo, X., Daniel, E., Lambeth, K., West, K., … Olson, E. N. (2013). Reprogramming of human fibroblasts toward a cardiac fate. *Proceedings of the National Academy of Sciences of the United States of America*, *110*(14), 5588–5593.

Narayanavari, S.A., Chilkunda, S.S., Ivics, Z. & Izsvák, Z. (2017). *Sleeping Beauty* transposition: from biology to applications. *Critical Reviews in Biochemistry and Molecular Biology*, 52:1, 18-44,

Noble, D. (1960). Cardiac action and pacemaker potentials based on the Hodgkin-Huxley equations. *Nature*. *188*, 495–7.

Noble, D. (1962). A modification of the Hodgkin-Huxley equations applicable to Purkinje fibre action and pacemaker potentials. *The Journal of Physiology,160*(2), 317-352.

Noma, A., Morad, M., & Irisawa, H. (1983). Does the 'pacemaker current' generate the diastolic depolarization in the rabbit SA node cells? *Pflugers Archiv European Journal of Physiology,397*(3), 190-194.

Nong, Y., Zhang, C., Wei, L., Zhang, Z., Cheng, J., Wen, L., & Song, Z. (2013). In situ investigation of allografted mouse HCN4 gene–transfected rat bone marrow mesenchymal stromal cells with the use of patch-clamp recording of ventricular slices. *Cytotherapy,15*(8), 905-919.

Ohnuki, M., Tanabe, K., Sutou, K., Teramoto, I., Sawamura, Y., Narita, M., … Takahashi, K. (2014). Dynamic regulation of human endogenous retroviruses mediates factor-induced reprogramming and differentiation potential. *Proceedings of the National Academy of Sciences of the United States of America*, *111*(34), 12426–12431.

Oikonomopoulos, A., Kitani, T., & Wu, J. C. (2018). Pluripotent Stem Cell-Derived Cardiomyocytes as a Platform for Cell Therapy Applications: Progress and Hurdles for Clinical Translation. *Molecular Therapy,26*(7), 1624-1634.

Okita, K., Matsumura, Y., Sato, Y., Okada, A., Morizane, A., Okamoto, S., . . . Yamanaka, S. (2011). A more efficient method to generate integration-free human iPS cells. Nature Methods, 8(5), 409-412.

Opthof, T., Dejonge, B., Mackaay, A., Bleeker, W., Massonpevet, M., Jongsma, H., & Bouman, L. (1985). Functional and morphological organization of the guinea-pig sinoatrial node compared with the rabbit sinoatrial node. *Journal of Molecular and Cellular Cardiology,17*(6), 549-564.

Orbán, T. I., Apáti, Á, Németh, A., Varga, N., Krizsik, V., Schamberger, A., . . . Sarkadi, B. (2009). Applying a "Double-Feature" Promoter to Identify Cardiomyocytes Differentiated from Human Embryonic Stem Cells Following Transposon-Based Gene Delivery. *Stem Cells,27*(5), 1077-1087.

Paige, S. L., Osugi, T., Afanasiev, O. K., Pabon, L., Reinecke, H., & Murry, C. E. (2010). Endogenous Wnt/β-Catenin Signaling Is Required for Cardiac Differentiation in Human Embryonic Stem Cells. *PLoS ONE*, *5*(6), e11134.

Park, D. S., & Fishman, G. I. (2011). Basic Science for Clinicians: The Cardiac Conduction System. *Circulation*, *123*(8), 904–915.

Park, I.-H., Arora, N., Huo, H., Maherali, N., Ahfeldt, T., Shimamura, A., … Daley, G. Q. (2008). Disease-specific induced pluripotent stem (iPS) cells. *Cell*, *134*(5), 877–886. http://doi.org/10.1016/j.cell.2008.07.041

Pastor, M., Johnen, S., Harmening, N., Quiviger, M., Pailloux, J., Kropp, M., . . . Marie, C. (2018). The Antibiotic-free pFAR4 Vector Paired with the Sleeping Beauty Transposon System Mediates Efficient Transgene Delivery in Human Cells. *Molecular Therapy - Nucleic Acids,11*, 57-67.

Plotnikov, A. N., Sosunov E.A., Qu J., Shlapakova I.N., Anyukhovsky E.P., Liu L.,... Rosen MR. (2004). Biological Pacemaker Implanted in Canine Left Bundle Branch Provides Ventricular Escape Rhythms That Have Physiologically Acceptable Rates. *Circulation,109*(4), 506-512.

Plotnikov, A. N., Shlapakova, I., Szabolcs, M. J., Danilo, P., Lorell, B. H., Potapova, I. A., . . . Rosen, M. R. (2007). Xenografted Adult Human Mesenchymal Stem Cells Provide a Platform for Sustained Biological Pacemaker Function in Canine Heart. *Circulation,116*(7), 706-713.

Plotnikov, A. N., Bucchi, A., Shlapakova, I., Danilo, P., Brink, P. R., Robinson, R. B., … Rosen, M. R. (2008). HCN212-channel biological pacemakers manifesting ventricular tachyarrhythmias are responsive to treatment with $I_f$blockade. *Heart Rhythm : The Official Journal of the Heart Rhythm Society*, *5*(2), 282–288.

Potapova, I., Plotnikov A., Lu Z., Danilo P. Jr., Valiunas V., Qu J., Doronin S., … Cohen I.S. (2004). Human Mesenchymal Stem Cells as a Gene Delivery System to Create Cardiac Pacemakers. *Circulation Research,94*(7), 952-959.

Protze, S. I., Liu, J., Nussinovitch, U., Ohana, L., Backx, P. H., Gepstein, L., & Keller, G. M. (2016). Sinoatrial node cardiomyocytes derived from human pluripotent cells function as a biological pacemaker. *Nature Biotechnology,35*(1), 56-68.

Qu, J., Barbuti, A., Protas, L., Santoro, B., Cohen, I. S., & Robinson, R. B. (2001). HCN2 Overexpression in Newborn and Adult Ventricular Myocytes : Distinct Effects on Gating and Excitability. *Circulation Research,89*(1).

Qu, J., Plotnikov A.N., Danilo P. Jr., Shlapakova I., Cohen I.S., Robinson R.B., Rosen M.R. (2003). Expression and Function of a Biological Pacemaker in Canine Heart. *Circulation,107*(8), 1106-1109.

Raatikainen, M. P., Arnar, D. O., Merkely, B., Nielsen, J. C., Hindricks, G., Heidbuchel, H., & Camm, J. (2017). A Decade of Information on the Use of Cardiac Implantable Electronic Devices and Interventional Electrophysiological Procedures in the European Society of Cardiology Countries: 2017 Report from the European Heart Rhythm Association. *EP Europace,19*(Suppl_2), Ii1-Ii90.

Ratcliffe, E., Thomas, R. J., & Williams, D. J. (2011). Current understanding and challenges in bioprocessing of stem cell-based therapies for regenerative medicine. *British Medical Bulletin,100*(1), 137-155.

Ravens U, Cerbai E. Role of potassium currents in cardiac arrhythmias. Europace. 2008 Oct;10(10):1133-7.

Refaey, M. M., & Mohler, P. J. (2017). Ankyrins and Spectrins in Cardiovascular Biology and Disease. *Frontiers in Physiology,8*.

Rezazadeh, S., & Duff, H. J. (2017). Genetic Determinants of Hereditary Bradyarrhythmias: A Contemporary Review of a Diverse Group of Disorders. *Canadian Journal of Cardiology,33*(6), 758-767.

Rimmbach, C., Jung, J. J., & David, R. (2015). Generation of Murine Cardiac Pacemaker Cell Aggregates Based on ES-Cell-Programming in Combination with Myh6-Promoter-Selection. *Journal of Visualized Experiments : JoVE*, (96), 52465. Advance online publication.

Robbins, J. P., & Price, J. (2017). Human induced pluripotent stem cells as a research tool in Alzheimer's disease. *Psychological Medicine*, *47*(15), 2587–2592.

Robinson, R. B., & Siegelbaum, S. A. (2003). Hyperpolarization-Activated Cation Currents: From Molecules to Physiological Function. *Annual Review of Physiology,65*(1), 453-480.

Ronaldson-Bouchard, K., Ma, S. P., Yeager, K., Chen, T., Song, L., Sirabella, D., . . . Vunjak-Novakovic, G. (2018). Advanced maturation of human cardiac tissue grown from pluripotent stem cells. *Nature,556*(7700), 239-243.

Rosen, M., Brink P.R., Cohen I.S., Robinson R.B. (2004). Genes, stem cells and biological pacemakers. *Cardiovascular Research,64*(1), 12-23.

Rostovskaya, M., Fu, J., Obst, M., Baer, I., Weidlich, S., Wang, H., . . . Stewart, A. F. (2012). Transposon-mediated BAC transgenesis in human ES cells. *Nucleic Acids Research,40*(19).

Rostovskaya, M., Naumann, R., Fu, J., Obst, M., Mueller, D., Stewart, A. F., & Anastassiadis, K. (2013). Transposon mediated BAC transgenesis via pronuclear injection of mouse zygotes. *Genesis,51*(2), 135-141.

Ruhparwar, A., Kallenbach, K., Klein, G., Bara, C., Ghodsizad, A., Sigg, D. C., . . . Niehaus, M. (2010). Adenylate-Cyclase VI Transforms Ventricular Cardiomyocytes into Biological Pacemaker Cells. *Tissue Engineering Part A,16*(6), 1867-1872.

Saito, Y., Nakamura, K., Yoshida, M., Sugiyama, H., Ohe, T., Kurokawa, J., … Ito, H. (2015). Enhancement of Spontaneous Activity by HCN4 Overexpression in Mouse Embryonic Stem Cell-Derived Cardiomyocytes - A Possible Biological Pacemaker. *PLoS ONE*, *10*(9), e0138193.

Saito, Y., Nakamura, K., Yoshida, M., Sugiyama, H., Takano, M., Nagase, S., . . . Ito, H. (2018). HCN4-Overexpressing Mouse Embryonic Stem Cell-Derived Cardiomyocytes Generate a New Rapid Rhythm in Rats with Bradycardia. *International Heart Journal,59*(3), 601-606.

Sánchez-Quintana D., Yen Ho S. (2003) [Anatomy of cardiac nodes and atrioventricular specialized conduction system]. Rev Esp Cardiol. 56(11), 1085-92.

Sánchez-Quintana, D., Cabrera, J. A., Farré, J., Climent, V., Anderson, R. H., & Ho, S. Y. (2005). Sinus node revisited in the era of electroanatomical mapping and catheter ablation. *Heart*, *91*(2), 189–194.

Sanders, P. (2004). Remodeling of Sinus Node Function in Patients With Congestive Heart Failure: Reduction in Sinus Node Reserve. *Circulation,110*(8), 897-903.

Satoh, H., Delbridge, L. M., Blatter, L. A., & Bers, D. M. (1996). Surface:volume relationship in cardiac myocytes studied with confocal microscopy and membrane capacitance measurements: species-dependence and developmental effects. *Biophysical Journal*, *70*(3), 1494–1504.

Satoh, H. (2003). Sino-Atrial Nodal Cells of Mammalian Hearts: Ionic Currents and Gene Expression of Pacemaker Ionic Channels. *Journal of Smooth Muscle Research*, 39(5), 175-193.

Sayed, N., Liu, C., & Wu, J. C. (2016). Translation of Human iPSCs: From Clinical Trial in a Dish to Precision Medicine. *Journal of the American College of Cardiology*, *67*(18), 2161–2176.

Schindelin, J., Arganda-Carreras, I., Frise, E., Kaynig, V., Longair, M., Pietzsch, T., … Cardona, A. (2012). Fiji - an Open Source platform for biological image analysis. *Nature Methods*, *9*(7), 10.1038/nmeth.2019.

Schulze-Bahr, E., Neu, A., Friederich, P., Kaupp, U. B., Breithardt, G., Pongs, O., & Isbrandt, D. (2003). Pacemaker channel dysfunction in a patient with sinus node disease. *Journal of Clinical Investigation,111*(10), 1537-1545.

Schweizer, P. A., Darche, F. F., Ullrich, N. D., Geschwill, P., Greber, B., Rivinius, R., … Thomas, D. (2017). Subtype-specific differentiation of cardiac pacemaker cell clusters from human induced pluripotent stem cells. *Stem Cell Research & Therapy*, *8*, 229.

Sharma, A., Marceau, C., Hamaguchi, R., Burridge, P. W., Rajarajan, K., Churko, J. M., … Wu, J. C. (2014). Human Induced Pluripotent Stem Cell-Derived Cardiomyocytes as an In Vitro Model for Coxsackievirus B3-Induced Myocarditis and Antiviral Drug Screening Platform. *Circulation Research*, *115*(6), 556–566.

Sharma, A., Burridge, P. W., McKeithan, W. L., Serrano, R., Shukla, P., Sayed, N., … Wu, J. C. (2017). High-Throughput Screening of Tyrosine Kinase Inhibitor Cardiotoxicity with Human Induced Pluripotent Stem Cells. *Science Translational Medicine*, *9*(377), eaaf2584.

Sharma, A., Toepfer, C. N., Ward, T., Wasson, L., Agarwal, R., Conner, D. A., . . . Seidman, C. E. (2018). CRISPR/Cas9-Mediated Fluorescent Tagging of Endogenous Proteins in Human Pluripotent Stem Cells. *Current Protocols in Human Genetics,96*(1).

Shiba, Y., Fernandes, S., Zhu, W.-Z., Filice, D., Muskheli, V., Kim, J., … Laflamme, M. A. (2012). hESC-Derived Cardiomyocytes Electrically Couple and Suppress Arrhythmias in Injured Hearts. *Nature*, *489*(7415), 322–325.

Silva, S. D., Mastrangelo, M. A., Lotta, L. T., Burris, C. A., Federoff, H. J., & Bowers, W. J. (2009). Extending the transposable payload limit of Sleeping Beauty (SB) using the Herpes Simplex Virus (HSV)/SB amplicon-vector platform. *Gene Therapy,17*(3), 424-431.

Sirenko, S. G., Yang, D., Maltseva, L. A., Kim, M. S., Lakatta, E. G., & Maltsev, V. A. (2017). Spontaneous, local diastolic subsarcolemmal calcium releases in single, isolated guinea-pig sinoatrial nodal cells. *PLoS ONE*, *12*(9), e0185222.

Snir, M., Kehat, I., Gepstein, A., Coleman, R., Itskovitz-Eldor, J., Livne, E., & Gepstein, L. (2003). Assessment of the ultrastructural and proliferative properties of human embryonic stem cell-derived cardiomyocytes. *American Journal of Physiology-Heart and Circulatory Physiology,285*(6).

Sommer, C. A., Capilla, A., Molina-Estevez, F. J., Gianotti-Sommer, A., Skvir, N., Caballero, I., … Mostoslavsky, G. (2018). Modeling APC mutagenesis and familial adenomatous polyposis using human iPS cells. *PLoS ONE*, *13*(7), e0200657.

Später, D., Abramczuk, M. K., Buac, K., Zangi, L., Stachel, M. W., Clarke, J., . . . Chien, K. R. (2013). A HCN4 cardiomyogenic progenitor derived from the first heart field and human pluripotent stem cells. *Nature Cell Biology,15*(9), 1098-1106.

Stein, R., Medeiros, C. M., Rosito, G. A., Zimerman, L. I., & Ribeiro, J. P. (2002). Intrinsic sinus and atrioventricular node electrophysiologic adaptations in endurance athletes. *Journal of the American College of Cardiology,39*(6), 1033-1038.

Sterneckert, J. L., Reinhardt, P., & Schöler, H. R. (2014). Investigating human disease using stem cell models. *Nature Reviews Genetics,15*(9), 625-639.

Stieber, J., Herrmann, S., Feil, S., Loster, J., Feil, R., Biel, M., . . . Ludwig, A. (2003). The hyperpolarization-activated channel HCN4 is required for the generation of pacemaker

action potentials in the embryonic heart. *Proceedings of the National Academy of Sciences,100*(25), 15235-15240.

Takahashi, K., Tanabe, K., Ohnuki, M., Narita, M., Ichisaka, T., Tomoda, K., & Yamanaka, S. (2007). Induction of Pluripotent Stem Cells from Adult Human Fibroblasts by Defined Factors. *Cell,131*(5), 861-872.

Takahashi, T., Nagai, T., Kanda, M., Liu, M., Kondo, N., Naito, A. T., . . . Kobayashi, Y. (2015). Regeneration of the Cardiac Conduction System by Adipose Tissue-Derived Stem Cells. *Circulation Journal,79*(12), 2703-2712.

Takayama, K., Inamura, M., Kawabata, K., Katayama, K., Higuchi, M., Tashiro, K., … Mizuguchi, H. (2012). Efficient Generation of Functional Hepatocytes From Human Embryonic Stem Cells and Induced Pluripotent Stem Cells by HNF4α Transduction. *Molecular Therapy*, *20*(1), 127–137.

Takeuchi, J. K., & Bruneau, B. G. (2009). Directed transdifferentiation of mouse mesoderm to heart tissue by defined factors. *Nature*, *459*(7247), 708–711.

Thomson, J. A., Itskovitz-Eldor J, Shapiro SS, Waknitz MA, Swiergiel JJ, Marshall VS, Jones JM. (1998). Embryonic Stem Cell Lines Derived from Human Blastocysts. *Science,282*(5391), 1145-1147.

Timmis, A., Townsend, N., Gale, C., Grobbee, R., Maniadakis, N., Flather, M., . . . Logstrup, S. (2017). European Society of Cardiology: Cardiovascular Disease Statistics 2017. *European Heart Journal,39*(7), 508-579.

Tohyama, S., Hattori, F., Sano, M., Hishiki, T., Nagahata, Y., Matsuura, T., . . . Fukuda, K. (2013). Distinct Metabolic Flow Enables Large-Scale Purification of Mouse and Human Pluripotent Stem Cell-Derived Cardiomyocytes. *Cell Stem Cell,12*(1), 127-137.

Tran, N., Proenza, C., Macri, V., Petigara, F., Sloan, E., Samler, S., & Accili, E. A. (2002). A Conserved Domain in the NH2Terminus Important for Assembly and Functional Expression of Pacemaker Channels. *Journal of Biological Chemistry,277*(46), 43588-43592.

Trillhaase, A., Haferkamp, U., Rangnau, A., Märtens, M., Schmidt, B., Trilck, M., . . . Aherrahrou, Z. (2018). Differentiation of human iPSCs into VSMCs and generation of VSMC-derived calcifying vascular cells. *Stem Cell Research,31*, 62-70.

Tsutsui, K., Monfredi, O. J., Sirenko-Tagirova, S. G., Maltseva, L. A., Bychkov, R., Kim, M. S., . . . Lakatta, E. G. (2018). A coupled-clock system drives the automaticity of human sinoatrial nodal pacemaker cells. *Science Signaling,11*(534).

Ueno, S., Weidinger, G., Osugi, T., Kohn, A. D., Golob, J. L., Pabon, L., … Murry, C. E. (2007). Biphasic role for Wnt/β-catenin signaling in cardiac specification in zebrafish and embryonic stem cells. *Proceedings of the National Academy of Sciences of the United States of America*, *104*(23), 9685–9690.

Unudurthi, S. D., Wolf, R. M., & Hund, T. J. (2014). Role of sinoatrial node architecture in maintaining a balanced source-sink relationship and synchronous cardiac pacemaking. *Frontiers in Physiology*, *5*, 446.

Vaccari, T., Moroni, A., Rocchi, M., Gorza, L., Bianchi, M., Beltrame, M., & Difrancesco, D. (1999). The human gene coding for HCN2, a pacemaker channel of the heart. *Biochimica Et Biophysica Acta (BBA) - Gene Structure and Expression,1446*(3), 419-425.

Valiunas, V., Doronin, S., Valiuniene, L., Potapova, I., Zuckerman, J., Walcott, B., . . . Cohen, I. S. (2004). Human mesenchymal stem cells make cardiac connexins and form functional gap junctions. *The Journal of Physiology,555*(3), 617-626.

Vedantham, V. (2015). New Approaches to Biological Pacemakers: Links to Sinoatrial Node Development. *Trends in Molecular Medicine*, *21*(12), 749–761.

Verkerk, A. O., Marcel M. G. J. Van Borren, Peters, R. J., Broekhuis, E., Lam, K. Y., Coronel, R., . . . Wilders, R. (2007). Single Cells Isolated from Human Sinoatrial Node: Action Potentials and Numerical Reconstruction of Pacemaker Current. *2007 29th Annual International Conference of the IEEE Engineering in Medicine and Biology Society*.

Verkerk, A. O., & Wilders, R. (2015). Pacemaker activity of the human sinoatrial node: an update on the effects of mutations in HCN4 on the hyperpolarization-activated current. *International Journal of Molecular Sciences*, 16(2), 3071–3094

Vinogradova, T. M., Brochet, D. X., Sirenko, S., Li, Y., Spurgeon, H., & Lakatta, E. G. (2010). Sarcoplasmic Reticulum Ca2 Pumping Kinetics Regulates Timing of Local Ca2 Releases and Spontaneous Beating Rate of Rabbit Sinoatrial Node Pacemaker Cells. *Circulation Research,107*(6), 767-775.

Warren, L., Manos, P. D., Ahfeldt, T., Loh, Y.-H., Li, H., Lau, F., … Rossi, D. J. (2010). Highly efficient reprogramming to pluripotency and directed differentiation of human cells using synthetic modified mRNA. *Cell Stem Cell*, *7*(5), 618–630.

Williams, D. A. (2008). Sleeping Beauty Vector System Moves Toward Human Trials in the United States. *Molecular Therapy,16*(9), 1515-1516.

Woods, W. T., Urthaler, F., & James, T. N. (1976). Spontaneous action potentials of cells in the canine sinus node. Circulation Research, 39(1), 76-82.

Wu, J., Schuessler, R. B., Rodefeld, M. D., Saffitz, J. E., & Boineau, J. P. (2001). Morphological and membrane characteristics of spider and spindle cells isolated from rabbit sinus node. *American Journal of Physiology-Heart and Circulatory Physiology,280*(3).

Wu, Y., Gao, Z., Chen, B., Koval, O. M., Singh, M. V., Guan, X., . . . Anderson, M. E. (2009). Calmodulin kinase II is required for fight or flight sinoatrial node physiology. *Proceedings of the National Academy of Sciences,106*(14), 5972-5977.

Xue, T., Cho H.C., Akar F.G., Tsang S.Y., Jones S.P., Marbán E., Tomaselli G.F. & Li R.A. (2005). Functional Integration of Electrically Active Cardiac Derivatives From Genetically Engineered Human Embryonic Stem Cells With Quiescent Recipient Ventricular

Cardiomyocytes: Insights Into the Development of Cell-Based Pacemakers. *Circulation,111*(1), 11-20.

Yang, L., Soonpaa, M. H., Adler, E. D., Roepke, T. K., Kattman, S. J., Kennedy, M., . . . Keller, G. M. (2008). Human cardiovascular progenitor cells develop from a KDR embryonic-stem-cell-derived population. *Nature,453*(7194), 524-528. doi:10.1038/nature06894

Yang, X., Zhou, Y., Li, H., Han, L., & Jiang, W. (2008). Mesenchymal Stem Cells as a Gene Delivery System to Create Biological Pacemaker Cells in vitro. *Journal of International Medical Research,36*(5), 1049-1055.

Yaniv, Y., Spurgeon, H. A., Lyashkov, A. E., Yang, D., Ziman, B. D., Maltsev, V. A., & Lakatta, E. G. (2012). Crosstalk between Mitochondrial and Sarcoplasmic Reticulum Ca2 Cycling Modulates Cardiac Pacemaker Cell Automaticity. *PLoS ONE,7*(5).

Yaniv, Y., Lakatta, E. G., & Maltsev, V. A. (2015). From two competing oscillators to one coupled-clock pacemaker cell system. *Frontiers in Physiology,6*.

Ye, L., Chang, Y.-H., Xiong, Q., Zhang, P., Zhang, L., Somasundaram, P., … Zhang, J. (2014). Cardiac repair in a porcine model of acute myocardial infarction with human induced pluripotent stem cell-derived cardiovascular cell populations. *Cell Stem Cell*, *15*(6), 750–761.

Yechikov, S., Copaciu, R., Gluck, J. M., Deng, W., Chiamvimonvat, N., Chan, J. W., & Lieu, D. K. (2016). Same-Single-Cell Analysis of Pacemaker-Specific Markers in Human Induced Pluripotent Stem Cell-Derived Cardiomyocyte Subtypes Classified by Electrophysiology. *Stem Cells (Dayton, Ohio)*, *34*(11), 2670–2680.

Yoshida, Y., & Yamanaka, S. (2011). IPS cells: A source of cardiac regeneration. *Journal of Molecular and Cellular Cardiology,50*(2), 327-332.

Young, L., Sung, J., Stacey, G., & Masters, J. R. (2010). Detection of Mycoplasma in cell cultures. *Nature Protocols,5*(5), 929-934.

Yu, F. H. (2005). Overview of Molecular Relationships in the Voltage-Gated Ion Channel Superfamily. *Pharmacological Reviews,57*(4), 387-395.

Yu, J., Chau, K. F., Vodyanik, M. A., Jiang, J., & Jiang, Y. (2011). Efficient Feeder-Free Episomal Reprogramming with Small Molecules. *PLoS ONE*, *6*(3), e17557.

Zayed, H., Izsvak, Z., Walisko, O., & Ivics, Z. (2004). Development of hyperactive sleeping beauty transposon vectors by mutational analysis. *Molecular Therapy, 9*(2), 292-304.

Zhang, J., Wilson, G. F., Soerens, A. G., Koonce, C. H., Yu, J., Palecek, S. P., … Kamp, T. J. (2009). Functional Cardiomyocytes Derived from Human Induced Pluripotent Stem Cells. *Circulation Research*, *104*(4), e30–e41.

Zhang, X., Wei, H., Šarić, T., Hescheler, J., Cleemann, L., & Morad, M. (2015). Regionally diverse mitochondrial calcium signaling regulates spontaneous pacing in developing cardiomyocytes. *Cell Calcium,57*(5-6), 321-336.

Zhou, H., Wu, S., Joo, J. Y., Zhu, S., Han, D. W., Lin, T., . . . Ding, S. (2009). Generation of Induced Pluripotent Stem Cells Using Recombinant Proteins. *Cell Stem Cell,4*(5), 381-384.

Zhou, Y., Yang, X., Li, H., Han, L., & Jiang, W. (2013). Genetically-engineered mesenchymal stem cells transfected with human HCN1 gene to create cardiac pacemaker cells. *Journal of International Medical Research,41*(5), 1570-1576. doi:10.1177/0300060513501123

Contributions

I performed all the experiments and analyzed all the data, with few exceptions already cited in the main text and summarized here:

The teratoma assay was performed by EPO GmbH - Experimental Pharmacology & Oncology, Berlin, Germany.

The SNP karyotyping was performed by the SCCF in cooperation with Prof. Hübner laboratory and analyzed by Dr. Sebastian Diecke at the MDC, Berlin, Germany.

Cardiac AP and I_f current recordings from SCVI 113 hiPSCs were performed by Dr. Mirko Moroni in the laboratory of Prof. Dr. Gary R. Lewin at MDC, Berlin, Germany. I_f currents from CMs and C6, C15 and IMR90 C8 hiPSC lines were recorded and analyzed by Dr. Xiaohua Zhang and I_f currents from HEK293T cells were recorded and analyzed by Nathaniel Jensen in the laboratory of Prof. Dr. Martin Morad at the MUSC, Charleston, South Carolina, USA.

Appendix

I. Plasmid maps

I.1 pCAGGS-SB100X

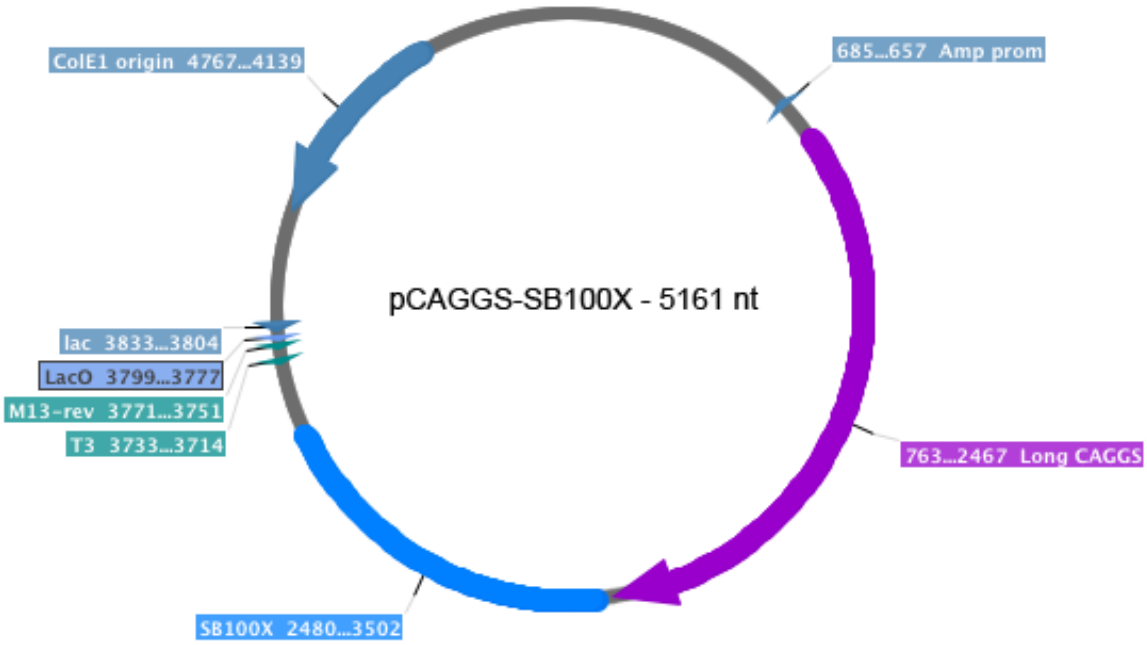

I.2 pT2CVIneo3

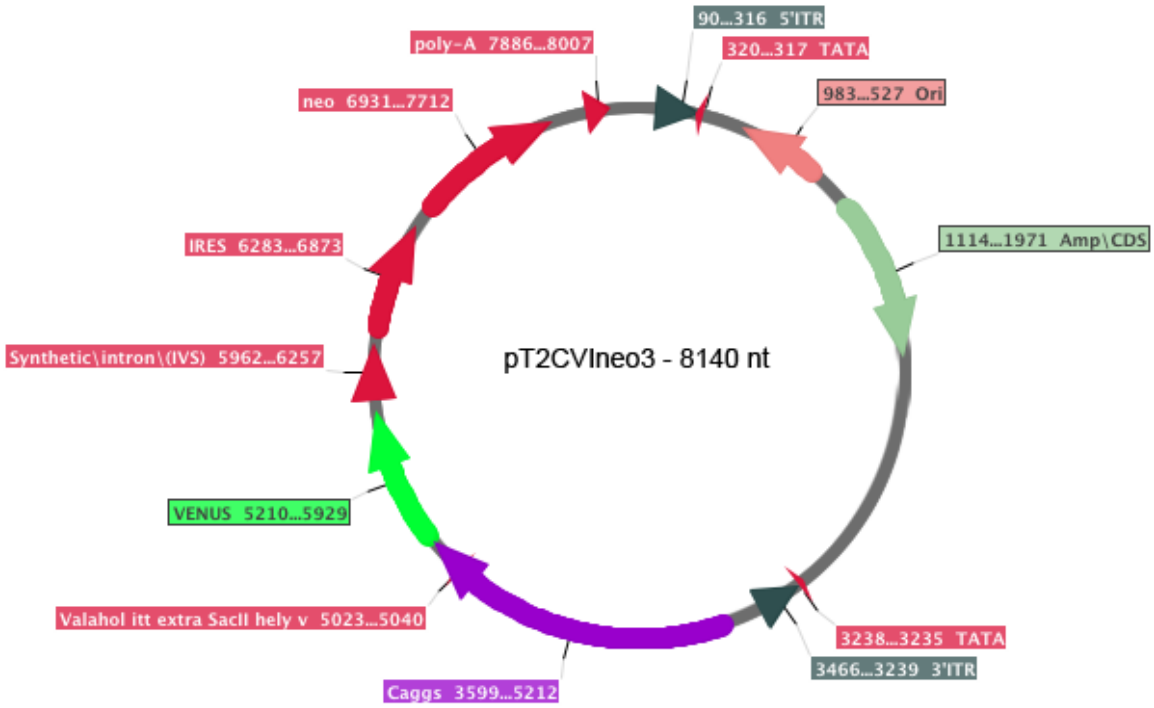

I.3 pT2-GFP

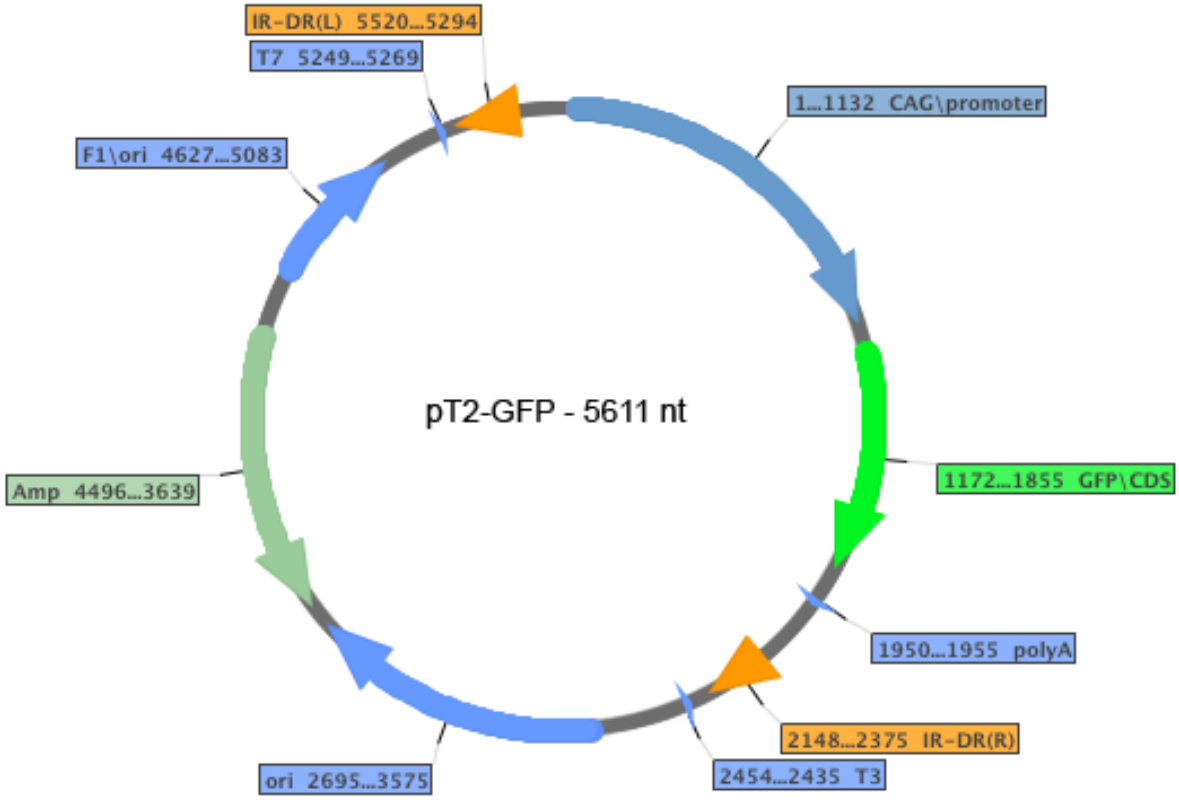

I.4 pJET1.2-IRESreverse

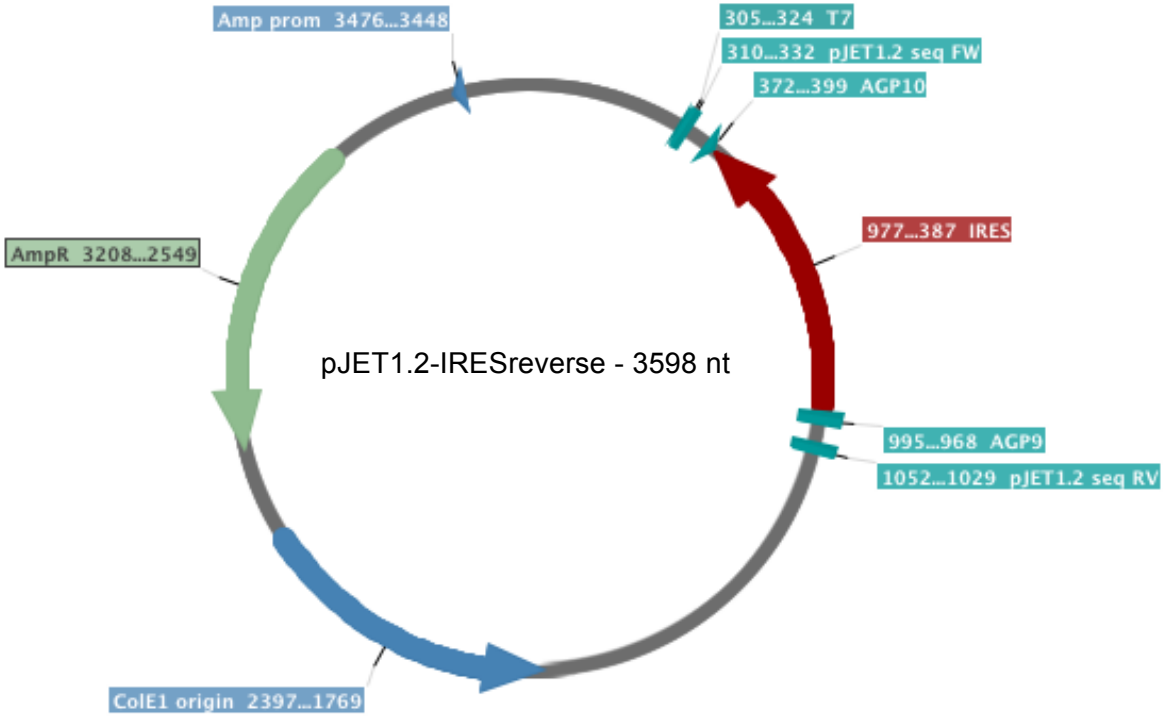

I.5 pT2-IRES-GFP

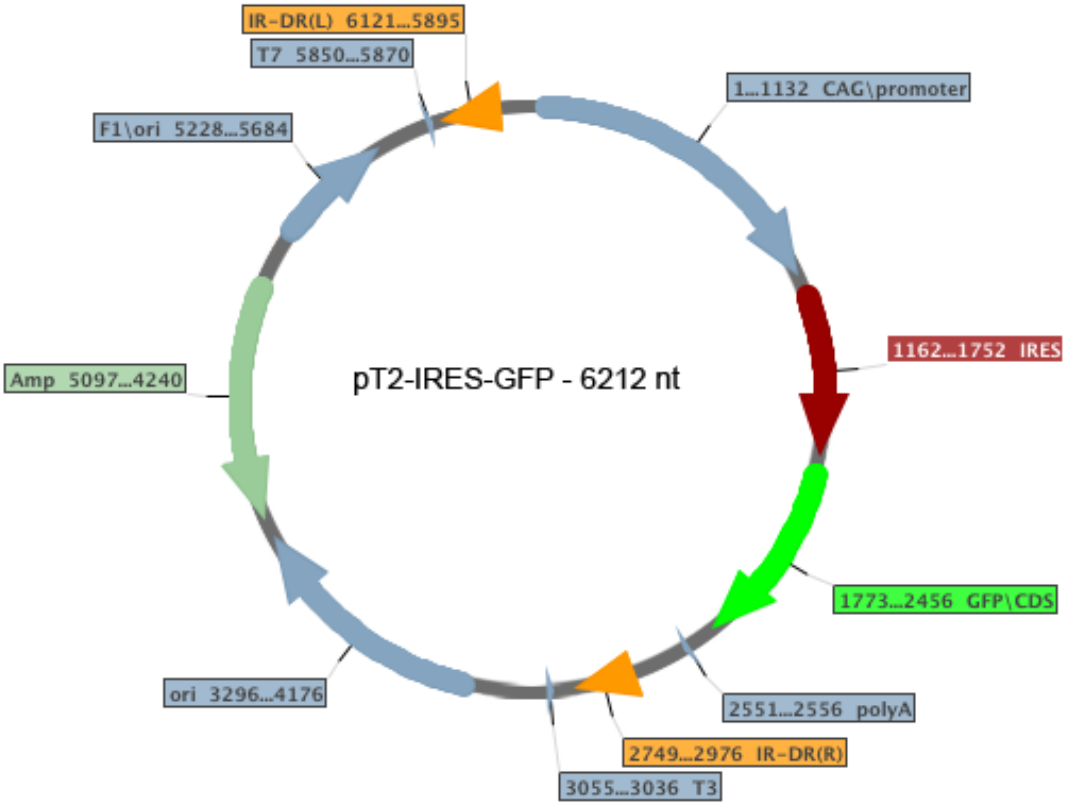

I.6 pT2-hHCN4-GFP

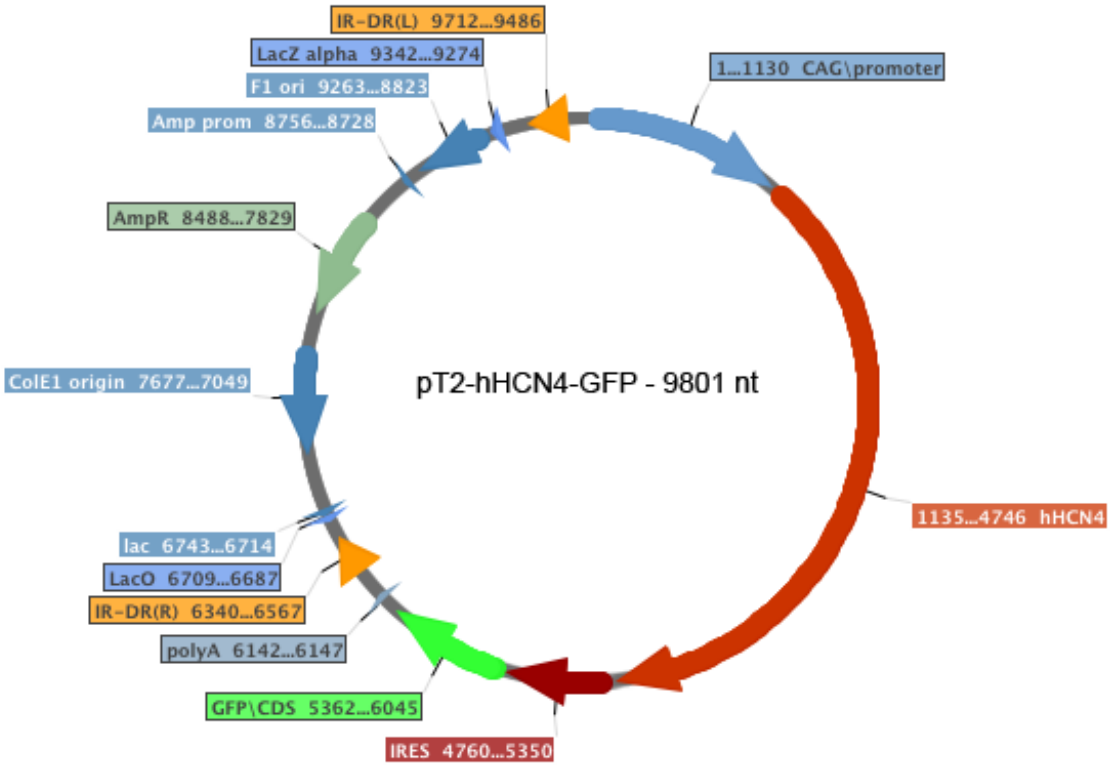

II. Antibodies summary table

Antibody	Clone	Host species	Cat. No.	Provider	RRID	Stock concentration	Working dilution	Application
α-Actinin (sarcomeric)	EA-53	Mouse	A7811	Sigma-Aldrich	AB_476766	10-22mg/ml	1:800/1:1000	IF
HCN4	Polyclonal	Rabbit	ab69054	Abcam	AB_1861080	1mg/ml	1:1000/1:2000 1:100/1:200	WB IF
Nanog	Polyclonal	Goat	AF1997	R&D Systems	AB_355097	0,2mg/ml	1:200	IF
Nkx2.5	E1Y8H	Rabbit	#8792	Cell Signaling			1:1000 1:800	FACS IF
Oct-3/4	C-10	Mouse	sc-5279	Santa Cruz Biotechnology	AB_628051	0,2mg/ml	1:300	IF
Sox-2 (Y-17)	Polyclonal	Goat	sc-17320	Santa Cruz Biotechnology	AB_2286684	0,2mg/ml	1:100	IF
TRA-1-60	TRA-1-60	Mouse	09-0010	Stemgent	AB_1512170	0,5mg/ml	1:80/1:100	IF
TRA-1-81	TRA-1-81	Mouse	09-0011	Stemgent	AB_1512171	0,5mg/ml	1:80/1:100	IF
Troponin T-C	CT3	Mouse	sc-20025	Santa Cruz Biotechnology	AB_628403	0,2mg/ml	1:200	FACS IF
anti-mouse IgG (H+L) Alexa Fluor 647	Polyclonal	Donkey	A-31571	Invitrogen™, Thermo Fisher Scientific	AB_162542	2mg/ml	1:1000	FACS IF
anti-mouse IgG (H+L) Alexa Fluor 555	Polyclonal	Donkey	A-31570	Invitrogen™, Thermo Fisher Scientific	AB_2536180	2mg/ml	1:1000	IF
anti-goat IgG (H+L) Alexa Fluor 555	Polyclonal	Donkey	A-21432	Invitrogen™, Thermo Fisher Scientific	AB_2535853	2mg/ml	1:1000	IF
anti-goat IgG (H+L) Cy™3	Polyclonal	Donkey	705-165-147	Jackson Immuno Research	AB_2307351	1,5mg/ml	1:500	IF
anti-rabbit IgG (H+L) Alexa Fluor 546	Polyclonal	Goat	A-11010	Invitrogen™, Thermo Fisher Scientific	AB_2534077	2mg/ml	1:1000	FACS IF
anti-rabbit IgG (H+L) Alexa Fluor 647	Polyclonal	Donkey	A-31573	Invitrogen™, Thermo Fisher Scientific	AB_2536183	2mg/ml	1:1000	IF
anti-rabbit IgG (H+L) Cy™3	Polyclonal	Donkey	711-165-152	Jackson Immuno Research	AB_2307443	1,5mg/ml	1:1000	IF
anti-rabbit IgG (H+L) HRP	Polyclonal	Goat	31462	Thermo Fisher Scientific	AB_228338	0,8mg/ml	1:3000/1:5000	WB